



**HAL**  
open science

# Frequency-Selective Precoding and Channel Estimation for MmWave Hybrid MIMO Systems

Mohammad Masarra

► **To cite this version:**

Mohammad Masarra. Frequency-Selective Precoding and Channel Estimation for MmWave Hybrid MIMO Systems. Micro and nanotechnologies/Microelectronics. Université Polytechnique Hauts-de-France, 2022. English. NNT : 2022UPHF0024 . tel-03895219

**HAL Id: tel-03895219**

**<https://theses.hal.science/tel-03895219>**

Submitted on 12 Dec 2022

**HAL** is a multi-disciplinary open access archive for the deposit and dissemination of scientific research documents, whether they are published or not. The documents may come from teaching and research institutions in France or abroad, or from public or private research centers.

L'archive ouverte pluridisciplinaire **HAL**, est destinée au dépôt et à la diffusion de documents scientifiques de niveau recherche, publiés ou non, émanant des établissements d'enseignement et de recherche français ou étrangers, des laboratoires publics ou privés.



**Thèse de doctorat**

**Pour obtenir le grade de Docteur de**

**l'UNIVERSITE POLYTECHNIQUE HAUTS-DE-FRANCE**

**et de l'INSA HAUTS-DE-FRANCE**

Discipline:

**Electronique, Microélectronique, nanoélectronique et micro-ondes**

**Présentée et soutenue par Mohammad MASARRA.**

**Le 07/07/2022, à Aulnoy-Lez-Valenciennes**

**Ecole doctorale :**

Ecole Doctorale Polytechnique Hauts-de-France (ED PHF n°635)

**Unité de recherche :**

Institut d'Electronique, de Micro-Electronique et de Nanotechnologie - Site de Valenciennes  
(IEMN - UMR CNRS 8520)

**Précodage et estimation des canaux sélectifs en fréquence pour les  
systèmes millimétriques MIMO hybrides**

## JURY

### Rapporteurs

- CHARGE, Pascal. M., Professeur. Polytech-Nantes.
- SHAIEK, Hmaied. M., Maître de conférences HDR. CNAM-Paris.

### Examineurs

- RAOOF, Kosai. M., Professeur. Le Mans Université.
- MOULIN, Emmanuel. M., Professeur. UPHF.
- FARES, Haïfa. Mme., Maître de conférences. CentraleSupélec/IETR-Rennes.

### Directeur de thèse

- DAYOUB, Iyad. M., Professeur. UPHF.

### Co-directeur de thèse :

- ZWINGELSTEIN-COLIN, Marie. Mme., Maître de conférences. UPHF.

### Co-encadrant :

- HASSAN, Kais. M., Maître de conférences. Université du Maine.



## **PhD Thesis**

**Submitted for the degree of Doctor of Philosophy from**  
**UNIVERSITE POLYTECHNIQUE HAUTS-DE-FRANCE**  
**and INSA HAUTS-DE-FRANCE**

Subject :

**Electronique, Microélectronique, nanoélectronique et micro-ondes**

**Presented and defended by Mohammad MASARRA.**

**On 07/07/2022, Aulnoy-Lez-Valenciennes**

**Doctoral school :**

Doctoral School Polytechnique Hauts-de-France (ED PHF n°635)

**Research unit :**

Institute of Electronics Microelectronics and Nanotechnology – Valenciennes site (IEMN – UMR CNRS 8520)

**Frequency-Selective Precoding and Channel Estimation for MmWave  
Hybrid MIMO Systems**

## JURY

### Reviewers

- CHARGE, Pascal. M., Professeur. Polytech-Nantes.
- SHAIEK, Hmaied. M., Maître de conférences HDR.

### Examiners

- RAOOF, Kosai. M., Professeur. Le Mans Université.
- MOULIN, Emmanuel. M., Professeur. UPHF.
- FARES, Haïfa. Mme., Maître de conférences.

### Thesis director

- DAYOUB, Iyad. M., Professeur. UPHF.

### Thesis co-director :

- ZWINGELSTEIN-COLIN, Marie. Mme., Maître de conférences. UPHF.

### Co-supervisor :

- HASSAN, Kais. M., Maître de conférences. Université du Maine.

Frequency-Selective Precoding and Channel Estimation for MmWave Hybrid MIMO  
Systems © 2022 by Mohammad MASARRA, UPHF is licensed under CC BY 4.0

*To my family, for their unconditional support and endless love*

# Acknowledgments

This dissertation is the result of three and a half years of hard working at UPHF and IEMN, hence, throughout this journey, I have encountered numerous life-changing events that necessitated the assistance and advice of many people.

First and foremost, I want to express my gratitude to my Ph.D directors, Iyad, Marie, and Kais, for their support during my Ph.D study. Without their guidance, this project would have not been possible. Whether through personal ties or professional experiences, everyone has made a significant contribution to my education. Thank you for your time, effort, good attitude, insightful remarks, and suggestions.

I exploit this opportunity to thank UPHF and IEMN for receiving me as a Ph.D. student, and for their financial support that allowed me to conduct my Ph.D. Their encouragement and friendliness aided me in maintaining a high level of motivation.

I would also like to express my gratitude to the members of my reviewing committee for agreeing to devote their time and effort to reviewing this work. Indeed, I would like to thank M. Pascal CHARGE and M. Hmaied SHAIK for accepting to review and evaluate the thesis. Also, I thank M. Kosai RAOOF, M. Emmanuel MOULIN, and Mme. Haïfa FARES for accepting to be members of the jury.

Special thanks to my friends and colleagues at IEMN and UPHF, my friends in valenciennes, Lille, and France, and to all who supported me during my Ph.D. journey. Special thanks to my close friends in Lebanon.

I thank my sisters and brothers, for their tremendous support and endless self-sacrifices. I appreciate their prayers and encouragement in difficult times, as well as the laughs and joys.

Lastly, but most importantly, I thank my Dad **علي** and Mum **تغريد**, I will use my native

---

arabic language to deliver something which is nothing compared to their sacrifices and love,

To my dad I say:

وأما حق أبيك، فان تعلم أنه أصلك ، وأنتك فرعه ، وأنتك لولاه لم تكن. فهما رأيت في نفسك مما  
يعجبك فاعلم أن أباك أصل النعمة عليك فيه.

And to my Mum I say:

وأما حق أمك فتعلم أنها حملتك، حيث لا يحمل أحد أحدا، وأطعمتك من ثمرة قلبها ما لا يطعم  
أحد أحدا.. وأنها وقتك بسمعها وبصرها، فرضيت أن تشبع وتجووع هي، وتكسوك وتعري، وترويك  
وتظماً.. تباشر حر الدنيا وبردها لك، ودونك.





# Abstract

Many new applications, such as connected cars, augmented reality, virtual reality, mixed reality, three-dimensional video, ultra-high definition video, industrial internet of things, smart cities, connected healthcare, and so on, will emerge in the next decade. These applications necessitate connecting a large number of new devices and exchanging more data. For example, between 2018 and 2024, global mobile traffic is predicted to climb by 30% yearly, while capacity demand is expected to increase 1000-fold in the next decade. When compared to fourth generation (4G), fifth generation (5G) objectives is to boost user data rate by 10 to 100 (up to 10 Gbit/s), reduce latency by 10, increase connectivity density by 10, and lower cost and power usage. Researchers are attempting to suggest innovative solutions in response to the rapidly expanding need for data traffic and large connectivity, as well as the scarcity of sub-6 GHz radio spectrum. These are mostly based on novel signal processing techniques, network densification, or the use of extra frequency bands.

Regarding new bands, the millimeter-wave (mmWave) spectrum is between 30 GHz and 300 GHz, and the large unused bandwidth in these bands can allow wireless systems to support massive increases in capacity demand, as capacity of wireless systems increases as exploited bandwidth increases. As a result, mmWave communications will be critical in 5G and future cellular network generations. However, implementing mmWave and large multiple-input multiple-output (MIMO) advantages in practice is fraught with difficulties. The fundamental obstacles in realizing mmWave are three key challenges: hardware limitations, channel acquisition costs, and precoding design complexity.

To address these difficulties, precoding and channel estimation algorithms for both mmWave and massive MIMO are developed in this dissertation. The suggested methods implement filter-bank multicarrier offset-quadrature amplitude modulation (FBMC-OQAM)

---

and hybrid analog/digital architectures that divide precoding and combining processing across the radio-frequency (RF) and baseband domains, resulting in cost and power savings. Furthermore, to reduce precoder design complexity and training cost, the developed algorithms take advantage of the structure and features of mmWave and massive MIMO channels. The following are the dissertation's major contributions: (a) developing hybrid precoding algorithms and codebooks for frequency-selective (FS) mmWave systems, (b) investigating the viability of using the FBMC-OQAM signaling waveform for next-generation mmWave communications, and (c) developing a channel estimation algorithm for hybrid architecture-based mmWave systems that takes advantage of the sparse nature of mmWave channels.

**Keywords**— Millimeter-wave communications, MIMO, FBMC, OFDM, hybrid precoding, channel estimation.

# Résumé

De nombreuses nouvelles applications, telles que la voiture connectée, la réalité augmentée, la réalité virtuelle, la réalité mixte, la vidéo tridimensionnelle, la vidéo ultra-haute définition, l'internet industriel des objets, les villes intelligentes, la santé connectée, etc., verront le jour dans la prochaine décennie. Ces applications nécessitent de connecter un grand nombre de nouveaux appareils et d'échanger davantage de données. Par exemple, entre 2018 et 2024, le trafic mobile mondial devrait augmenter de 30% par an, tandis que la demande de capacité devrait être multipliée par 1 000 au cours de la prochaine décennie. Par rapport à la quatrième génération (4G), la cinquième génération (5G) promet d'augmenter le débit de données utilisateur de 10 à 100 (jusqu'à 10 Gbit/s), de réduire la latence de 10, d'augmenter la densité de connectivité de 10 et de réduire les coûts et la consommation d'énergie. Les chercheurs tentent de proposer des solutions innovantes en réponse au besoin croissant de trafic de données et de connectivité étendue, ainsi qu'à la rareté du spectre radio inférieur à 6 GHz. Celles-ci reposent principalement sur de nouvelles techniques de traitement du signal, la densification du réseau ou l'utilisation de bandes de fréquences supplémentaires. En ce qui concerne les nouvelles bandes, le spectre des ondes millimétriques (mmWave) se situe entre 30 GHz et 300 GHz, et la large bande passante inutilisée dans ces bandes peut permettre aux systèmes sans fil de supporter des augmentations massives de la demande de capacité. Par conséquent, les communications mmWave seront essentielles dans la 5G et les futures générations de réseaux cellulaires.

Cependant, la mise en œuvre des communications millimétriques avec les antennes multiples MIMO (multiple-input multiple-output) reste un challenge. Ainsi, trois défis majeurs sont à surmonter à savoir : 1) la limitation matérielle, 2) le coût d'acquisition des canaux et 3) la complexité de la conception du précodage. Afin de faire face à ces difficultés majeures, des algorithmes de précodage et d'estimation de canal pour mmWave et MIMO massif sont développés dans cette thèse. Les méthodes proposées mettent en œuvre une modulation multiporteuse d'amplitude en quadrature décalée à banque de filtres (FBMC-OQAM) et des architectures hy-

brides analogiques/numériques qui divisent le précodage et combinent le traitement dans les domaines RF et en bande de base, ce qui résulte en une économie de coûts et d'énergie. De plus, pour réduire la complexité de conception du précodeur et les coûts de formation de voies, les algorithmes développés dans la thèse tirent parti de la structure et des fonctionnalités des canaux mmWave et MIMO massifs.

Ainsi, les principales contributions de la thèse sont : (a) le développement d'algorithmes de précodage hybrides et des livres de codes pour les systèmes mmWave sélectifs en fréquence (FS), (b) l'étude de la viabilité de l'utilisation de la forme d'onde de signalisation FBMC-OQAM pour les communications mmWave de prochaine génération, et (c) le développement d'un algorithme d'estimation de canal pour les systèmes à ondes millimétriques basés sur une architecture hybride profitant de la nature parcimonieuse des canaux à ondes millimétriques.

**Keywords**— Millimeter-wave communications, MIMO, FBMC, OFDM, hybrid precoding, channel estimation.

# Table of Contents

<b>Abstract</b>	<b>viii</b>
<b>Résumé</b>	<b>x</b>
<b>Table of Contents</b>	<b>xii</b>
<b>List of Tables</b>	<b>xv</b>
<b>List of Figures</b>	<b>xvi</b>
<b>Mathematical Notations and Acronyms</b>	<b>xix</b>
<b>General Introduction</b>	<b>2</b>
<b>Chapter 1:</b>	
<b>Fundamentals And Background Of MmWave Communications</b>	<b>6</b>
1.1 Introduction and Background . . . . .	6
1.2 Characteristics of MmWave Communications . . . . .	9
1.2.1 Propagation Characteristics . . . . .	10
1.2.2 Technical Potential . . . . .	11
1.2.3 Enabling Technologies . . . . .	12
1.3 Massive MIMO for MmWave Systems . . . . .	13
1.3.1 MIMO Architectures for MmWave Communications . . . . .	15
1.3.2 Spatial MmWave MIMO Channel Modeling . . . . .	18
1.3.3 MmWave MIMO System Model . . . . .	20

1.4	Multi-Carrier Modulation Techniques . . . . .	22
1.4.1	Multi-Carrier Modulation History and Motivations . . . . .	22
1.4.2	Multi-Carrier Modulation Principles . . . . .	23
1.4.3	Multi-Carrier Modulation Techniques for MmWave Systems . . . . .	25
1.5	Compressive Sensing : Mathematical Tool for Channel Estimation . . . . .	29
1.6	Conclusions . . . . .	32

## Chapter 2:

### Hybrid Precoding For Frequency-Selective MmWave MIMO FBMC-OQAM

<b>Systems</b>		<b>34</b>
2.1	Introduction . . . . .	34
2.2	Review of Existing Works . . . . .	36
2.3	FS MmWave Hybrid FBMC-OQAM MIMO System Model . . . . .	37
2.4	Spatially Sparse Precoding . . . . .	40
2.5	Spatially Sparse MMSE Combining . . . . .	50
2.6	Results . . . . .	54
2.7	Conclusions . . . . .	56

## Chapter 3:

### Hybrid Precoding And Channel Estimation For Frequency-Selective MmWave

<b>MIMO OFDM Systems</b>		<b>60</b>
3.1	Introduction . . . . .	60
3.2	Review of Channel Estimation Techniques for Hybrid Architecture Systems . . . . .	61
3.2.1	Techniques for Narrowband Systems . . . . .	61
3.2.2	Techniques for Wideband Systems . . . . .	71
3.2.3	Conclusions . . . . .	74
3.3	System Model . . . . .	74
3.4	Frequency-Selective Hybrid Training Codebook Design . . . . .	76
3.4.1	Codebook Structure . . . . .	76
3.4.2	Design of the Codebook Beamforming Vectors . . . . .	77

---

3.5	Channel Model . . . . .	79
3.5.1	Channel in the Time-Domain . . . . .	79
3.5.2	Channel in the Frequency-Domain . . . . .	80
3.5.3	Grid Quantization . . . . .	80
3.6	A Sparse Formulation of the mmWave Channel Estimation Problem . . . . .	81
3.7	Channel Estimation for Frequency-Selective MmWave Channels . . . . .	83
3.8	Results . . . . .	87
3.9	Conclusions . . . . .	90
	<b>General Conclusions and Perspectives</b>	<b>92</b>
	<b>Bibliography</b>	<b>98</b>

# List of Tables

2.1	Summary of existing works on mmWave hybrid OFDM and MIMO-FBMC-OQAM systems. . . . .	35
3.1	Channel estimation algorithms for narrowband hybrid mmWave systems. . . . .	62
3.2	Channel estimation algorithms for wideband hybrid mmWave systems. . . . .	71

# List of Figures

1.1	General system architecture of mmWave transceiver. . . . .	14
1.2	Different MIMO architectures (a) fully-analog architecture; (b) hybrid architecture; (c) lens array architecture (d) few-bit ADCs architecture . . . . .	15
1.3	FBMC-QAM resource grid structure . . . . .	27
1.4	FBMC-OQAM resource grid structure . . . . .	28
2.1	Architecture of mmWave hybrid MIMO FBMC BS and MS. . . . .	37
2.2	The BER versus SNR of the proposed hybrid algorithms for mmWave $32 \times 16$ MIMO FBMC-OQAM system, compared to the OFDM counterpart, $N_S = 2, N_{RF} = 4$ . . . . .	53
2.3	The SEs of the proposed hybrid precoding and digital SVD algorithms versus SNR for mmWave $32 \times 16$ MIMO FBMC-OQAM system, $N_S = N_{RF} = 3$ . . . . .	54
2.4	The SEs of the proposed hybrid precoding and digital SVD algorithms versus the number of quantization bits for mmWave $32 \times 16$ MIMO FBMC-OQAM system, $N_S = 1, N_{RF} = 2, \text{SNR} = 0$ dB. . . . .	55
2.5	The SEs of the proposed hybrid precoding and digital SVD algorithms versus the number of streams for mmWave $32 \times 8$ MIMO FBMC-OQAM system, $N_S = N_{RF}, \text{SNR} = 0$ dB. . . . .	56
3.1	An example of the beam patterns adopted in the first (a) and second (b) stages in [111] when $K = 3$ , where $S_k, k \in \{1, \dots, K\}$ denotes the sub-ranges in each stage. . . . .	63

3.2	Illustration of the two-stage estimation algorithm in [166], the blue colored arrows represent the AoAs and AoDs at the BS and MS; (a) the BS sends an omnidirectional signal over all directions, (b) the MS scans the directions, in this case we have two AoAs at MS at $135^\circ$ and $180^\circ$ , (c) the MS sends through its AoDs, (d) the BS scans the directions, in this case we have two AoAs at BS at $0^\circ$ and $45^\circ$ . . .	65
3.3	The overlapped beam patterns adopted in the first (a) and second (b) stages when $V = 3$ . . . . .	65
3.4	Hybrid mmWave MS architecture implementing switches instead of phase shifters .	68
3.5	The two-stage asymmetric estimation approach in [116] . . . . .	69
3.6	Different sparse matrix types (a) unstructured sparse matrix (b) sparse rows matrix (c) sparse Hermitian matrix. . . . .	69
3.7	Architecture of mmWave hybrid MIMO OFDM TX and RX. . . . .	75
3.8	SEs of a $64 \times 32$ MIMO OFDM mmWave system, based on the proposed hybrid precoding and channel estimation algorithms, as a function of SNR. . . . .	85
3.9	SEs of a $64 \times 32$ MIMO OFDM mmWave system employing the proposed hybrid precoding and channel estimation algorithms versus the number of resolution N when SNR = 10 dB. . . . .	89
3.10	SEs of a $64 \times 32$ MIMO OFDM mmWave system employing the proposed hybrid precoding and channel estimation algorithms versus the number of quantization bits when SNR = 13dB. . . . .	89



# Mathematical Notations and Acronyms

## List of Mathematical Notations and Operators

$(\cdot)^T$	Transpose operation.
$(\cdot)^*$	Hermitian conjugate transpose.
diag	Matlab diag function.
$\otimes$	Kronecker product.
$ \cdot $	Absolute value operator.
$\langle \cdot \rangle$	Imaginary part of complex number.
tr	Trace operator.
$[\cdot]_{i,j}$	The $(i, j)$ th entry of the matrix argument.
$\ \cdot\ _F$	Frobenius norm.
$\ \cdot\ _2$	Euclidean norm.
$\ \cdot\ _0$	$\ell_0$ norm or number of non-zero entries.
vec{.}	Vectorization of the matrix.
$\circ$	Matrix entrywise product.

## List of Acronyms

<b>1D</b>	One-Dimensional
<b>2D</b>	Two-Dimensional
<b>3D</b>	Three-Dimensional

---

<b>4G</b>	Fourth Generation
<b>5G</b>	Fifth Generation
<b>AAVE</b>	Antenna Array with Virtual Elements
<b>ADC</b>	Analog to Digital Converter
<b>AoAs</b>	Angles-Of-Arrivals
<b>AoDs</b>	Angles-Of-Drivals
<b>AWGN</b>	Additive White Gaussian Noise
<b>BER</b>	Bit Error Rate
<b>BLT</b>	Balian Low Theorem
<b>AMP</b>	Approximate Message Passing
<b>BP</b>	Basis Pursuit
<b>BS</b>	Base Station
<b>CFR</b>	Channel Frequency Response
<b>CMOS</b>	Complementary Metal Oxide Semiconductor
<b>C-OMP</b>	Covariance OMP
<b>CoSaMP</b>	COmpressive SAmping Matching Pursuit
<b>CP</b>	Cyclic-Prefix
<b>C/P</b>	CANDECOMP/PARAFAC
<b>CS</b>	Compressive Sensing
<b>CSI</b>	Channel State Information
<b>DC-OMP</b>	Dynamic Covariance OMP

---

<b>DFT</b>	Discrete Fourier Transform
<b>DGMP</b>	Distributed Grid Matching Pursuit
<b>DL</b>	DownLink
<b>DS-OMP</b>	Dynamic Simultaneous OMP
<b>FBMC</b>	Filter-Bank MultiCarrier
<b>FBMC-OQAM</b>	Filter-Bank MultiCarrier Offset-QAM
<b>FCC</b>	Federal Communications Commission
<b>FDD</b>	Frequency-Division Duplexing
<b>FDM</b>	Frequency-Division Multiplexing
<b>F-OFDM</b>	Filtered OFDM
<b>FS</b>	Frequency-Selective
<b>FT</b>	Frequency-Time
<b>GOMP</b>	Generalized OMP
<b>ICI</b>	Inter-Carrier Interference
<b>IoT</b>	Internet Of Things
<b>ISI</b>	Inter-Symbol Interference
<b>JCE+LS</b>	Joint Channel Estimation + Local Search
<b>LASSO</b>	Least Absolute Shrinkage and Selection Operator
<b>LSE</b>	Least-Squares Estimation
<b>MCM</b>	Multi-Carrier Modulation
<b>MFO</b>	MIMO-FBMC-OQAM

---

<b>MG-OMP</b>	Multi-Grid OMP
<b>MIMO</b>	Multiple-Input Multiple-Output
<b>MMP</b>	Multipath Matching Pursuit
<b>MMSE</b>	Minimum Mean-Square Error
<b>MmWave</b>	Millimeter-Wave
<b>M-OMP</b>	Multiple measurement vector OMP
<b>MS</b>	Mobile Station
<b>MSE</b>	Mean-Square Error
<b>MU</b>	Multi-User
<b>MUSIC</b>	MUltiple SIgnal Classification
<b>NLOS</b>	Non-Line-Of-Sight
<b>OFDM</b>	Orthogonal Frequency-Division Multiplexing
<b>OMP</b>	Orthogonal Matching Pursuit
<b>OOB</b>	Out-Of-Band
<b>OQAM</b>	Offset-QAM
<b>PCSI</b>	Perfect Channel State Information
<b>QAM</b>	Quadrature Amplitude Modulation
<b>RF</b>	Radio-Frequency
<b>RX</b>	Receiver
<b>SC-FDE</b>	Single Carrier-Frequency Domain Equalization
<b>SdMP</b>	Stage-Determined Matching Pursuit

---

<b>SE</b>	Spectral Efficiency
<b>SNR</b>	Signal-to-Noise Ratio
<b>S-OMP</b>	Simultaneous OMP
<b>SSAMP</b>	Structured Sparsity Adaptive Matching Pursuit
<b>SS-SW-OMP+Th</b>	Subcarrier Selection SW-OMP + THresholding
<b>SU</b>	Single-User
<b>SVD</b>	Singular Value Decomposition
<b>SW-OMP</b>	Simultaneous Weighted OMP
<b>TDD</b>	Time-Division Duplexing
<b>TFL</b>	Time Frequency Localization
<b>TX</b>	Transmitter
<b>UDNs</b>	Ultra-Dense Networks
<b>UFMC</b>	Universal Filtered MultiCarrier
<b>UL</b>	UpLink
<b>ULA</b>	Uniform Linear Array
<b>ULPA</b>	Uniform Linear Planar Array





# General Introduction

## Context and Motivations

MIMO communication is predicted to play a prominent role in future wireless systems through the deployment of a large number of antennas at the transmitters and receivers. Massive MIMO provides large multiplexing gains in low-frequency systems, boosting system spectral efficiency. To ensure sufficient received signal power in millimeter-wave (mmWave) systems, massive antenna arrays must be deployed at both the base station and mobile users. However, putting these methods into practice necessitates addressing a number of significant issues: (i) Fully digital solutions are expensive and power-hungry, (ii) precoder design optimization problems are complex, (iii) and channel training and estimation processes have a large overhead. In this dissertation, precoding and channel estimation techniques for both mmWave and massive MIMO are developed to overcome these issues. The proposed solutions adopt FBMC-OQAM and use hybrid analog/digital architectures that split precoding and combining processing between the RF and baseband domains, resulting in cost and power reductions. Furthermore, the developed techniques take advantage of the structure and properties of mmWave and massive MIMO channels to reduce precoder design complexity and training overhead.

### Thesis contributions

- Building hybrid precoding algorithms and codebooks for FS mmWave systems
- Examining the viability of using the FBMC-OQAM signaling waveform for next-generation mmWave communications
- Developing a channel estimation solution for hybrid architecture-based mmWave systems that takes use of the sparse nature of mmWave channels

The proposed solutions' promising performance is demonstrated by numerical simulations, establishing them as enabling technologies for mmWave and massive MIMO systems.

## Thesis Organization

In chapter 1, the reader will be introduced to mmWave communications and all of its supporting technologies. Thereafter, the viability of adopting the FBMC-OQAM signaling waveform for next-generation mmWave communications was investigated in chapter 2. Orthogonal matching pursuit (OMP)-based hybrid precoding and combining algorithms have been developed to utilize FBMC-OQAM filter banks in mmWave hybrid MIMO systems. Afterwards, in chapter 3, both algorithms are presented, the first is a proposed approach for developing an FS hybrid multi-resolution codebook which is based on OMP technique, and the second is a proposed FS channel estimation algorithm for next-generation mmWave communications. As we shall discuss in the conclusions and perspectives, more research and analysis are still needed and envisioned for future studies.

## Publications

The following is a list of publications in refereed journals and international conference proceedings, and other publications produced during my Ph.D. candidature.

### International Journal papers

- Hassan, Kais, Mohammad Masarra, Marie Zwingelstein, and Iyad Dayoub. "Channel estimation techniques for millimeter-wave communication systems: Achievements and challenges." IEEE Open Journal of the Communications Society 1 (2020): 1336-1363.
- M. Masarra, K. Hassan, M. Zwingelstein, and I. Dayoub, "Hybrid precoding and channel estimation for frequency-selective mmWave MIMO OFDM systems", in IEEE Sensors Letters, Submitted.

- M. Masarra, K. Hassan, M. Zwingelstein, and I. Dayoub, “Channel estimation for frequency-selective mmWave MIMO FBMC-OQAM systems” Journal Paper, On going.

## International Conference Papers

- M. Masarra, K. Hassan, M. Zwingelstein and I. Dayoub, ”FBMC-OQAM for frequency-selective mmWave hybrid MIMO systems,” 2022 IEEE Wireless Communications and Networking Conference (WCNC), 2022, pp. 1593-1598, doi: 10.1109/WCNC51071.2022.9771667.
- M. Masarra, K. Hassan, M. Zwingelstein, and I. Dayoub, “RF Codebook-based frequency-selective hybrid precoding for MIMO FBMC-OQAM mmWave systems” in 2022 ITC-EGYPT2021, ACCEPTED.

## Miscellaneous Publications

### Scientific Reports

- Masarra, M. Rapport d’avancement de thèse et CSI, IEMN-DOAE, UPHF, September 2019.
- Masarra, M. Rapport d’avancement de thèse et CSI, IEMN-DOAE, UPHF, September 2021.

### Posters and Presentations

- Masarra, M. ”The next-generation mmWave communication systems”, IEMN-DOAE, Lille, November 2019.
- Masarra, M. ”Different channel estimation techniques for mmWave systems”, Workshop, LILLIAD, Lille, November 2019.



# Chapter 1

## Fundamentals And Background Of MmWave Communications

### 1.1 Introduction and Background

The next decade will encounter many emerging applications such as connected cars, augmented reality, virtual reality, mixed reality, three-dimensional (3D) video, ultra-high definition video, industrial internet of things (IoT), smart cities, connected healthcare, etc. These applications require to massively connect new devices and to exchange more data. For instance, the global mobile traffic is expected to grow annually by 30 percent between 2018 and 2024, and the capacity demand in the next decade is expected to witness a 1000-fold increase [1]. Among the future communication systems promises, when compared to fourth generation (4G), is to increase user data rate by 10 to 100 (up to 10 Gbit/s), to reduce latency by 10, to increase connectivity density by 10, and also to reduce the cost and power consumption [2]. Due to this hugely increasing demand for data traffic and massive connectivity as well as to the scarcity in the sub-6 GHz radio spectrum, researchers are trying to propose new solutions. These are mainly based either on the new signal processing techniques, or on densifying the network, or on exploiting additional frequency bands.

In regards of exploiting new bands, the mmWave spectrum is between 30 GHz and 300 GHz (i.e. wavelengths between 1mm to 10mm) where the large unused bandwidth in these bands can allow the

wireless systems to support the enormously increase in capacity demand since capacity of wireless systems increases when the exploited bandwidth increases. Hence, mmWave communications will play an essential role in upcoming future generations of cellular networks [3, 4, 5, 6].

Despite their bandwidth attractivity, mmWave communications systems suffer from high free-space path-loss when compared to the sub-6 GHz ones. In addition, a substantial attenuation is observed in some mmWave bands due to atmospheric absorption, and rain and snow effects. Therefore, the mmWave signal risks to propagate over a few meters in some scenarios, and hence mmWave communications may be only suitable for very close-range communications such as in indoor applications. This difficulty can be overcome for outdoor mobile communications, where a greater transmission range is expected, by either increasing the transmission power or by using high-gain, high-directional antennas. Since the transmission power is always limited by regulations, mmWave systems must enable narrow steering beams such as the transmitter (TX) and the receiver (RX) steer towards each other which results in high directional gain in the wanted directions and low gain in the unwanted ones. The desirable high directivity is based on signal processing techniques such as beamforming which requires to increase the number of antennas of the antenna arrays at the TX and/or RX, i.e. massive antenna arrays are needed. This approach is facilitated by the short wavelength of mmWave signals which makes possible to compact more antennas while keeping the array size small. Another aspect of mmWave system design comes from the impossibility to directly apply the traditional digital transceiver architectures, which are employed in sub-6 GHz, directly to mmWave systems because of the high power consumption of mmWave RF chains. Recently, new tailored MIMO architectures were proposed to solve this problem namely *fully-analog*, *hybrid* and *few-bit analog to digital converters (ADC)* architectures. The objective is to reduce the total consumed power by either reducing the number of RF chains or the power consumption per each one.

Hence, mmWave communications are a key technology enabler for the upcoming future generations of cellular networks, not only thanks to the huge available bandwidth, but also by means of its complementary with other fifth generation (5G) technologies such as ultra-dense networks (UDNs) and massive MIMO. MmWave links are suitable for wireless backhauling and short-range communications in the small cells of UDNs while still capable of mitigating interferences by using

the high-directional antenna arrays. This high directivity is enabled by the beamforming ability of massive MIMO. However, the evolution of mmWave communications is hindered by challenges that require more insight to propose the needed solutions to reach their full potential. Some of these challenges come from the propagation characteristics in the mmWave bands (the path-loss, penetration loss, and the atmospheric attenuation), others come from the high power consumption and the hardware impairments of mmWave circuits. As can be concluded, mmWave systems will play a crucial role in the structure of next-generation communication systems, this has shaped the motivations beyond later analysis and developments in this Ph.D thesis. In this chapter, the reader will be introduced to mmWave communications with all its enabling technologies. In the upcoming section, an illustration of the organization of this chapter is given.

## Scope and Organization

This chapter is organized as follows:

- First, in section 1.2 the characteristics of mmWave channels such as the differences between the propagation behavior in the mmWave bands and in the sub-6 GHz ones are illustrated. This will help to understand the technical potential of mmWave communications, the challenges which have to be addressed to reach this potential, and the enabler-technologies to reply to these challenges.
- Then in section 1.3, we discuss the different existing system architectures which are proposed for massive MIMO mmWave systems. The spatial MIMO channel models which present the special nature of highly-directive mmWave communications are also introduced before presenting the massive MIMO system model.
- In section 1.4 we present multi-carrier modulation (MCM) techniques alongside with the modulation waveforms that have been used in this Ph.D. thesis. FBMC-OQAM waveform has been used in chapter 2, and orthogonal frequency-division multiplexing (OFDM) waveform has been used in 3.
- Afterwards, compressive sensing (CS) as a mathematical tool for channel estimation is intro-

duced in section 1.5. This tool is crucial for the proposed channel estimation algorithm in chapter 3.

- Finally, the conclusions of this chapter are given in section 1.6.

## 1.2 Characteristics of MmWave Communications

An increased attention has recently been drawn to the huge spectrum in the mmWave frequency bands to meet the increase in the global mobile data traffic and to achieve up to hundreds of times more capacity compared to 4G cellular networks [7, 8, 9].

MmWave communications have been employed for applications such as radar and point-to-point communication for 100 years ago [10]. In the last decade, some mmWave standards have emerged including IEEE 802.15.3c [11], IEEE 802.11ad [12] and WirelessHD [13] which are intended to wireless personal area networks, wireless local area networks and wireless HDMI, respectively. Recently, the mobile network research community dedicated a lot of attention to the sub-100 GHz systems operating in the 28 GHz, 38 GHz, 60 GHz, 71 GHz and 81 GHz bands, while the band above 100 GHz has been studied by only a few very recent papers [14]. Some proof of concept studies had been conducted in the last years. In May 2013, Samsung realized a 1.056 Gb/s transmission in the 28 GHz band to a distance of up to 2 km [15]. In April 2015, a peak rate of 15 Gbps at 73 GHz was achieved by Nokia in collaboration with National Instruments [5]. In February 2018, Deutsche Telekom and Huawei have successfully completed the world's first multi-cell field tests at 73 GHz [16].

However, the propagation characteristics at mmWave frequencies are different from that at the traditional sub-6 GHz ones, that is why we will show in the following subsections the main technical advantages and challenges of the mmWave technology.

### 1.2.1 Propagation Characteristics

A major difference between sub-6 GHz and mmWave systems in terms of propagation characteristics is in their free-space path-loss ( $\rho_{\text{FS}}$ ) [17] which is described by,

$$\rho_{\text{FS}} \propto \frac{d^\zeta}{\lambda^2}, \quad (1.1)$$

where  $d$  is the distance between the TX and RX,  $\zeta$  is the path-loss exponent which typically equals 2, and  $\lambda$  is the wavelength of the signal. However,  $\zeta$  is less than 2 in some scenarios of cellular networks and indoor applications [18]. On the other hand, path-loss exponent can reach the value of 6 in some severe environments of propagation [19]. A comparison between the microwave propagation in the 1.8 GHz GSM band and the mmWave one in the 73 GHz bands, under the same configuration (transmission distance, propagation environment, antenna array), shows an additional loss of 32 dB in the mmWave band [20]. Recent urban model experiments also show a degradation of 40 dB in path-loss at 28 GHz compared to 2.8 GHz [21, 19]. Thus, the severe path-loss of mmWave propagation required to be compensated by a strong directionality.

The *atmospheric* attenuation of mmWave signals, which is caused particularly by the absorption of oxygen and water vapor, as well as the scattering of rain, must be added to the path-loss. The atmospheric attenuation depends on the operating frequency. The atmospheric oxygen absorption is especially severe at 60 GHz and 120 GHz, and the water vapor absorption is particularly very high at 180 GHz [22]. Also, rain attenuation at mmWave frequencies is much greater than that of sub-6 GHz frequencies [23].

Another factor which affects the propagation of mmWave signals is their severe penetration loss which results in susceptibility to the static and dynamic blockage effect. In fact, some obstacles, such as human bodies, doors, glass and walls, attenuate and even can block mmWaves signals. For instance, attenuation of a 28 GHz signal can be as high as 24 dB and 45 dB if penetrating respectively through two walls and four doors [24]. Hence, it is not realistic to employ outdoor base stations (BS)s to serve indoor users for example.

The severe path-loss, the vulnerability of mmWave transmissions to blockages, and the atmospheric attenuation affect the choice of the operating frequencies, and require important changes to

the system design and architecture. however, even after removing many of the unusable frequency bands due to the aforementioned challenges, it is anticipated that mmWave bands may provide 100 GHz of new bandwidth for mobile communications, which is more than 200 times the spectrum now allocated for this purpose below 3 GHz [25].

## 1.2.2 Technical Potential

Despite the challenging characteristics of the mmWave channel, mmWave communications is an important part of the 5G cellular system and beyond. This is due to the potential of mmWave communications in terms of large bandwidth availability and short wavelength.

### Large Bandwidth

The requirements of upcoming telecommunications systems in terms of very high data rate may not be achievable by focusing only on the heavily-occupied conventional sub-6 GHz frequency bands. On the contrary, an abandon of the mmWave bands is available to be exploited opening the door to multi-Gigabit data exchange in spite of the low spectral efficiency (SE) since a very large bandwidth is hopefully sufficient to support very high data rates [26]. For instance, more than 12 GHz of bandwidth is available between 60 GHz and 90 GHz which is also called the E-band. Furthermore, the low SE means less complexity and more robustness making mmWave systems more feasible. Actually, the 3rd Generation Partnership Project (3GPP) Release 15 selected the 24~29 GHz and 37~43 GHz frequency bands for the deployment of 5G mmWave systems [27]. The International Telecommunication Union (ITU) and the 3GPP will allocate two frequency bands around 40 GHz and 100 GHz for commercial use [28]. In July 2016, the Federal Communications Commission (FCC) dedicated several mmWave bands for wireless services including around 28 GHz and 39 GHz for licensed allocation, and 64~71 GHz for unlicensed usage [29].

### Short Wavelength

The short wavelength is the main reason behind the strong path-loss of mmWave signals and hence the need for high directivity antennas which can be realised with antenna arrays and beamforming

techniques. Narrower beams require higher number of antennas in the array which is compatible with mmWave communications thanks to the short wavelength. Indeed, the shorter the wavelength is, the smaller the antenna arrays' sizes are (since the distance between any two antennas in the array is basically half of the wavelength) and thus the higher the number of antennas to be packed into the same physical array size is, and also the higher the beamforming gain is [7, 5, 28]. It is worth noting that a typical antenna length at 60 GHz is less than 2.5 mm for example [28]. Another benefit of highly directional communications, based on narrow beams at the TX and at RX, is that it helps to secure the mmWave communication link against eavesdropping and jamming as well as to increase the interference immunity [5, 30].

### 1.2.3 Enabling Technologies

The mmWave communications technology is, at the same time, enabled by and complementary to some other technologies such as massive MIMO, advances in signal processing, network densification and finally advances in circuit design and integration.

#### Massive MIMO

The use of a large number of antennas at BSs and for mobile stations MSs is called Massive MIMO and is an essential technology to increase the capacity of cellular networks. Massive MIMO has been studied for conventional sub-6 GHz systems, and is also very crucial for mmWave systems where high directivity is mandatory [31]. Higher frequency bands offered by mmWave systems grant the ability to design antenna arrays with a huge number of antennas [32]. However, this will not be possible without the recent advances in complementary metal oxide semiconductor (CMOS) circuits which increase the capacity of circuit integration [33].

#### Enhanced Signal Processing Techniques

It is clear that the conventional *fully-digital* MIMO system, in which one RF chain is dedicated to each antenna, is infeasible for mmWave systems because of the high implementation cost and high energy consumption [34, 9, 35]. Indeed, it has been shown that RF components can consume

up to 70% of the total transceiver power consumption [36]. For these reasons, several mmWave *hybrid* architectures were proposed as alternatives to the fully-digital one, see section 1.3.1. These solutions offer a good balance between system performance and hardware complexity. However, they require to develop new signal processing techniques for beamforming, channel estimation, and more generally for improving system performance.

### Network Densification

Network densification means increasing the density of BSs deployment in the network via several tiers and an hierarchy of macro, micro, pico and femto cells, and leads to a multi-tier heterogeneous network [37]. Increasing the small cells density increases capacity and SE of served users at the expense of increasing the cost of interference management [38]. MmWave communications are a very good candidate for small cell deployment mainly for three reasons i) a small cell means a short-range communication which makes the high path-loss of mmWave communications less unfavorable, ii) the larger bandwidth of mmWave frequencies means higher capacity which is the main goal of small cells deployment, iii) and the high directivity of mmWave communications, at the TX and RX, results in better interference control.

## 1.3 Massive MIMO for MmWave Systems

Millimeter-wave communication systems need to employ a large number of antennas at the TX and RX sides. Some early research works suggested arrays of 32 to 256 antennas at BSs and 4 to 16 ones at MSs [39, 8]. Fortunately, it is now possible to pack such number of antennas into small packages [40, 41]. However, other aspects such as the power consumption and cost influence the maximum number of antennas that can be integrated in the mmWave system. If digital signal processing techniques are employed for baseband precoding at the TX and combining at the RX then one dedicated RF chain per antenna is needed, where each RF chain includes an ADC. These techniques are usually used for sub-6 GHz systems. However, they are not affordable actually at mmWave frequencies as the bandwidths become wider and the antenna arrays become larger. This results in high-resolution ADCs and high energy consumption of each RF chain. For instance, 30

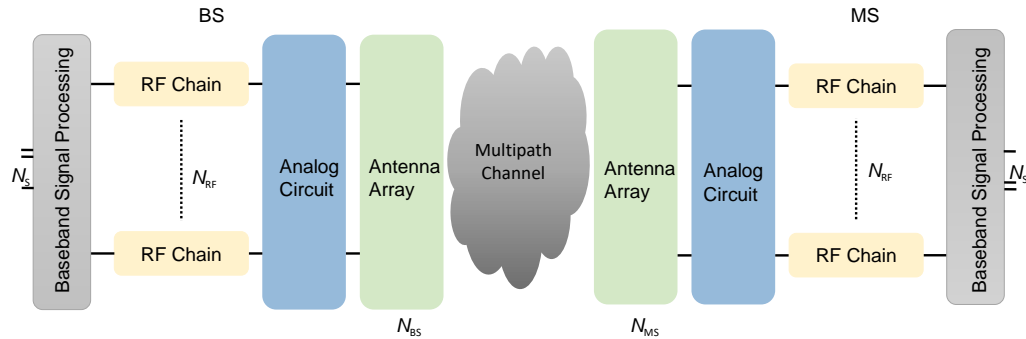


Figure 1.1: General system architecture of mmWave transceiver.

mW per RF chain is consumed at sub-6 GHz frequencies, while 250 mW per RF chain is needed at mmWave frequency bands [9].

Figure 1.1 is a block diagram that illustrates the general architecture of a hybrid mmWave transceiver. Without loss of generality, a BS equipped with  $N_{\text{RF}}$  RF chains and  $N_{\text{BS}}$  antennas ( $N_{\text{RF}} < N_{\text{BS}}$ ) is assumed to communicate with an MS equipped with  $N_{\text{RF}}$  RF chains and  $N_{\text{MS}}$  antennas ( $N_{\text{RF}} < N_{\text{MS}}$ ) in order to exchange some data streams [4]. In practice, the number of RF chains at the MSs is usually less than that at the BSs. A point to point communication is considered here, however, this architecture could be easily extended to the case of multi-users (MU)s. The combined role of the baseband digital processing and the analog circuit of the hybrid architecture is to direct the beams at the TX or/and RX. In contrast with the traditional fully-digital architecture that does not consider an analog circuit behind (before) the RF chains at the TX (RX) and considers one RF chain per antenna, i.e.  $N_{\text{RF}} = N_{\text{BS}} = N_{\text{MS}}$  [5, 42]. For this reason, fully-digital architecture must be avoided nowadays when it comes to mmWave communication systems although it could be possible at some point in the future. This leads to introducing some new hybrid architectures in order to make the massive MIMO mmWave systems feasible. The idea is to figure out how to reduce the number of RF chains and/or the resolution of the ADCs which consequently will reduce the total power consumption and the total cost. Different transceiver architectures for mmWave communication will be introduced in the following subsection.

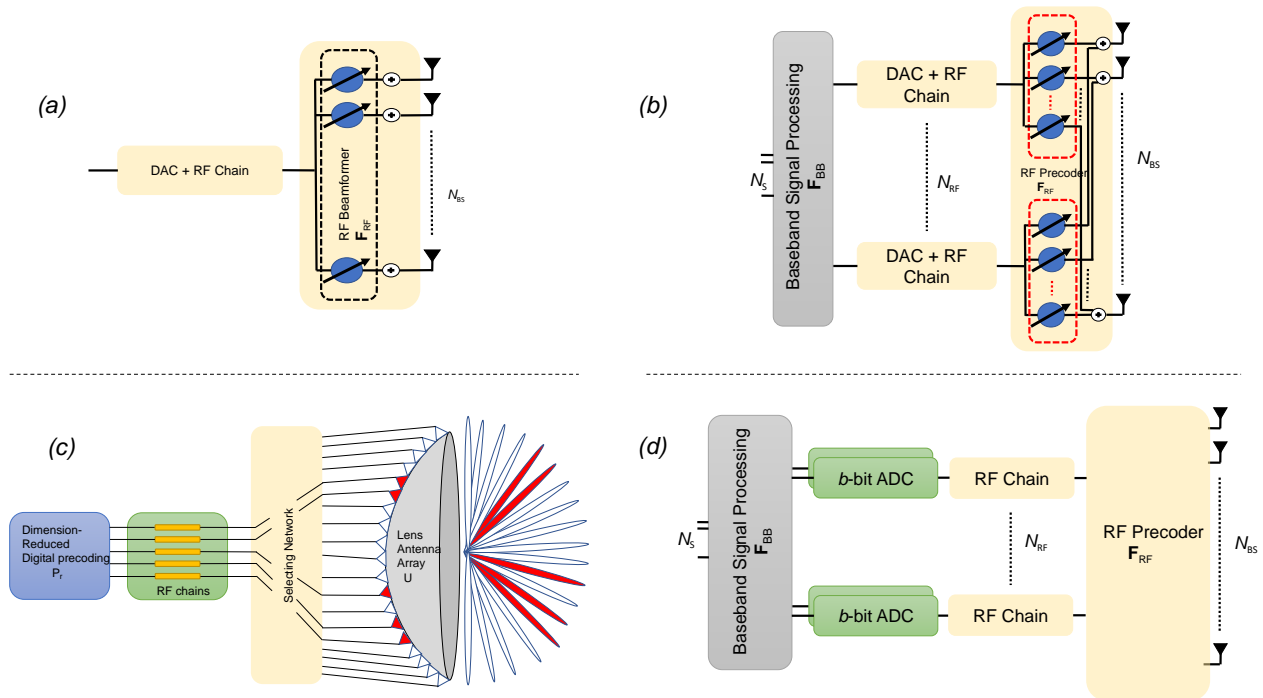


Figure 1.2: Different MIMO architectures (a) fully-analog architecture; (b) hybrid architecture; (c) lens array architecture (d) few-bit ADCs architecture .

### 1.3.1 MIMO Architectures for MmWave Communications

#### Fully-Analog Architecture

One solution is to reduce the number of RF chains to one and to perform beamforming entirely using the analog processing. As illustrated in figure 1.2(a) [5, 42], this is achieved by analog shifters employed in the RF domain to adjust the phase of the RF signals at each antenna. This solution drastically reduces the hardware cost and power consumption.

Many studies have been carried out on the *fully-analog* architecture. A codebook-based analog beamformer for mmWave wireless personal area networks via beam switching is discussed in [43]. [44, 45] which propose an alternative codebook-based beamforming for outdoor backhaul based on a joint TX-RX beam scanning employing a tree-structured codebook. Moreover, an iterative channel estimation and analog beamforming algorithm has been investigated in [46, 47, 48, 49], where the coefficients at the TX and RX sides are calculated to reach asymptotically singular value decomposition (SVD) elements.

Unfortunately, these solutions suffer from hardware limitations due to the constant modulus constraint imposed by the implementation of the phase shifters, hence the signals can only be partially adjusted [5, 42]. Another drawback of the fully-analog architecture is that it supports only one data stream, which makes its usage for MU communications tricky. However, this architecture is still a good fit for some standards such as WirelessHD for instance.

## Hybrid Architecture

The hybrid architecture represents a compromise between the fully-digital architecture (where the number of RF chains equals that of the antennas) and the fully-analog one (where only one RF chain is employed). Precoding (at the TX) and combining (at the RX) are performed in both the analog and the digital domains as shown in figure 1.2(b). The idea is to employ a dimension-reduced precoder/combiner with a small number of RF chains ( $N_{\text{RF,BS}} \ll N_{\text{BS}}, N_{\text{RF,MS}} \ll N_{\text{MS}}$ ) while still relying on full-size analog precoder/combiner, where  $N_{\text{RF,BS}}, N_{\text{RF,MS}}$  stand for the number of RF chains at BS and MS, respectively. Despite the reduced number of RF chains, the performance of these architectures has been shown to be not far from the fully-digitally ones [39, 9, 50]. This can be explained by the sparse nature of the mmWave channel (since the number of scatters is small), which makes the channel matrix low-rank [51, 6], see section 1.5 for further illustration about sparsity. In addition, this solution supports easily several users/data streams, their number being equal or less than the number of RF chains. The 3GPP included the hybrid architecture in its recommendation for 5G systems in 2016 [52].

Furthermore, the analog processing (precoding/combining) can be realized through different analog networks with phase shifters, namely the fully-connected networks [53] and the sub-connected ones [39, 54]. The idea is either to connect each RF chain to all the antennas, or to connect it to a subset of them. It seems that the sub-connected choice could be practically more interesting since it reduces the cost and complexity while still achieving a good performance when compared to the fully-connected network [39, 54, 55]. Another alternative is to replace the phase shifters (and all the required complementary components such as power combiners/splitters, control lines) with switches [55, 56]. Using switching networks could reduce the power consumption and complexity at the expense of lesser spectral-efficiency. One perspective is to combine switches and

phase shifters to obtain an advantageous trade-off between them [57].

### **Lens Array Architecture**

All the above mentioned architectures consider one-dimensional (1D) or two-dimensional (2D) planar antenna arrays. An attractive emerging approach is to combine *lens antenna arrays* with switching networks [58, 59]. A lens array is an electromagnetic lens with feed antennas located on the focal surface of the lens, which allows to concentrate the signal arriving from different directions on different antennas as depicted in figure 1.2(c). Hence, the spatial model of the channel can be seen as a beamspace model. Furthermore, the beamspace of mmWave channels is sparse since the scattering is not rich and the power is propagated over a small number of paths [51, 6]. Due to the sparsity of the mmWave channel, a reduced-size switching network is used to select the dominant beams in the beamspace, which greatly reduces the number of RF chains [58, 59]. The authors in [59] had shown that the number of required switches (or RF chains) to achieve near-optimal capacity in lens array systems depends on the number of signal beams (and not on the number of antennas on the lens), and they proposed a spatial multiplexing scheme for mmWave communications, namely the path-division multiplexing.

### **Few-Bit ADCs Architecture**

Reducing the power consumption can be done either by reducing the number of RF chains (as proposed in the above presented architectures) and/or by reducing the energy consumed per RF chain. The latest is the key motivation behind proposing to replace the high-resolution ADCs with few-bit (e.g., 1 to 4 bit) ADCs, since high-frequency high-resolution ADCs are well known to consume a lot of power [9, 60, 61]. The mmWave system with few-bit ADCs is shown in figure 1.2(d). Using few-bit ADCs could even open the door to the feasibility of fully-digital mmWave systems [9]. However, the high non-linearity errors of quantization and the wide bands of mmWave channels pose a lot of challenges to the design of signal processing solutions for mmWave communications despite some recent research works [62, 63].

## Conclusion

In this subsection, we have presented the different MIMO architectures for mmWave communications, and the differences between them. In this Ph.D. thesis, we have developed our work in chapters 2 and 3 based on the hybrid architecture.

### 1.3.2 Spatial MmWave MIMO Channel Modeling

MmWave channel models are classified into two categories [6], physical models and analytical models. The physical models are based on the electromagnetic characteristics of the signal propagation between the transmit and receive antenna arrays. They can efficiently reflect the measured parameters and they are popular for MIMO channels, hence they are a good choice for mmWave MIMO channels. On the other hand, the analytical models are based on the mathematical analysis of the channel, and they are convenient for algorithm development and system analysis. The physical channel models are divided into two categories. Deterministic models, which characterize the real effects of the environment on the system, but need high computational complexity, and stochastic channel models, which require low computational complexity, hence they are the popular choice for mmWave system design and simulation. Thus the considered channel model for this thesis is the Saleh-Valenzuela stochastic channel model.

Since the number of scatters is limited [51, 6], most research works had adopted the geometric channel model to describe mmWave channels [4, 53, 54]. Let us consider again the system presented in figure 1.1. In the geometric channel model, the  $N_{\text{MS}} \times N_{\text{BS}}$  complex matrix  $\mathbf{H}_{\text{DL}}$  of the narrowband downlink (DL) channel is expressed as,

$$\mathbf{H}_{\text{DL}} = \sqrt{\frac{N_{\text{BS}}N_{\text{MS}}}{L\varrho_{\text{DL}}}} \sum_{l=1}^L \alpha_{l,\text{DL}} \mathbf{a}_{\text{MS}}(\theta_{l,\text{MS}}, \phi_{l,\text{MS}}) \mathbf{a}_{\text{BS}}^*(\theta_{l,\text{BS}}, \phi_{l,\text{BS}}), \quad (1.2)$$

$$\mathbf{H}_{\text{DL}} = \mathbf{A}_{\text{MS}} \mathbf{H}_{\alpha} \mathbf{A}_{\text{BS}}^*, \quad (1.3)$$

where  $\varrho_{\text{DL}}$  is the DL path-loss,  $\alpha_{l,\text{DL}}$  is the DL complex gain of path  $l$ .  $\mathbf{A}_{\text{BS}} \in \mathbb{C}^{N_{\text{BS}} \times L}$  and  $\mathbf{A}_{\text{MS}} \in \mathbb{C}^{N_{\text{MS}} \times L}$  are, respectively, the aggregation of the  $L$  steering vectors  $\mathbf{a}_{\text{BS}}(\theta_{l,\text{BS}}, \phi_{l,\text{BS}})$  and  $\mathbf{a}_{\text{MS}}(\theta_{l,\text{MS}}, \phi_{l,\text{MS}})$  for  $l = 1, 2, \dots, L$ , and

$$\mathbf{H}_\alpha = \sqrt{\frac{N_{\text{BS}}N_{\text{MS}}}{L\alpha_\theta}} \text{diag}(\alpha_{1,\text{DL}}, \alpha_{2,\text{DL}}, \dots, \alpha_{L,\text{DL}}).$$

The channel is FS when the system is wideband, hence equation (1.2) must be rewritten to represent the  $D$ -delay DL channel model. The  $d$ -th delay tap is given by [64],

$$\mathbf{H}_{\text{DL},d} = \sqrt{\frac{N_{\text{BS}}N_{\text{MS}}}{L\varrho_{\text{DL}}}} \sum_{l=1}^L \alpha_{l,\text{DL}} p_{\text{ps}}(dT_s - \tau_l) \mathbf{a}_{\text{MS}}(\theta_{l,\text{MS}}, \phi_{l,\text{MS}}) \mathbf{a}_{\text{BS}}^*(\theta_{l,\text{BS}}, \phi_{l,\text{BS}}), \quad (1.4)$$

where  $p_{\text{ps}}(\cdot)$  is the combination of pulse shaping filter and other filters,  $T_s, \tau_l$  are the sampling period and the delay. For OFDM modulation, the MIMO channel frequency response matrix at each subcarrier  $k$  follows the expression [64],

$$\mathbf{H}_{\text{DL}}[k] = \sqrt{\frac{N_{\text{BS}}N_{\text{MS}}}{L\varrho_{\text{DL}}}} \sum_{l=1}^L \alpha_{l,\text{DL}} q_l[k] \mathbf{a}_{\text{MS}}(\theta_{l,\text{MS}}, \phi_{l,\text{MS}}) \mathbf{a}_{\text{BS}}^*(\theta_{l,\text{BS}}, \phi_{l,\text{BS}}), \quad (1.5)$$

where  $q_l[k]$  is given by,

$$q_l[k] = \sum_{d=1}^D p_{\text{ps}}(dT_s - \tau_l) e^{-\frac{2\pi jkd}{K}}, \quad (1.6)$$

and  $K$  is the number of subcarriers.

The response vectors for the uniform linear planar array (ULPA) is given as follows.

### ULPA Response Vector

A ULPA is a rectangular array that consists of  $N_h$  antennas in each row and  $N_v$  antennas in each column, in the horizontal and vertical directions, uniformly separated by a distance  $d_A$ . Typically,  $d_A = \lambda/2$  where  $\lambda$  is the signal wavelength. The total number of antennas within the array is  $N = N_h \times N_v$ , and each row or column is a uniform linear array (ULA) which is considered as a special case of ULPA. The response vector of an  $N$ -element ULA is given by,

$$\mathbf{a}_{\text{ULA}}(\theta) = \frac{1}{\sqrt{N}} \left[ \mathbf{1} \ e^{j2\pi \frac{d_A}{\lambda} \sin(\theta)} \ \dots \ e^{j(N-1)2\pi \frac{d_A}{\lambda} \sin(\theta)} \right]^T \quad (1.7)$$

The array response for the ULPA configuration is given by [65],

$$\mathbf{a}_{\text{ULPA}}(\theta, \phi) = \mathbf{a}_h(\theta) \otimes \mathbf{a}_v(\phi) \quad (1.8)$$

where  $\theta$  and  $\phi$  are, respectively, the azimuth and elevation angles, and  $\mathbf{a}_h$  and  $\mathbf{a}_v$  are the horizontal and vertical steering vectors which are derived from (1.7) with the corresponding angle and number of antennas, and  $\otimes$  is the Kronecker product.

Recently, 3D beamforming techniques for mmWave communications had been introduced [66, 67, 68]. However, few papers studied the estimation of the 3D mmWave channel [69, 70, 71]. On the other hand, most existing research works had considered only the 2D beamforming case, i.e. the elevation is neglected and only the horizontal scattering is taken into consideration. Under these assumptions, the ULPA response is rewritten as,

$$\mathbf{a}_{\text{ULPA}}(\theta) = \mathbf{a}_h(\theta) \otimes \mathbf{1}_{N_v} \tag{1.9}$$

where  $\mathbf{1}_{N_v}$  is an  $N_v \times 1$  unity vector.

### 1.3.3 MmWave MIMO System Model

Let us first consider a narrowband system model for a hybrid architecture. The downlink is described by the  $N_{\text{MS}} \times 1$  received signal vector at the MS, which is given by

$$\mathbf{r} = \mathbf{H}_{\text{DL}}\mathbf{F}\mathbf{s} + \mathbf{n}, \tag{1.10}$$

where  $\mathbf{H}_{\text{DL}}$  is the DL channel matrix as defined in equation (1.2),  $\mathbf{s}$  is the  $N_{\text{S}} \times 1$  normalized transmitted symbols vector with  $E[\mathbf{s}\mathbf{s}^H] = (P_{\text{BS}}/N_{\text{S}})\mathbf{I}_{N_{\text{S}}}$ , and  $P_{\text{BS}}$  is the average transmission power of the BS.  $\mathbf{F} = \mathbf{F}_{\text{RF}}\mathbf{F}_{\text{BB}}$  is the  $N_{\text{BS}} \times N_{\text{S}}$  precoding matrix of the BS which combines the baseband precoder  $\mathbf{F}_{\text{BB}} \in \mathbb{C}^{N_{\text{RF}} \times N_{\text{S}}}$  and the RF precoder  $\mathbf{F}_{\text{RF}} \in \mathbb{C}^{N_{\text{BS}} \times N_{\text{RF}}}$ . Finally, the vector  $\mathbf{n}$  of size  $N_{\text{MS}} \times 1$  is the additive white Gaussian noise (AWGN). The received vector  $\mathbf{r}$  is processed at the MS such as,

$$\mathbf{y} = \mathbf{W}^*\mathbf{H}_{\text{DL}}\mathbf{F}\mathbf{s} + \mathbf{W}^*\mathbf{n}, \tag{1.11}$$

where  $\mathbf{W} = \mathbf{W}_{\text{RF}}\mathbf{W}_{\text{BB}}$  is the  $N_{\text{MS}} \times N_{\text{S}}$  combiner matrix of the MS which is assumed to consecutively apply the RF combiner  $\mathbf{W}_{\text{RF}} \in \mathbb{C}^{N_{\text{MS}} \times N_{\text{RF}}}$  and the baseband combiner  $\mathbf{W}_{\text{BB}} \in \mathbb{C}^{N_{\text{RF}} \times N_{\text{S}}}$ . It is worth noting that the constant modulus constraint must be applied to the RF precoder and

to the RF combiner when analog shifters are used, that is all the entries of the matrix must have the same magnitude.

The same logic can be employed for the uplink (UL) by replacing  $\mathbf{H}_{\text{DL}}$  by the UL channel matrix  $\mathbf{H}_{\text{UL}}$  and by reversing the combiners and precoders roles. Under the widely-adopted assumption of *channel reciprocity* [72], the UL channel is a Hermitian transposition of the DL channel  $\mathbf{H}_{\text{UL}} = \mathbf{H}_{\text{DL}}^*$ , and one between them must be estimated to have channel state information (CSI) [73]. In practice, it is not obvious how to guarantee the channel reciprocity in mmWave communications, even for time-division duplexing (TDD) systems (where the same carrier frequency is used for both DL and UL), due to different issues, for instance the synchronization and calibration errors of RF chains [73]. However, it should be pointed out that the number of paths and the angle-of-arrivals (AoAs), angle-of-departures (AoDs) for each path are strongly correlated for both DL and UL channels even for frequency-division duplexing (FDD) communication systems where separated DL and UL frequencies are employed. This property is called the *path reciprocity* [74].

Assuming the path reciprocity, the  $N_{\text{BS}} \times N_{\text{MS}}$  complex matrix  $\mathbf{H}_{\text{UL}}$  of the UL channel is given by,

$$\mathbf{H}_{\text{UL}} = \sqrt{\frac{N_{\text{BS}}N_{\text{MS}}}{L\varrho_{\text{UL}}}} \sum_{l=1}^L \alpha_{l,\text{UL}} \mathbf{a}_{\text{MS}}(\theta_{l,\text{MS}}, \phi_{l,\text{MS}}) \mathbf{a}_{\text{BS}}^*(\theta_{l,\text{BS}}, \phi_{l,\text{BS}}), \quad (1.12)$$

where  $\alpha_{l,\text{UL}}$  is the complex gain of the  $l^{\text{th}}$  path in the UL channel, and is in general different from  $\alpha_{l,\text{DL}}$  as introduced in Equation (1.2).  $\varrho_{\text{UL}}$  is the UL path-loss

For wideband systems, equation (1.11) is reformulated to express the received signal at each subcarrier  $k$ . It is rewritten as

$$\mathbf{y}[k] = \mathbf{W}^*[k]\mathbf{H}_{\text{DL}}[k]\mathbf{F}[k]\mathbf{s}[k] + \mathbf{W}^*[k]\mathbf{n}[k], \quad (1.13)$$

where  $\mathbf{H}_{\text{DL}}[k]$  is given by (1.5).

In section 1.5, we explain why compressive sensing techniques are good candidates to estimate the sparse mmWave channels.

## 1.4 Multi-Carrier Modulation Techniques

In the previous sections, we explored the different mmWave enabling technologies. On the other hand, the MCM techniques are regarded crucial for ensuring optimum exploitation of limited time and frequency resources. In this section, we look at the MCM in depth, as well as some of the MCM techniques that have been used in this work.

### 1.4.1 Multi-Carrier Modulation History and Motivations

The MCM approach was first developed in the late 1950s [75]. The concept was to split data into many bit streams and modulate each stream with a distinct subcarrier. Different steep bandpass filters completely separate these subcarriers. The so-called frequency division multiplexing (FDM) technology was born as a result of this. A US patent [76] from 1970 offered a high data rate FDM variant with closely spaced subcarriers and overlapped spectrum. Despite the fact that OFDM waveforms provided for complete SE while dealing with FS challenges, single carrier technologies dominated early communication systems. MCM in general, and OFDM in particular, have generated significant attention only with the full digitization of the deployed IFFT/FFT modem [77, 78].

The OFDM technology was developed to combat single carrier techniques' vulnerability to FS channels [79]. This is owing to the fact that in single carrier techniques, the symbol length must be as short as feasible in order to convey high data rates in a given bandwidth. In FS channel settings, however, the symbol duration is substantially shorter than the channel coherence time, resulting in severe inter-symbol interference (ISI). This necessitates the use of non-linear complex receivers. OFDM was a crucial solution for achieving the desired high data rate for a FS channel while keeping the RX simple. This is accomplished by breaking the allocated bandwidth into a number of sub-channels (subcarriers) with narrow bandwidth for each one. As a result, the FS channel becomes roughly flat per each sub-channel.

A cyclic-prefix (CP) addition was added to OFDM to prevent ISI, resulting in the CP-OFDM waveform. CP- OFDM has seen widespread acceptance in a variety of wireless and wireline stan-

dards, including VDSL, IEEE 802.11a/g, IEEE 802.16, 4G, and, more recently, 5G. CP-OFDM, on the other hand, has two major flaws. Due to its rectangular pulse structure, it has poor spectral confinement. Second, the duplicated CP component degrades SE directly. As a result, the urgent necessity for a novel MCM approach has lately surfaced [80]. Many MCM strategies have been presented while presenting various tradeoffs, which has resulted in an intriguing quantity of studies [81, 81, 82, 83]. Various methods have been used to make minor changes to the (CP)-OFDM.

Another viewpoint utilized the filtering view point to better reduce out-of-band (OOB) emission. Subband and subcarrier based filtering methods are two types of filtering techniques used in MCM. Subband filtering divides the system bandwidth into many subbands, with each subband performing a standard OFDM operation. As a result, different settings may be used in different subbands to meet the needs of different applications. Different subband-based filtering MCM approaches, such as the universal filtered multicarrier (UFMC) [84] and the filtered OFDM (F-OFDM), have been suggested in the literature [85].

Filter-bank multicarrier (FBMC) waveforms, on the other hand, take the extreme situation of filtering each subcarrier separately. This yields the best frequency localisation, but at the expense of other features [83]. For example, FBMC systems based on quadrature amplitude modulation (QAM) forfeit SE while FBMC systems based on offset-QAM (OQAM) suffer from a new built-in interference. Several works [86, 83] have been undertaken in the literature to compare various aspects of different MCM approaches. Waveforms based on the FBMC have been shown to have the best spectral confinement, making them ideal for efficient spectrum reuse and asynchronous communications.

## 1.4.2 Multi-Carrier Modulation Principles

In MCM schemes, the messages to be sent are first mapped into a 2-dimensional space, such as a frequency-time (FT) space. They are then converted into signal space using the basis function  $\chi[k, n]\{m\}$  of the  $k$ th subcarrier and the  $n$ th time symbol defined as:

$$\chi[k, n]\{m\} = p\{m - nT\}e^{j2\pi km/K}e^{j\psi[k, n]}, \quad (1.14)$$

where  $p\{m\}$  is the impulse response of the prototype filter of the system, and it is different for each MCM technique, and  $m$  denotes the sampling index.  $T = \frac{1}{F}$  is the symbol duration while  $F$  is the subcarrier spacing. The phase factor  $\psi[k, n]$  is different for each MCM technique.

The TX and RX prototype filters' overall goal will be to better combine the transmitted symbol's dispersed energy in the FT grid. As a result, the combined impacts of the analysis and synthesis filters might be used to determine the performance of an MCM approach.

### Balian Low Theorem

According to the Balian low theorem (BLT) [83], three main characteristics are used to determine the overall performance of an MCM system:

1. Orthogonality: The basis functions are said to be orthogonal if they satisfy the following orthogonality condition

$$\sum_{m=-\infty}^{+\infty} \chi[k, n]\{m\}\chi^*[\bar{k}, \bar{n}]\{m\} = \delta_{k, \bar{k}}\delta_{n, \bar{n}}, \quad (1.15)$$

where  $\delta_{l_1, l_2}$  is the Kronecker delta with  $\delta_{l_1, l_2} = 1$  if  $l_1 = l_2$  and zero otherwise. While orthogonality demands that the TX and RX utilize the same prototype filters, bi-orthogonality is more flexible and allows for the use of alternative prototype filters.

2. Time frequency localization (TFL): A pulse shape's time and frequency localization ( $\sigma_t$  and  $\sigma_f$ ) define the time and frequency variance of its energy, respectively. This can be expressed in the FT continuous domain as follows:

$$\sigma_t = \sqrt{\int_{-\infty}^{+\infty} (t - \bar{t})|p(t)|^2 dt} \quad (1.16)$$

$$\sigma_f = \sqrt{\int_{-\infty}^{+\infty} (f - \bar{f})|P(f)|^2 df} \quad (1.17)$$

where  $P(f)$  is the Fourier transformation of  $p(t)$ , and  $\bar{t}$  and  $\bar{f}$  are the mean time and mean frequency of the pulse  $p(t)$ , respectively. The MCM system is referred to as having TFL localized filters if  $\sigma_t\sigma_f < \infty$ ; otherwise, they are non-localized.

3. Symbol density: The SE of an MCM technique is expressed by its symbol density. In other words, how effective the MCM technique is at utilizing the given time and frequency resources. The MCM technique is designed to achieve maximum SE by setting  $F = 1/T$ , which corresponds to a symbol density of  $TF = 1$ .

The BLT states that no MCM approach can attain all these three features at the same time. Depending on the required characteristics, trade-offs must be made.

### 1.4.3 Multi-Carrier Modulation Techniques for MmWave Systems

Different waveforms have been proposed based on the BLT. The two MCM techniques that have been used in this work, are presented in this subsection. First we present the well-known OFDM waveform, afterwards, we present the subcarrier filtering-based waveform which is known as FBMC-OQAM.

#### OFDM

For analysis and synthesis filtering, the OFDM waveform uses a rectangular pulse shape

$$p_{tx}(t) = p_{rx}(t) = \begin{cases} \frac{1}{T_0}, & -\frac{T_0}{2} \leq t \leq \frac{T_0}{2} \\ 0, & \text{otherwise} \end{cases}$$

where  $p_{tx}(t), p_{rx}(t)$  are the TX and RX pulse shaping filters respectively.

The OFDM waveform can preserve two key advantages by using these pulse forms with a symbol duration of  $T = T_0$  and subcarrier spacing of  $F = 1/T_0$ . First, being the complex orthogonality condition. The full symbol density ( $TF = 1$ ) is the second. However, the receiver's complex orthogonality is conditioned by the channel's frequency selectivity. In other words, the channel within each subcarrier must be flat, with the channel maximum delay spread ( $\tau_{\max}$ ) being significantly lower than the symbol duration  $\tau_{\max} \ll T$ ). This isn't always the case, though. An enhanced variant of the OFDM waveform, known as CP-OFDM, is utilized to manage this.

In CP-OFDM each OFDM symbol's last  $T_{CP}$  part is copied and attached to the beginning of the same symbol, where  $T_{CP}$  denotes the duration of the cyclic prefix. We ensure that the FS

induced ISI will reside in the  $T_{CP}$  section exclusively by creating the CP  $T_{CP} > \tau_{\max}$ . Before the demodulation procedure, the redundant and ISI-polluted CP is removed at the RX. As a result, it ensures the complex orthogonality criterion once more.

The main advantage of the CP-OFDM waveform is the simplicity with which its modem (IFFT/FFT) is implemented. Furthermore, because to the CP-OFDM complex orthogonality criterion, basic one-tap equalizers function effectively. CP-OFDM, on the other hand, suffers from a loss in SE due to the use of the CP, where  $TF = 1 + T_{CP}/T_0$ . Furthermore, the CP-rectangular OFDM's pulse form translates to poor frequency localisation, i.e.,  $\sigma_f = \infty$  with strong OOB emission.

## FBMC

FBMC waveforms have the best spectrum confinement characteristics since each subcarrier is filtered separately. There are two types of FBMC waveforms: QAM based FBMC (FBMC-QAM) and Offset QAM (OQAM) based FBMC (FBMC-OQAM).

## FBMC-QAM

The prototype filter  $p(t)$  in FBMC-QAM is designed to achieve the TFL property and the complex orthogonality condition at the expense of a significant decrease in symbol density. The time and frequency separation between FBMC-QAM symbols is depicted in Fig. 1.3. This mapping results in a symbol density of  $TF = 2$  where the loss is due to the large frequency spacing  $F = 2/T_0$ . PHYDYAS, Hermite, and the root raised cosine prototype filters are among the TFL prototype filters utilized for FBMC-QAM waveform [83]. We illustrate the PHYDYAS prototype filter which has been used in this work, for the other prototype filters please refer to [83]. The PHYDYAS prototype filter is described as follows:

$$p(t) = \begin{cases} \frac{1+2\sum_{i=1}^{O-1} a_i \cos(\frac{2\pi t}{OT_0})}{O\sqrt{T_0}}, & -\frac{OT_0}{2} \leq t \leq \frac{OT_0}{2} \\ 0, & \text{otherwise} \end{cases}$$

PHYDYAS coefficients  $a_i$  depend on the overlapping factor  $O$ .

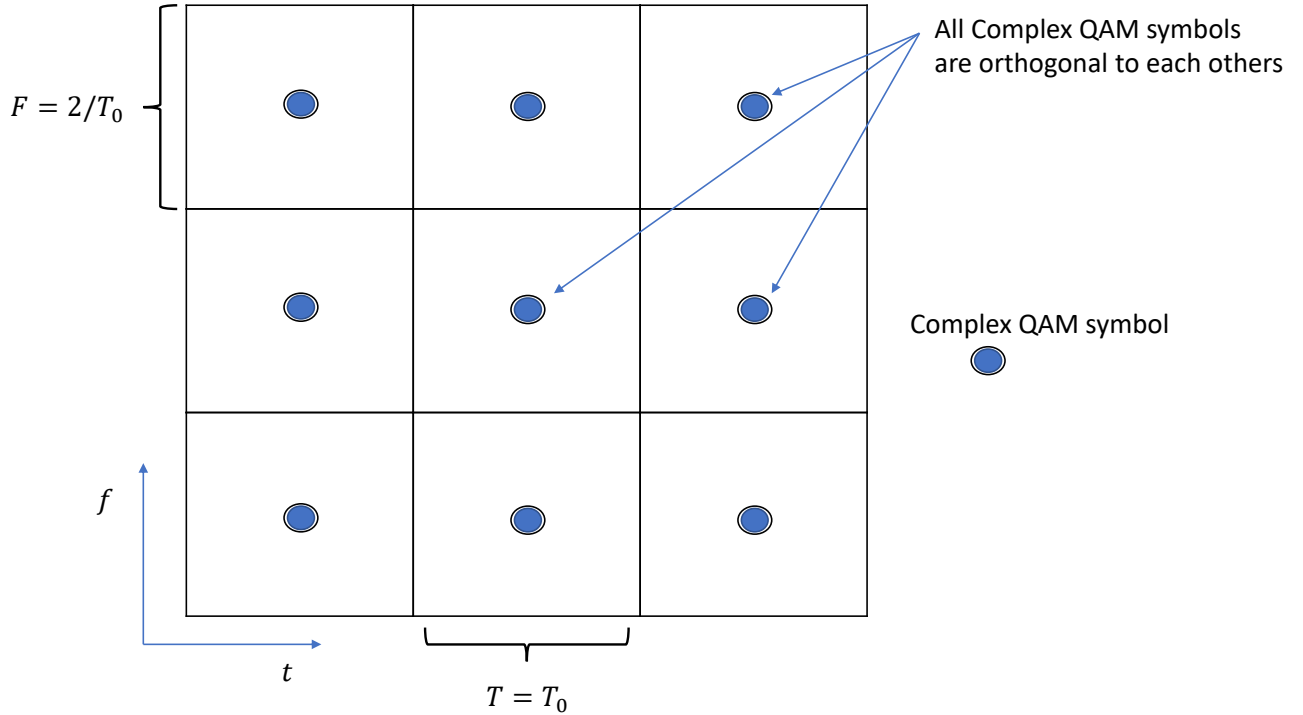


Figure 1.3: FBMC-QAM resource grid structure

### FBMC-OQAM

The goal of FBMC-OQAM is to keep the entire symbol density ( $TF = 1$ ) as well as the TFL property ( $\sigma_t \sigma_f < \infty$ ). This is accomplished by substituting the complex orthogonality criteria with a real-domain-only orthogonality. To do so, FBMC-OQAM is constructed from the FBMC-QAM waveform as follows:

1. The prototype filter is developed in the same way as the FBMC-QAM filter, which guarantees complex orthogonality for  $T = T_0$  and  $F = 2/T_0$ .
2. The time and frequency spacings are reduced to obtain the desired symbol density  $TF = 1$ , where  $F_{\text{FBMC-OQAM}} = \frac{F_{\text{FBMC-QAM}}}{2} = 1/T_0$ , and  $T_{\text{FBMC-OQAM}} = \frac{T_{\text{FBMC-QAM}}}{2} = T_0/2$ . As a result,  $TF = 1/2$  is obtained, as well as a new built-in interference.
3. Two procedures are taken to eliminate the new built-in interference component:

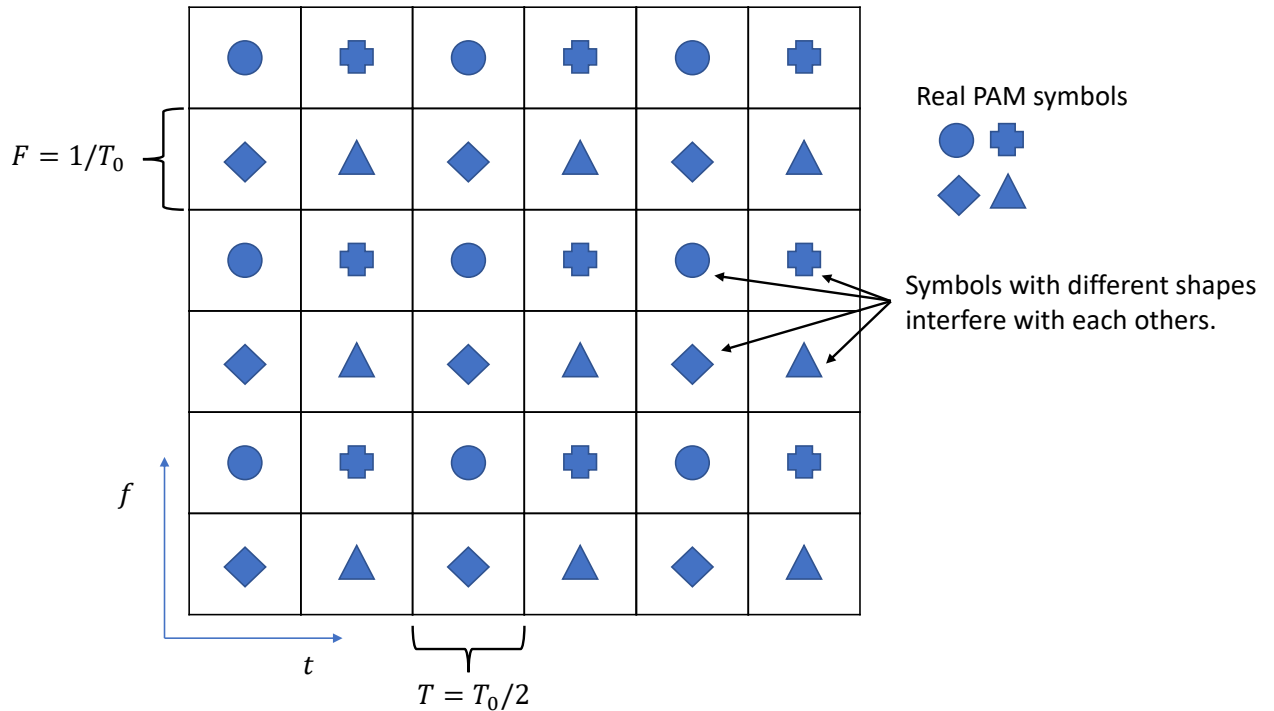


Figure 1.4: FBMC-OQAM resource grid structure

- (a) Real PAM symbols are used instead of complex QAM symbols.
- (b) The interference caused by the Step 2's new time and frequency spacings is shifted to the imaginary part. This is done by defining the phase factor  $\psi[k, n]$  as  $\frac{\pi}{2}(k+n) - \pi kn$  in (1.14).

The structure of the FBMC-OQAM resource grid is depicted in Fig. 1.4. By comparing Fig. 1.4 and Fig. 1.3, we can see that the time and frequency spacing in FBMC-OQAM is half that of FBMC-QAM. As a result, the spectral density of FBMC-OQAM is equal to  $TF = 1/2$ . However, because FBMC-OQAM sends real symbols, the equivalent complex symbol density is equal to 1, as in the case of OFDM.

## 1.5 Compressive Sensing : Mathematical Tool for Channel Estimation

In this section, we present the compressive sensing tool which is crucial for hybrid precoding and channel estimation techniques that have been used in this Ph.D. thesis.

The multi-path signal components of mmWave systems tend to be distributed into few clusters such as mmWave channels look sparse [65, 87]. This sparsity characteristic is also verified by measurements, for instance, [88, 21, 19, 89] showed that mmWave channels typically exhibit only 3-4 scattering clusters in dense-urban non-line-of-sight (NLOS) environments. Thus a convenient representation of such channels needs a comprehensive study of sparsity. The traditional training-based channel estimation methods seem to be not optimal under these sparse conditions due to the huge channel size (big number of antennas at the TX and RX) and the fact that most of what we get will be thrown away. Hence, the aim is to estimate the non-zero elements of the channel and one approach to solve this type of problems is to use CS techniques [90, 91, 92]. CS is widely employed in wireless communication applications like channel estimation, spectrum sensing for cognitive radio, and localization among others [93]. CS tools handle the problem of estimating any sparse signal by directly acquiring a compressive signal representation with a lot fewer number of samples than that required by the Shannon-Nyquist theorem, and from which the sparse signal can be recovered through an optimization process [94, 91].

A signal represented by an  $N_n \times 1$  vector  $\mathbf{s} \in \mathbb{C}^{N_n}$  is said to be exactly  $N_k$ -sparse signal if all but just  $N_k \ll N_n$  values in the vector are zeros, in other words, there is a very small number of non-zero values in the vector and the rest are zero value elements. Mathematically, we can represent it as  $\|\mathbf{s}\|_0 \leq N_k$ . The same idea can be generalized to 2D and 3D signals. Consider a discrete-time signal  $\mathbf{x}$ , which can be represented by an  $N_n \times 1$  vector in  $\mathbb{C}^{N_n}$ . If  $\mathbf{x}$  is not sparse, it can be transformed into another domain via a transformation matrix  $\Psi \in \mathbb{C}^{N_n \times N_n}$  as follows

$$\mathbf{x} = \Psi \mathbf{s} \tag{1.18}$$

such as  $\mathbf{s}$  represents an exactly  $N_k$ -sparse signal. It is very essential to employ a careful transfor-

mation matrix which can further expose the sparse nature of the original signal.

The objective of CS tools is to compress the dimension of measurements by projecting the high-dimensional sparse signals of dimension  $N_n$  into a reduced-dimension spaces of dimension  $N_m \ll N_n$  via a measurement or sensing matrix  $\Phi$  such as

$$\mathbf{y} = \Phi \mathbf{x} = \Phi \Psi \mathbf{s} = \Theta \mathbf{s} \quad (1.19)$$

where  $\Theta = \Phi \Psi$  is an  $N_m \times N_n$  matrix. This requires first to design a stable sensing (measurement) matrix  $\Phi$ , and consequently a matrix  $\Theta$ , before proposing a reconstruction algorithm to recover the signal  $\mathbf{x}$  from only  $N_m \approx N_k$  measurement vector  $\mathbf{y}$  with the best reconstruction reliability and hence the minimum information loss. This problem is ill-posed in general, but can be resolved for the class of signals that have a sparse expansion. This requires that the design of the compression matrix  $\Theta$  respects some properties such as *the restricted isometry property* and *the small coherence* one [95, 96, 97]. The first represents a necessary and sufficient condition for the CS problem to be well conditioned, while the later makes the CS technique more effective.

Many algorithms have been proposed to recover  $N_k$ -sparse signals with high probability [98], where some of them used tractable mixed-norm optimization methods [99, 100, 101], efficient greedy algorithms [102, 97, 103, 104], fast iterative thresholding methods [105], statistical sparse recovery [106], and many more [94, 97, 107, 93]. We give a glance and point out some of these algorithms. The non-convex  $\ell_0$ -norm problem is transformed into a convex  $\ell_1$ -norm one, and basis pursuit (BP) solutions [99], such as least absolute shrinkage and selection operator (LASSO) [101], are used. However, the BP approach is rarely implemented in real-time wireless applications because of its high computational cost. OMP is a greedy algorithm [97] which was proposed as an effective alternative to the BP ones [99]. In [104], compressive sampling matching pursuit (CoSaMP), which is a parallel greedy algorithm, was introduced. Moreover, the authors in [103] proposed a modified version of the OMP, called multi-grid OMP (MG-OMP), in order to reduce the complexity, and to make the reconstruction more adaptive. Another low-complexity approach, which tries to solve the problem by iteratively refining the sparse estimate, is a thresholding approach illustrated in [105]. Three algorithms were proposed in [108, 109, 110] that select more than one candidate per

iteration to decrease the running time, while for OMP one candidate is selected per each iteration. An algorithm termed as multipath matching pursuit (MMP) was proposed in [108], where it performs the tree search, in which all combinations of  $k$ -sparse indices are the candidates in the tree, and the algorithm tries to find the best candidate from this tree that minimizes the residual. The aforementioned algorithm imposes reasonable computational overhead while achieving better performance over existing greedy algorithms. A generalization algorithm of the OMP was proposed in [109] termed as generalized OMP (GOMP) that selects more than one index per iteration corresponding to largest correlation in magnitude with the residual. Similar to the MMP and GOMP, a stage-determined matching pursuit (SdMP) was proposed in [110] that aims at selecting more than one index per iteration that surpass a carefully designed threshold. A small difference compared to MMP and GOMP is that the StMP adds a pruning step after the end of some latter iterations (after satisfying a certain sparsity level condition) in order to refine the selection. Finally, approximate message passing (AMP) algorithm, which combines the thresholding methods with the message passing ones, performs well for highly structured measurement matrices [92].

**A Sparse Formulation of the MmWave Channel Estimation Problem** The mmWave system model is described in equation (1.11). In what follows, some indices will be omitted for simplicity. Let us consider the received signal at  $Q$  successive instants when the same precoder,  $\mathbf{F}$ , and the same combiner,  $\mathbf{W}$ , are employed. To exploit the sparse nature of the channel, the concatenated  $Q \times N_S$  matrix is vectorized, the resultant vectorized vector,  $\mathbf{y}_v$ , can then be written as [111, 89],

$$\mathbf{y}_v = \sqrt{P}\mathbf{F}^T \mathbf{A}_{\text{BS,D}}^* \mathbf{z}_{\text{BS}} \otimes \mathbf{W}^* \mathbf{A}_{\text{MS,D}}^* \mathbf{z}_{\text{MS}} + \mathbf{n}_v, \tag{1.20}$$

where the  $N \times 1$  sparse vectors,  $\mathbf{z}_{\text{BS}}$  and  $\mathbf{z}_{\text{MS}}$ , have non-zero elements that correspond to the actual AoDs and AoAs.  $\mathbf{A}_{\text{BS,D}}$  and  $\mathbf{A}_{\text{MS,D}}$  are, respectively, the  $N_{\text{BS}} \times N$  and  $N_{\text{MS}} \times N$  beamforming dictionary matrices at the BS and MS. Each dictionary consists of column vectors which represent the complex antenna steering vectors corresponding to the  $N$  spatially quantized directions, i.e. it is assumed that each direction is defined by an angle which is taken from  $\{0, \frac{2\pi}{N}, \dots, \frac{2\pi(N-1)}{N}\}$ . Equation (1.20) introduces a sparse formulation of this problem by employing a compression matrix which can be expressed as a function of beamforming dictionaries, precoder and combiner matrices

[111, 89], this formulation will be reused in chapter 3 when it comes to propose a new method to estimate the mmWave channel. This allows to estimate the channel by detecting and estimating the non-zero elements of  $\mathbf{z}_{\text{BS}}$  and  $\mathbf{z}_{\text{MS}}$  with a small number of measurements. The CS tools will be able to guarantee that if only the compression matrix is well-designed which in turn requires an efficient design of the precoder and the combiner.

Hence, the estimation of mmWave channels is enabled by reformulating the matrix system model into a sparse problem, before compressing the sparse matrices into reduced-size ones, and finally employing the appropriate CS reconstruction method. Basically, CS-based methods have a significant improvement over most traditional ones, a conclusion made in almost all recent studies on mmWave channel estimation [9]. Such conclusion motivated the practical usage of CS solutions for estimating mmWave channels as will be shown in the upcoming sections [111, 103, 87, 112, 113, 114, 115, 116, 117, 118, 119, 120, 121, 122, 123, 64, 124, 125, 62, 126].

## 1.6 Conclusions

This chapter provided an overview of mmWave communications and the technologies that enable it. The features of mmWave channels, such as the variations between propagation behavior in mmWave bands and sub-6 GHz bands, are first illustrated in section 1.2. This will aid in comprehending the technical promise of mmWave communications, the problems that must be overcome in order to realize their potential, and the enabler technologies that will address these challenges. Then, in section 1.3, we went over the various existing system architectures for massive MIMO mmWave systems. Before presenting the huge MIMO system model, the spatial MIMO channel models have been presented, which demonstrate the unique character of highly-directive mmWave communications. In section 1.4, we have described MCM techniques and presented the modulation waveforms utilized in this Ph.D. thesis, such as the FBMC-OQAM waveform in chapter 2 and the OFDM waveform in chapter 3. Finally, section 1.5 introduced compressive sensing as a mathematical method for channel estimation. This will pave the way for the proposed channel estimation algorithm in chapter 3, on which such an algorithm is based.



# Chapter 2

## Hybrid Precoding For Frequency- Selective MmWave MIMO FBMC- OQAM Systems

### 2.1 Introduction

The hardware complexity of implementing the conventional fully-digital architecture for mmWave MIMO systems is too expensive. An eminently compromised solution is to use the hybrid MIMO architecture [127], where precoding and combining are performed in both the analog and digital domains as to decrease the number of the costly RF chains in the system. Despite the reduced number of RF chains, the performance of this architecture has been shown to be not far from the fully-digital ones [128]. Moreover, it supports easily several users/data streams.

For simplicity, the initial works on mmWave systems have adopted frequency-flat (FF) mmWave channels [127, 129], which turned out to be not realistic. In fact, mmWave channels are wideband channels, having a sparse behavior with few available paths that can be used to send data [25]. To cope with this behavior and to combat multipath fading, OFDM waveform has been commonly used for such mmWave systems [130, 25]. Nevertheless, OFDM has its drawbacks: The utilization of OFDM leads to significant OOB radiation owing to the rectangular time-domain window pulse. In addition, the limited frequency localization characteristic of such pulse makes it vulnerable to synchronization errors, and turns out to be undesirable for high-velocity mobile scenarios, where

Table 2.1: Summary of existing works on mmWave hybrid OFDM and MIMO-FBMC-OQAM systems.

References	[127, 132]	[130]	[133]	[134]	[86, 135, 136, 137, 138]	[139, 140, 141, 142, 143]	[144]	[145]	<b>Proposed</b>
FBMC	<b>X</b>	<b>X</b>	✓	✓	✓	✓	✓	✓	✓
OFDM	<b>X</b>	✓	✓	<b>X</b>	✓	<b>X</b>	<b>X</b>	✓	✓
MmWave	✓	✓	<b>X</b>	<b>X</b>	<b>X</b>	<b>X</b>	✓	✓	✓
Hybrid	✓	✓	<b>X</b>	<b>X</b>	<b>X</b>	<b>X</b>	✓	<b>X</b>	✓
MIMO	✓	✓	<b>X</b>	<b>X</b>	✓	✓	✓	✓	✓
Wideband	<b>X</b>	✓	✓	✓	✓	✓	✓	✓	✓
Narrowband	✓	<b>X</b>	<b>X</b>	<b>X</b>	<b>X</b>	<b>X</b>	<b>X</b>	<b>X</b>	<b>X</b>

Doppler shifts aren't easy to track [131]. Nonetheless, the main transmission technology considered in almost all mmWave hybrid MIMO studies so far is OFDM, please refer to Table-2.1. The reasons behind this popularity are the simplicity of implementing OFDM and the adequacy of such waveform to cope with multipath fading channels. These two reasons clarify why OFDM has been the favorite modulation choice for mmWave hybrid MIMO systems until now.

FBMC-OQAM is an alternative to OFDM waveform, which has some advantages due to the characteristics of its prototype filter [83]. The FBMC-OQAM prototype filter is localized in both time and frequency domains, which makes such filter immune to the OOB emission. In contrast to the OFDM filter, the FBMC-OQAM filter meets the desired synchronization requirements for systems with high mobility and Doppler shifts [131]. Therefore, FBMC-OQAM can be a feasible challenger of OFDM for future mmWave hybrid MIMO systems.

In this chapter, the viability of using the FBMC-OQAM signaling waveform for next-generation mmWave communications is studied. To incorporate FBMC-OQAM filter banks in mmWave hybrid MIMO systems, OMP-based hybrid precoding and combining techniques have been developed. According to simulation studies, the FBMC-OQAM waveform could be a good fit for future mmWave MIMO communication systems, especially when SE is a top priority. Before delving into the details of this work, we first brief the recent contributions in the regard of FBMC-OQAM for mmWave systems.

## 2.2 Review of Existing Works

In this paragraph, we focus our review on mmWave hybrid MIMO systems. There are a lot of works that have treated this topic in details. The authors in [127] proposed a novel hybrid precoding algorithm based on OMP compressive sensing technique to design the precoders' and combiners' matrices for narrowband mmWave MIMO systems. A minimum sum mean-square error (MSE) hybrid precoding algorithm to improve the bit error rate (BER) for narrowband mmWave MIMO systems was proposed in [132]. Novel codebook design and Gram Schmidt based hybrid precoding algorithms for FS mmWave MIMO systems have been proposed in [130]. Finally, the authors in [146] have theoretically revealed the optimality of FF precoding for FS mmWave MIMO systems. In fact, none of the works mentioned earlier has apoted FBMC-OQAM signaling.

In this paragraph we briefly illustrate some existing works on FBMC-OQAM systems. The performance of FBMC-OQAM with other OFDM's versions for high speed railway channels was evaluated in [133]. In addition, an efficient equalization technique using the Wiener filter for FBMC-OQAM system for very high-speed scenarios was proposed in [134]. In [86] a detailed signal processing study has been conducted for MIMO-FBMC-OQAM (MFO) systems. In [139, 140] Singh *et al.* studied the performance of a minimum mean-square error (MMSE) RX for MFO systems with perfect and imperfect channel state information, respectively. In [135] a study has been conducted on Alamouti's encoder and decoder for FBMC system in highly FS channels. In [141] Singh *et al.* proposed a two-step preamble-based approach to estimate the channel and carrier frequency offset for MFO systems. The same authors proposed also in [136] semiblind, training, and data-aided channel estimation schemes for MFO. A sparse channel estimation for MFO in smart city applications has been proposed in [142]. Some further studies have been conducted in [137, 143, 138] on the benefits of FBMC compared to OFDM waveform.

Few works have been proposed on MFO for mmWave systems as can be seen from Table-2.1. A very recent study on FBMC-OQAM for mmWave hybrid MIMO systems has been published by Srivastava *et al.* [144]. The authors proposed two novel channel estimation techniques, one is based on Bayesian learning, and the other is based on OMP. In [145] Nissel *et al.* tested FBMC-OQAM over real world 60 GHz  $2 \times 1$  multiple-input single-output mmWave channels. The authors showed

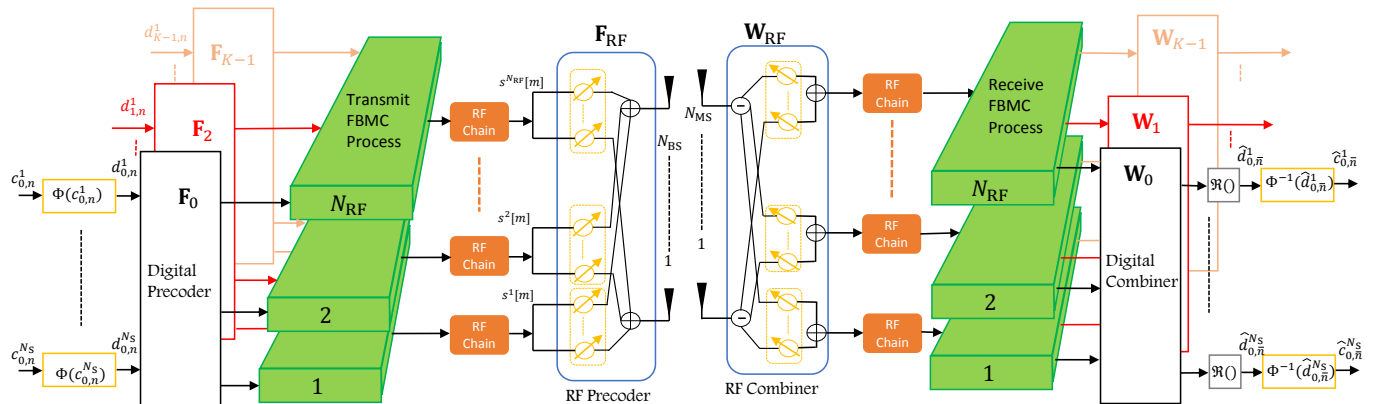


Figure 2.1: Architecture of mmWave hybrid MIMO FBMC BS and MS.

that FBMC-OQAM works fine for mmWave systems once they spread symbols in time. Clearly, a small spot of light was given to FBMC-OQAM signaling for mmWave MIMO systems, which supports our motivation to investigate in this regard.

## 2.3 FS MmWave Hybrid FBMC-OQAM MIMO System Model

Consider the FBMC system model given in Fig. 2.1 where we have a BS with  $N_{\text{BS}}$  antennas and  $N_{\text{RF}}$  RF chains is communicating with a MS with  $N_{\text{MS}}$  antennas and  $N_{\text{RF}}$  RF chains. We will examine the proposed algorithms for the DL system model. The same work, however, can be directly applied to the UL system. We assume that the BS is using  $N_S$  streams of data, where each stream is length- $K$  symbol block as seen in Fig. 2.1, such that  $N_S \leq N_{\text{RF}} \leq N_{\text{BS}}$  and  $N_S \leq N_{\text{RF}} \leq N_{\text{MS}}$ . Actually, the number of RF chains at the BS is usually greater than that of the MS's, but for simplicity we do not assume this fact.

Let  $c^i[k, n]$  denote the QAM symbol in the  $i$ th data stream, at subcarrier  $k$ , and time instant  $n$ . The function  $\Phi(c^i[k, n])$  separates from the complex QAM symbol  $c^i[k, n]$  the real and imaginary parts to extract real OQAM symbols  $d^i[k, 2n]$  and  $d^i[k, 2n + 1]$  [144]. If  $T_S$  is the QAM symbols' duration, then  $\frac{T_S}{2}$  is the OQAM symbols' duration. The real and imaginary parts of the QAM symbol are assumed to be spatially and temporally independent and identically distributed (i.i.d.)

with power  $\mathbb{E}[d^i[k, 2n](d^i[k, 2n])^*] = P$ . Let  $\mathbf{d}[k, n] \in \mathbb{C}^{N_S \times 1}$  be the symbol vector defined as

$$\mathbf{d}[k, n] = [d^1[k, n], d^2[k, n], \dots, d^{N_S}[k, n]]^T \quad (2.1)$$

After performing digital precoding on the vector  $\mathbf{d}[k, n]$ , we get the vector  $\tilde{\mathbf{d}}[k, n] = \mathbf{F}[k]\mathbf{d}[k, n]$ , where  $\mathbf{F}[k]$  is an  $N_{\text{RF}} \times N_S$  digital precoding matrix at subcarrier  $k$ . The baseband signal  $s^q\{m\}$  at the output of the  $q$ th transmit RF chain  $1 \leq q \leq N_{\text{RF}}$  can be expressed as

$$s^q\{m\} = \sum_{k=1}^K \sum_{n \in \mathbb{Z}} \tilde{d}^q[k, n] \chi[k, n]\{m\}, \quad (2.2)$$

where  $m$  denotes the sample index corresponding to the sampling interval  $\frac{T_S}{K}$ ,  $\tilde{d}^q[k, n]$  is  $q$ th element of  $\tilde{\mathbf{d}}[k, n]$ , and  $\chi[k, n]\{m\}$  is the basis function of the FBMC system and which is defined as

$$\chi[k, n]\{m\} = p\{m - nK/2\} e^{j2\pi km/K} e^{j\psi[k, n]}, \quad (2.3)$$

where  $p\{m\}$  is the impulse response of the prototype filter of the FBMC system. The phase factor  $\psi[k, n]$  is defined as  $\frac{\pi}{2}(k+n) - \pi kn$ , which will guarantee shifting the interference caused by the neighboring symbols to the imaginary part. The basis functions are required to satisfy the following real field orthogonality condition

$$\underbrace{\Re\left\{ \sum_{m=-\infty}^{+\infty} \chi[k, n]\{m\} \chi^*[\bar{k}, \bar{n}]\{m\} \right\}}_{\xi_{k,n}^{\bar{k}, \bar{n}}} = \delta_{k, \bar{k}} \delta_{n, \bar{n}}, \quad (2.4)$$

where  $\delta_{l_1, l_2}$  is the Kronecker delta with  $\delta_{l_1, l_2} = 1$  if  $l_1 = l_2$  and zero otherwise. Hence, we have  $\xi_{k,n}^{\bar{k}, \bar{n}} = 1$  if  $(k, n) = (\bar{k}, \bar{n})$ , and  $\xi_{k,n}^{\bar{k}, \bar{n}} = j \langle \xi \rangle_{k,n}^{\bar{k}, \bar{n}}$  if  $(k, n) \neq (\bar{k}, \bar{n})$ , where  $\langle \xi \rangle_{k,n}^{\bar{k}, \bar{n}}$  denotes the imaginary part of  $\xi_{k,n}^{\bar{k}, \bar{n}}$  [144], please refer to section 1.4.3 for more details. The discrete-time transmitted complex baseband signal can be written as

$$\tilde{\mathbf{s}}\{m\} = \mathbf{F}_{\text{RFS}}\{m\}, \quad (2.5)$$

where  $\mathbf{s}\{m\} = [s^1\{m\}, s^2\{m\}, \dots, s^{N_{\text{RF}}}\{m\}]^T$ . As can be seen that the baseband digital precoders

$\mathbf{F}[k]$  are FS matrices, thus can be different for each subcarrier, while the analog precoder  $\mathbf{F}_{\text{RF}}$  is an FF matrix. Indeed the analog precoder  $\mathbf{F}_{\text{RF}}$  is implemented using analog phase shifters, hence the entries of  $\mathbf{F}_{\text{RF}}$  should be of constant modulus. In the following, we take normalized values  $|[\mathbf{F}_{\text{RF}}]_{m,n}|^2 = 1$ . Furthermore, we impose a quantized set of angles for the phase shifters, by having  $[\mathbf{F}_{\text{RF}}]_{m,n} = e^{j\vartheta_{m,n}}$ , where  $\vartheta_{m,n}$  is a quantized angle, since in practice we only have quantized values. We consider in this paper a unitary power constraint, such that the hybrid precoders satisfy  $\mathbf{F}_{\text{RF}}\mathbf{F}[k] \in \mathcal{U}_{N_{\text{BS}} \times N_{\text{S}}}$ ,  $k = 1, \dots, K$ , with the set of semi-unitary matrices  $\mathcal{U}_{N_{\text{BS}} \times N_{\text{S}}} = \{\mathbf{U} \in \mathbb{C}^{N_{\text{BS}} \times N_{\text{S}}} | \mathbf{U}^* \mathbf{U} = \mathbf{I}\}$ . The unitary power constraint requires that the transmit power be distributed equally among the subcarriers and data streams on each subcarrier. Despite the fact that the unitary power constraint causes some performance loss when compared to the more relaxed total power constraint, the unitary power constraint usually results in more efficient codebooks and codeword selection algorithms for restricted feedback systems [130]. The total power constraint is a power constraint that enables the transmit power to be spread non-uniformly among the subcarriers and data streams on each subcarrier. At the MS, assuming perfect carrier and frequency offset synchronization, the received signal is combined using the analog and digital combiners  $\mathbf{W}_{\text{RF}} \in \mathbb{C}^{N_{\text{MS}} \times N_{\text{RF}}}$ ,  $\mathbf{W}[k] \in \mathbb{C}^{N_{\text{RF}} \times N_{\text{S}}}$ , respectively. The received signal after analog combining can be expressed as [144]

$$\tilde{\mathbf{f}}[\bar{k}, \bar{n}] = \mathbf{W}_{\text{RF}}^* \mathbf{H}[\bar{k}] \mathbf{F}_{\text{RF}} \tilde{\mathbf{b}}[\bar{k}, \bar{n}] + \tilde{\boldsymbol{\eta}}[\bar{k}, \bar{n}], \quad (2.6)$$

where  $\mathbf{H}_k$  denotes the  $N_{\text{MS}} \times N_{\text{BS}}$  mmWave MIMO channel frequency response (CFR) matrix for the  $k$ th subcarrier, and  $\tilde{\boldsymbol{\eta}}[\bar{k}, \bar{n}] = [\tilde{\eta}^1[\bar{k}, \bar{n}], \tilde{\eta}^2[\bar{k}, \bar{n}], \dots, \tilde{\eta}^{N_{\text{RF}}}[\bar{k}, \bar{n}]]^T \in \mathbb{C}^{N_{\text{RF}} \times 1}$  is the noise vector corrupting the received signal, such that  $\mathbb{E}[\tilde{\boldsymbol{\eta}}[\bar{k}, \bar{n}] \tilde{\boldsymbol{\eta}}^*[\bar{k}, \bar{n}]] = \sigma_{\eta}^2 \mathbf{W}_{\text{RF}}^* \mathbf{W}_{\text{RF}}$ . The vector  $\tilde{\mathbf{b}}[\bar{k}, \bar{n}] = [\tilde{b}^1[\bar{k}, \bar{n}], \tilde{b}^2[\bar{k}, \bar{n}], \dots, \tilde{b}^{N_{\text{RF}}}[\bar{k}, \bar{n}]]^T \in \mathbb{C}^{N_{\text{RF}} \times 1}$  contains the precoded virtual symbols  $\{\tilde{b}^q[\bar{k}, \bar{n}]\}_{q=1}^{N_{\text{RF}}}$  that obey  $\tilde{b}^q[\bar{k}, \bar{n}] = \tilde{d}^q[\bar{k}, \bar{n}] + j\tilde{I}^q[\bar{k}, \bar{n}]$ . Where the term  $\tilde{I}^q[\bar{k}, \bar{n}]$  consists of the ISI and inter-carrier interference (ICI) coming from the adjacent FT symbols in the neighborhood of the desired symbol  $\tilde{d}^q[\bar{k}, \bar{n}]$  in the FT grid. This is a fundamental difference compared to OFDM system, where the ISI and ICI are tackled by adding cyclic prefix and through the orthogonality among the subcarriers, respectively. This term is known as the intrinsic interference component which is from

the characteristics of FBMC systems. It can be expressed as

$$\tilde{I}^q[\bar{k}, \bar{n}] = \sum_{(m,n) \in \Omega_{\bar{k}, \bar{n}}} \tilde{d}^q[k, n] \langle \xi \rangle_{k,n}^{\bar{k}, \bar{n}}, \quad (2.7)$$

where  $\Omega_{\bar{k}, \bar{n}} = \{(\bar{k} \pm 1, \bar{n} \pm 1), (\bar{k} \pm 1, \bar{n}), (\bar{k}, \bar{n} \pm 1)\}$  is the first-order neighborhood of the FT point  $(\bar{k}, \bar{n})$ .

## 2.4 Spatially Sparse Precoding

The major goal of this chapter is to create efficient RF and baseband precoding matrices for hybrid analog/digital precoding architectures with limited feedback. In this chapter, we assume perfect channel knowledge at the MS with a limited feedback between the BS and MS [127]. Moreover, to simplify the channel equalization task and use the demonstrated algorithms, we assume that the CFR is sufficiently smooth in the passband region of each subcarrier. The complete calculations of the precoders' matrices are done at the MS, afterwards, the calculated precoders are quantized and fed back to the BS via the limited feedback. The detailed quantization procedure of the calculated precoders can be found in [127].

When transmitting Gaussian symbols over the mmWave channel, the SE attained by the system is given by [147]

$$\mathcal{I}(\mathbf{F}_{\text{RF}}, \{\mathbf{F}_{\text{BB}}[k]\}_{k=1}^K, \mathbf{W}_{\text{RF}}, \{\mathbf{W}_{\text{BB}}[k]\}_{k=1}^K) = \frac{1}{K} \sum_{k=1}^K \log_2 \left| \mathbf{I}_{N_s} + \frac{\rho}{N_s} \mathbf{R}_n^{-1}[k] \mathbf{W}_{\text{BB}}^*[k] \mathbf{W}_{\text{RF}}^* \mathbf{H}[k] \mathbf{F}_{\text{RF}} \mathbf{F}_{\text{BB}}[k] \mathbf{F}_{\text{BB}}^*[k] \mathbf{F}_{\text{RF}}^* \mathbf{H}^*[k] \mathbf{W}_{\text{RF}} \mathbf{W}_{\text{BB}}[k] \right|, \quad (2.8)$$

where  $\rho = \frac{P}{K\sigma_n^2}$  is the signal-to-noise ratio (SNR), and  $\mathbf{R}_n[k] = \mathbf{W}_{\text{BB}}^*[k] \mathbf{W}_{\text{RF}}^* \mathbf{W}_{\text{RF}} \mathbf{W}_{\text{BB}}[k]$  is the noise covariance matrix after combining.

To gain a further simplification of the hybrid precoders design, we assume that the MS can perform optimal nearest neighbor decoding based on the  $N_{\text{MS}}$ -dimensional received signal with fully-digital hardware. This assumption allows to decouple the transceiver design problem, hence focusing only on designing the precoders. Therefore, instead of maximizing SE, we design  $\mathbf{F}_{\text{RF}}, \{\mathbf{F}_{\text{BB}}[k]\}_{k=1}^K$

to maximize the mutual information achieved by Gaussian signaling over the mmWave channel as [130]

$$\mathcal{I}(\mathbf{F}_{\text{RF}}, \{\mathbf{F}_{\text{BB}}[k]\}_{k=1}^K) = \frac{1}{K} \sum_{k=1}^K \log_2 \left| \mathbf{I} + \frac{\rho}{N_S} \mathbf{H}[k] \mathbf{F}_{\text{RF}} \mathbf{F}_{\text{BB}}[k] \mathbf{F}_{\text{BB}}^*[k] \mathbf{F}_{\text{RF}}^* \mathbf{H}^*[k] \right| \quad (2.9)$$

We emphasize here that by abstracting RX operation, and concentrating on mutual information rather than the SE expression in (2.8), successfully yields to accepting that the RX can perform ideal nearest-neighbor decoding based on the  $N_{\text{MS}}$ -dimensional received signal. Tragically, such a decoder is impractical to realize with actual mmWave systems, in which decoders don't have access to the  $N_{\text{MS}}$ -dimensional signal. In practical mmWave systems, the received signals must be combined in the analog domain, before possibly combining in the digital domain. Thus, we will revisit this problem of designing feasible mmWave receivers in section 3.5.

Focusing only on the design of  $\mathbf{F}_{\text{RF}}, \{\mathbf{F}_{\text{BB}}[k]\}_{k=1}^K$ , the precoder optimization problem under the unitary power constraint can be written as

$$\begin{aligned} (\mathbf{F}_{\text{RF}}^*, \{\mathbf{F}_{\text{BB}}^*[k]\}_{k=1}^K) &= \underset{\mathbf{F}_{\text{RF}}, \{\mathbf{F}_k\}_{k=1}^K}{\text{argmax}} \mathcal{I}(\mathbf{F}_{\text{RF}}, \{\mathbf{F}_{\text{BB}}[k]\}_{k=1}^K), \\ \text{s.t. } \mathbf{F}_{\text{RF}} &\in \mathcal{F}_{\text{RF}}, \\ \|\mathbf{F}_{\text{RF}} \mathbf{F}_{\text{BB}}[k]\|_{\text{F}}^2 &\in \mathcal{U}_{N_{\text{BS}} \times N_S}, k = 1, 2, \dots, K, \end{aligned} \quad (2.10)$$

where  $\mathcal{F}_{\text{RF}}$  is the set of possible RF precoders, in other words, it is the set of  $N_{\text{BS}} \times N_{\text{RF}}$  matrices with constant modulus elements.

To our humble knowledge, no general solutions to problem (2.10) with the non-convex feasibility constraint  $\mathbf{F}_{\text{RF}} \in \mathcal{F}_{\text{RF}}$  has been proposed yet. Hence, we propose to solve an approximation to (2.10) for the sake of finding practical near-optimal precoders which can be implemented in the system of Figure 2.1. We solve this problem, using a combination of the spatially sparse precoding design algorithm proposed for narrowband mmWave channels in [127], and the FS precoding design algorithm proposed for OFDM mmWave systems in [130].

We begin by considering the mutual information achieved by the hybrid precoders  $\mathbf{F}_{\text{RF}}, \{\mathbf{F}_{\text{BB}}[k]\}_{k=1}^K$  and rewriting (2.9) in terms of the distance between the hybrid precoders

$\mathbf{F}_{\text{RF}}, \{\mathbf{F}_{\text{BB}}[k]\}_{k=1}^K$  and the channel's optimal unconstrained precoders  $\mathbf{F}_{\text{svd}}[k]$ . Thus, we start by defining the SVD of the channel as  $\mathbf{H}[k] = \mathbf{U}[k]\mathbf{\Sigma}[k]\mathbf{V}^*[k]$ , where  $\mathbf{U}[k]$  is an  $N_{\text{MS}} \times \text{rank}(\mathbf{H}[k])$  unitary matrix,  $\mathbf{\Sigma}[k]$  is a  $\text{rank}(\mathbf{H}[k]) \times \text{rank}(\mathbf{H}[k])$  diagonal matrix of singular values arranged in decreasing order, and  $\mathbf{V}^*[k]$  is an  $N_{\text{BS}} \times \text{rank}(\mathbf{H}[k])$  unitary matrix.

Using the SVD of the channel and standard mathematical manipulation, (2.9) can be rewritten as

$$\mathcal{I}(\mathbf{F}_{\text{RF}}, \{\mathbf{F}_{\text{BB}}[k]\}_{k=1}^K) = \frac{1}{K} \sum_{k=1}^K \log_2 \left| \mathbf{I} + \frac{\rho}{N_{\text{S}}} \mathbf{\Sigma}^2[k] \mathbf{V}^*[k] \mathbf{F}_{\text{RF}} \mathbf{F}_{\text{BB}}[k] \mathbf{F}_{\text{BB}}^*[k] \mathbf{F}_{\text{RF}}^* \mathbf{V}[k] \right| \quad (2.11)$$

Furthermore, let's define the following two partitions of the matrices  $\mathbf{\Sigma}[k]$  and  $\mathbf{V}[k]$  as

$$\mathbf{\Sigma}[k] = \begin{bmatrix} \mathbf{\Sigma}_1[k] & 0 \\ 0 & \mathbf{\Sigma}_2[k] \end{bmatrix}, \quad \mathbf{V}[k] = \begin{bmatrix} \mathbf{V}_1[k] & \mathbf{V}_2[k] \end{bmatrix}, \quad (2.12)$$

where  $\mathbf{\Sigma}_1[k]$  is of dimension  $N_{\text{S}} \times N_{\text{S}}$  and  $\mathbf{V}_1[k]$  is of dimension  $N_{\text{BS}} \times N_{\text{S}}$ , note that the optimal unconstrained unitary precoder of  $\mathbf{H}[k]$  is simply  $\mathbf{F}_{\text{svd}}[k] = \mathbf{V}_1[k]$ . Another important observation is that the precoder  $\mathbf{V}_1[k]$  cannot in general be expressed as  $\mathbf{F}_{\text{RF}}, \{\mathbf{F}_{\text{BB}}[k]\}_{k=1}^K$  with  $\mathbf{F}_{\text{RF}} \in \mathcal{F}_{\text{RF}}$ , hence cannot be implemented in the mmWave hybrid architecture under consideration. Nevertheless, if we can make  $\mathbf{F}_{\text{RF}}, \{\mathbf{F}_{\text{BB}}[k]\}_{k=1}^K$  sufficiently close to the optimal precoder  $\mathbf{V}_1[k]$ , in other words if we can make them roughly equal each others, then the mutual information resulting from  $\mathbf{F}[k]$  and  $\mathbf{F}_{\text{RF}}, \{\mathbf{F}_{\text{BB}}[k]\}_{k=1}^K$  can be made comparable. Indeed, to facilitate our handling of  $\mathcal{I}(\mathbf{F}_{\text{RF}}, \{\mathbf{F}_{\text{BB}}[k]\}_{k=1}^K)$ , we make the following system assumption:

*Approximation1:* We assume that the mmWave system parameters ( $N_{\text{S}}, N_{\text{RF}}, N_{\text{BS}}, N_{\text{MS}}$ ), as well as the mmWave channel ( $L, N_{\text{ray}}, \dots$ ), are such that the assumption of the hybrid precoders  $\mathbf{F}_{\text{RF}} \mathbf{F}_{\text{BB}}[k]$  are very close to the optimal unitary precoders  $\mathbf{F}_{\text{svd}}[k] = \mathbf{V}_1[k]$ , where  $N_{\text{ray}}$  is the number of sub-paths per each path  $l$ . Mathematically, this can be described as follows:

1. The eigenvalues of the matrix  $\mathbf{I}_{N_{\text{S}}} - \mathbf{V}_1^*[k] \mathbf{F}_{\text{RF}} \mathbf{F}_{\text{BB}}[k] \mathbf{F}_{\text{BB}}^*[k] \mathbf{F}_{\text{RF}}^* \mathbf{V}_1[k]$  are very small. In other words, and in the context of mmWave precoding, this means that  $\mathbf{V}_1^*[k] \mathbf{F}_{\text{RF}} \mathbf{F}_{\text{BB}}[k] \approx \mathbf{I}_{N_{\text{S}}}$ .

2. The singular values of the matrix  $\mathbf{V}_2^*[k]\mathbf{F}_{\text{RF}}\mathbf{F}_{\text{BB}}[k]$  are very small, in other words,  $\mathbf{V}_2^*[k]\mathbf{F}_{\text{RF}}\mathbf{F}_{\text{BB}}[k] \approx 0$ .

This assumption is reasonable in our mmWave system under consideration, where we have: (1) a large number of antennas  $N_{\text{BS}}$ , (2) a number of transmit chains  $N_{\text{S}} \leq N_{\text{RF}} \leq N_{\text{BS}}$ , (3) and correlated channel matrices  $\mathbf{H}[k]$ .

Basically, Approximation 1 grants us the ability to further simplify the expression of the mutual information  $\mathcal{I}(\mathbf{F}_{\text{RF}}, \{\mathbf{F}_{\text{BB}}[k]\}_{k=1}^K)$ . With the aim of doing that, we need to use the expressions defined in (2.12), over and above we need to define the following new partition of the matrix  $\mathbf{V}^*[k]\mathbf{F}_{\text{RF}}\mathbf{F}_{\text{BB}}[k]\mathbf{F}_{\text{BB}}^*[k]\mathbf{F}_{\text{RF}}^*\mathbf{V}[k]$  as

$$\begin{aligned}
& \mathbf{V}^*[k]\mathbf{F}_{\text{RF}}\mathbf{F}_{\text{BB}}[k]\mathbf{F}_{\text{BB}}^*[k]\mathbf{F}_{\text{RF}}^*\mathbf{V}[k] \\
&= \begin{bmatrix} \mathbf{V}_1^*[k]\mathbf{F}_{\text{RF}}\mathbf{F}_{\text{BB}}[k]\mathbf{F}_{\text{BB}}^*[k]\mathbf{F}_{\text{RF}}^*\mathbf{V}_1[k] & \mathbf{V}_1^*[k]\mathbf{F}_{\text{RF}}\mathbf{F}_{\text{BB}}[k]\mathbf{F}_{\text{BB}}^*[k]\mathbf{F}_{\text{RF}}^*\mathbf{V}_2[k] \\ \mathbf{V}_2^*[k]\mathbf{F}_{\text{RF}}\mathbf{F}_{\text{BB}}[k]\mathbf{F}_{\text{BB}}^*[k]\mathbf{F}_{\text{RF}}^*\mathbf{V}_1[k] & \mathbf{V}_2^*[k]\mathbf{F}_{\text{RF}}\mathbf{F}_{\text{BB}}[k]\mathbf{F}_{\text{BB}}^*[k]\mathbf{F}_{\text{RF}}^*\mathbf{V}_2[k] \end{bmatrix} \\
&= \begin{bmatrix} \mathbf{Q}_{11}[k] & \mathbf{Q}_{12}[k] \\ \mathbf{Q}_{21}[k] & \mathbf{Q}_{22}[k] \end{bmatrix}, \tag{2.13}
\end{aligned}$$

using this partition, we can express the mutual information as

$$\begin{aligned}
& \mathcal{I}(\mathbf{F}_{\text{RF}}, \{\mathbf{F}_{\text{BB}}[k]\}_{k=1}^K) \\
&= \frac{1}{K} \sum_{k=1}^K \log_2 \left| \mathbf{I} + \frac{\rho}{N_S} \boldsymbol{\Sigma}^2[k] \mathbf{V}^*[k] \mathbf{F}_{\text{RF}} \mathbf{F}_{\text{BB}}[k] \mathbf{F}_{\text{BB}}^*[k] \mathbf{F}_{\text{RF}}^* \mathbf{V}[k] \right| \\
&= \frac{1}{K} \sum_{k=1}^K \log_2 \left| \mathbf{I} + \frac{\rho}{N_S} \begin{bmatrix} \boldsymbol{\Sigma}_1^2[k] & 0 \\ 0 & \boldsymbol{\Sigma}_2^2[k] \end{bmatrix} \begin{bmatrix} \mathbf{Q}_{11}[k] & \mathbf{Q}_{12}[k] \\ \mathbf{Q}_{21}[k] & \mathbf{Q}_{22}[k] \end{bmatrix} \right| \\
&\stackrel{(a)}{=} \frac{1}{K} \sum_{k=1}^K \log_2 \left| \mathbf{I}_{N_S} + \frac{\rho}{N_S} \boldsymbol{\Sigma}_1^2[k] \mathbf{Q}_{11}[k] \right| + \frac{1}{K} \sum_{k=1}^K \log_2 \left| \mathbf{I} + \frac{\rho}{N_S} \boldsymbol{\Sigma}_2^2[k] \mathbf{Q}_{22}[k] \right. \\
&\quad \left. - \frac{\rho^2}{N_S^2} \boldsymbol{\Sigma}_2^2[k] \mathbf{Q}_{21}[k] \left( \mathbf{I}_{N_S} + \frac{\rho}{N_S} \boldsymbol{\Sigma}_1^2[k] \mathbf{Q}_{11}[k] \right)^{-1} \boldsymbol{\Sigma}_1^2[k] \mathbf{Q}_{12}[k] \right| \\
&\stackrel{(b)}{\approx} \frac{1}{K} \sum_{k=1}^K \log_2 \left| \mathbf{I}_{N_S} + \frac{\rho}{N_S} \boldsymbol{\Sigma}_1^2[k] \mathbf{V}_1^*[k] \mathbf{F}_{\text{RF}} \mathbf{F}_{\text{BB}}[k] \mathbf{F}_{\text{BB}}^*[k] \mathbf{F}_{\text{RF}}^* \mathbf{V}_1[k] \right|,
\end{aligned} \tag{2.14}$$

where in (a) we have used the Schur complement identity for matrix determinants, and (b) is a result of using Approximation 1 which implies that  $\mathbf{Q}_{12}[k]$ ,  $\mathbf{Q}_{21}[k]$  and  $\mathbf{Q}_{22}[k]$  are approximately

zero. Continuing with (2.14), we can further simplify the mutual information as

$$\begin{aligned}
 \mathcal{I}(\mathbf{F}_{\text{RF}}, \{\mathbf{F}_{\text{BB}}[k]\}_{k=1}^K) & \\
 & \stackrel{(a)}{\approx} \frac{1}{K} \sum_{k=1}^K \log_2 \left| \mathbf{I}_{N_S} + \frac{\rho}{N_S} \boldsymbol{\Sigma}_1^2[k] \right| + \frac{1}{K} \sum_{k=1}^K \log_2 \left| \mathbf{I}_{N_S} - \left( \mathbf{I}_{N_S} + \frac{\rho}{N_S} \boldsymbol{\Sigma}_1^2[k] \right)^{-1} \right. \\
 & \quad \left. \times \frac{\rho}{N_S} \boldsymbol{\Sigma}_1^2[k] \left( \mathbf{I}_{N_S} - \mathbf{V}_1^*[k] \mathbf{F}_{\text{RF}} \mathbf{F}_{\text{BB}}[k] \mathbf{F}_{\text{BB}}^*[k] \mathbf{F}_{\text{RF}}^* \mathbf{V}_1[k] \right) \right| \\
 & \stackrel{(b)}{\approx} \frac{1}{K} \sum_{k=1}^K \log_2 \left| \mathbf{I}_{N_S} + \frac{\rho}{N_S} \boldsymbol{\Sigma}_1^2[k] \right| - \frac{1}{K} \sum_{k=1}^K \text{tr} \left( \left( \mathbf{I}_{N_S} + \frac{\rho}{N_S} \boldsymbol{\Sigma}_1^2[k] \right)^{-1} \right. \\
 & \quad \left. \times \frac{\rho}{N_S} \boldsymbol{\Sigma}_1^2[k] \left( \mathbf{I}_{N_S} - \mathbf{V}_1^*[k] \mathbf{F}_{\text{RF}} \mathbf{F}_{\text{BB}}[k] \mathbf{F}_{\text{BB}}^*[k] \mathbf{F}_{\text{RF}}^* \mathbf{V}_1[k] \right) \right) \\
 & \stackrel{(c)}{\approx} \frac{1}{K} \sum_{k=1}^K \log_2 \left| \mathbf{I}_{N_S} + \frac{\rho}{N_S} \boldsymbol{\Sigma}_1^2[k] \right| \\
 & \quad - \frac{1}{K} \sum_{k=1}^K \text{tr} \left( \mathbf{I}_{N_S} - \mathbf{V}_1^*[k] \mathbf{F}_{\text{RF}} \mathbf{F}_{\text{BB}}[k] \mathbf{F}_{\text{BB}}^*[k] \mathbf{F}_{\text{RF}}^* \mathbf{V}_1[k] \right) \\
 & = \frac{1}{K} \sum_{k=1}^K \log_2 \left| \mathbf{I}_{N_S} + \frac{\rho}{N_S} \boldsymbol{\Sigma}_1^2[k] \right| \\
 & \quad - \frac{1}{K} \sum_{k=1}^K \left( N_S - \|\mathbf{V}_1^*[k] \mathbf{F}_{\text{RF}} \mathbf{F}_{\text{BB}}[k]\|_{\text{F}}^2 \right), \tag{2.15}
 \end{aligned}$$

where (a) is obtained given (2.14) and by defining the matrices  $\mathbf{B} = \frac{\rho}{N_S} \boldsymbol{\Sigma}_1^2[k]$  and  $\mathbf{A} = \mathbf{V}_1^*[k] \mathbf{F}_{\text{RF}} \mathbf{F}_{\text{BB}}[k] \mathbf{F}_{\text{BB}}^*[k] \mathbf{F}_{\text{RF}}^* \mathbf{V}_1[k]$  and using  $\mathbf{I} + \mathbf{B}\mathbf{A} = (\mathbf{I} + \mathbf{B})(\mathbf{I} - (\mathbf{I} + \mathbf{B})^{-1}\mathbf{B}(\mathbf{I} - \mathbf{A}))$ . Step (b) follows from Approximation 1 which implies that the eigenvalues of the matrix  $\mathbf{X} = ((\mathbf{I}_{N_S} + \frac{\rho}{N_S} \boldsymbol{\Sigma}_1^2[k])^{-1} \frac{\rho}{N_S} \boldsymbol{\Sigma}_1^2[k] (\mathbf{I}_{N_S} - \mathbf{V}_1^*[k] \mathbf{F}_{\text{RF}} \mathbf{F}_{\text{BB}}[k] \mathbf{F}_{\text{BB}}^*[k] \mathbf{F}_{\text{RF}}^* \mathbf{V}_1[k]))$  are small, hence this grants us the ability to use this following approximation  $\log_2 |\mathbf{I}_{N_S} - \mathbf{X}| \approx \log_2 (1 - \text{tr}(\mathbf{X})) \approx -\text{tr}(\mathbf{X})$ . Lastly, (c) is a result from assuming a high effective-SNR approximation which leads to  $(\mathbf{I} + \frac{\rho}{N_S} \boldsymbol{\Sigma}_1^2[k])^{-1} \frac{\rho}{N_S} \boldsymbol{\Sigma}_1^2[k] \approx \mathbf{I}_{N_S}$  which provides the final result in (2.15). It's important to note that the nominal SNR  $\rho = \frac{P}{K\sigma_\eta^2}$ , isn't the one that's assumed to be high. In mmWave systems, this might be a problematic assumption. However, only the effective-SNRs in the channel's dominant  $N_S$  subspaces, are believed to be high enough. Because these effective SNRs incorporate the huge array gain from mmWave beam-

forming, this is a realistic assumption [127]. We observe that the first term after the last equality sign of (2.15)

$$\frac{1}{K} \sum_{k=1}^K \log_2 \left| \mathbf{I}_{N_S} + \frac{\rho}{N_S} \boldsymbol{\Sigma}_1^2[k] \right|$$

is the mutual information achieved by the optimal precoder  $\mathbf{F}_{\text{svd}}[k] = \mathbf{V}_1[k]$  and that the dependence of  $\mathcal{I}(\mathbf{F}_{\text{RF}}, \{\mathbf{F}_{\text{BB}}[k]\}_{k=1}^K)$  on the hybrid precoders  $\mathbf{F}_{\text{RF}}\mathbf{F}_{\text{BB}}[k]$  is now captured in the second term following the last equality sign in (2.15)

$$\frac{1}{K} \sum_{k=1}^K \left( N_S - \|\mathbf{V}_1^*[k]\mathbf{F}_{\text{RF}}\mathbf{F}_{\text{BB}}[k]\|_{\text{F}}^2 \right). \quad (2.16)$$

We note that the term in (2.16) is the squared chordal distance between the two points  $\mathbf{F}_{\text{svd}}[k] = \mathbf{V}_1[k]$  and  $\mathbf{F}_{\text{RF}}\mathbf{F}_{\text{BB}}[k]$  on the Grassmann manifold. Using Approximation 1 which states that these two points are close enough, we can utilize the manifold's locally Euclidean property to substitute the chordal distance by the Euclidean distance  $\|\mathbf{F}_{\text{svd}}[k] - \mathbf{F}_{\text{RF}}\mathbf{F}_{\text{BB}}[k]\|_{\text{F}}$  [148]. Thus, near-optimal hybrid precoders that approximately maximize  $\mathcal{I}(\mathbf{F}_{\text{RF}}, \{\mathbf{F}_{\text{BB}}[k]\}_{k=1}^K)$  can be obtained by instead minimizing  $\|\mathbf{F}_{\text{svd}}[k] - \mathbf{F}_{\text{RF}}\mathbf{F}_{\text{BB}}[k]\|_{\text{F}}$ . Actually, we can infer from Approximation 1 that  $\|\mathbf{V}_1^*[k]\mathbf{F}_{\text{RF}}\mathbf{F}_{\text{BB}}[k]\|_{\text{F}}^2$  and consequently (2.15), can be approximately maximized by instead maximizing  $\text{tr}(\mathbf{V}_1^*[k]\mathbf{F}_{\text{RF}}\mathbf{F}_{\text{BB}}[k])$ . This is due to the fact that the magnitude of the off-diagonal elements of  $\mathbf{V}_1^*[k]\mathbf{F}_{\text{RF}}\mathbf{F}_{\text{BB}}[k]$  is insignificant, and all the diagonal elements of  $\mathbf{V}_1^*[k]\mathbf{F}_{\text{RF}}\mathbf{F}_{\text{BB}}[k]$  must be made close to one. Hence,  $\|\mathbf{V}_1^*[k]\mathbf{F}_{\text{RF}}\mathbf{F}_{\text{BB}}[k]\|_{\text{F}}^2$ , or the  $\ell_2$  norm of  $\mathbf{V}_1^*[k]\mathbf{F}_{\text{RF}}\mathbf{F}_{\text{BB}}[k]$ 's diagonals can be maximized by optimizing  $\text{tr}(\mathbf{V}_1^*[k]\mathbf{F}_{\text{RF}}\mathbf{F}_{\text{BB}}[k])$ , i.e., the  $\ell_1$  norm of the diagonals [149, 150, 151].

Since maximizing  $\text{tr}(\mathbf{V}_1^*[k]\mathbf{F}_{\text{RF}}\mathbf{F}_{\text{BB}}[k])$  is much the same as minimizing  $\|\mathbf{F}_{\text{svd}}[k] - \mathbf{F}_{\text{RF}}\mathbf{F}_{\text{BB}}[k]\|_{\text{F}}$ , the precoder design problem can be reformulated as

$$\begin{aligned} (\mathbf{F}_{\text{RF}}^*, \{\mathbf{F}_{\text{BB}}^*[k]\}_{k=1}^K) &= \underset{\mathbf{F}_{\text{RF}}, \{\mathbf{F}_k\}_{k=1}^K}{\text{argmin}} \|\mathbf{F}_{\text{svd}}[k] - \mathbf{F}_{\text{RF}}\mathbf{F}_{\text{BB}}[k]\|_{\text{F}}, \\ \text{s.t. } \mathbf{F}_{\text{RF}} &\in \mathcal{F}_{\text{RF}}, \\ \|\mathbf{F}_{\text{RF}}\mathbf{F}_{\text{BB}}[k]\|_{\text{F}}^2 &\in \mathcal{U}_{N_{\text{BS}} \times N_S}, k = 1, 2, \dots, K, \end{aligned} \quad (2.17)$$

which is now the problem of finding the projections of  $\mathbf{F}_{\text{svd}}[k]$  onto the set of hybrid precoders of the form  $\mathbf{F}_{\text{RF}}\mathbf{F}_{\text{BB}}[k]$  with  $\mathbf{F}_{\text{RF}} \in \mathcal{F}_{\text{RF}}$ , where this projection is realized with respect to the standard Frobenius norm  $\|\cdot\|_{\text{F}}^2$ . Unluckily, the feasible set  $\mathcal{F}_{\text{RF}}$  is complex and non-convex, hence it makes finding such a projection both algorithmically and analytically troublesome [152].

Nevertheless, to deliver near-optimal solutions to the problem in (2.17), we suggest to make use of the structure of the mmWave MIMO channels which are generated by the clustered channel model that has been introduced in section 1.3.2. Specifically, we exploit the following observations on mmWave precoding:

1. *Structure of optimal precoders:* The optimal unitary precoder is  $\mathbf{F}_{\text{svd}}[k] = \mathbf{V}_1[k]$ , and that the columns of the unitary matrix  $\mathbf{V}[k]$  form an orthonormal basis for the channel's row space.
2. *Structure of clustered mmWave channels:* Observing the channel model in 1.3.2, we notice that the array response vectors  $\mathbf{a}_{\text{BS}}(\theta_l), \forall l$ , form a finite spanning set for the channel's row space as well. Indeed, if we have  $LN_{\text{ray}} \leq N_{\text{BS}}$ , we assure that the array response vectors are linearly independent with probability one, thus they form another minimal basis for the channel's row space for  $LN_{\text{ray}} \leq \min(N_{\text{BS}}, N_{\text{MS}})$ . To realize the fact of linear independence of the array response vectors  $\mathbf{a}_{\text{BS}}(\theta_l)$ , let us consider the typical ULAs case. For the case of ULAs, the  $N_{\text{BS}} \times LN_{\text{ray}}$  matrix established by gathering the vectors  $\mathbf{a}_{\text{BS}}(\theta_l), \forall l$ , will be a Vandermonde matrix that has full rank whenever the angles  $\theta_l$  are different. This happens with probability one once the angles  $\theta_l$  are generated from a continuous distribution. The same thing can be realized for the case of uniform planar arrays (ULPA)s, where linear independence can be established by expressing the response vectors as a Kronecker product of two ULPA response vectors [153].
3. *Relation between  $\mathbf{F}_{\text{svd}}[k]$  and  $\mathbf{a}_{\text{BS}}(\theta_l)$ :* Through examining observation 1, No matter if  $LN_{\text{ray}} \leq N_{\text{BS}}$  or not, we notice that the columns of the optimal precoders  $\mathbf{F}_{\text{svd}}[k] = \mathbf{V}_1[k]$  are connected to the vectors  $\mathbf{a}_{\text{BS}}(\theta_l)$  through a linear transformation. Consequently, the columns of  $\mathbf{F}_{\text{svd}}[k]$  can be expressed as linear combinations of  $\mathbf{a}_{\text{BS}}(\theta_l), \forall l$ .
4. *Vectors  $\mathbf{a}_{\text{BS}}(\theta_l)$  as columns of  $\mathbf{F}_{\text{RF}}$ :* Notice that the entries of the vectors  $\mathbf{a}_{\text{BS}}(\theta_l)$  are constant-

magnitude phase-only, this allows the vectors  $\mathbf{a}_{\text{BS}}(\theta_l)$  to be applied by the analog phase shifters. As a result, we can apply  $N_{\text{RF}}$  different vectors of  $\mathbf{a}_{\text{BS}}(\theta_l)$  at the TX via the RF precoder, and constructing arbitrary linear combinations of them using its digital precoder  $\mathbf{F}_{\text{BB}}[k]$ . Therefore, we can establish our main goal and build the linear combinations that minimizes  $\|\mathbf{F}_{\text{svd}}[k] - \mathbf{F}_{\text{RF}}\mathbf{F}_{\text{BB}}[k]\|_{\text{F}}$ .

Thus, by exploiting the structure of  $\mathbf{H}[k]$ , we can find near-optimal hybrid precoders by limiting the feasible set  $\mathcal{F}_{\text{RF}}$  to take values from the set of vectors of the form  $\mathbf{a}_{\text{BS}}(\theta_l)$ , and further solving

$$\begin{aligned} (\mathbf{F}_{\text{RF}}^*, \{\mathbf{F}_{\text{BB}}^*[k]\}_{k=1}^K) &= \underset{\mathbf{F}_{\text{RF}}, \{\mathbf{F}_k\}_{k=1}^K}{\text{argmin}} \|\mathbf{F}_{\text{svd}}[k] - \mathbf{F}_{\text{RF}}\mathbf{F}_{\text{BB}}[k]\|_{\text{F}}, \\ \text{s.t. } \mathbf{F}_{\text{RF}}^{(i)} &\in \{\mathbf{a}_{\text{BS}}(\theta_l), \forall i\}, \\ \|\mathbf{F}_{\text{RF}}\mathbf{F}_{\text{BB}}[k]\|_{\text{F}}^2 &\in \mathcal{U}_{N_{\text{BS}} \times N_{\text{S}}}, k = 1, 2, \dots, K, \end{aligned} \quad (2.18)$$

which can be interpreted as finding the best low dimensional representation of  $\mathbf{F}_{\text{svd}}[k]$  utilizing the basis vectors  $\mathbf{a}_{\text{BS}}(\theta_l)$ . It is good to notice that we can extend the basis vectors to include array response vectors in directions other than  $\{\mathbf{a}_{\text{BS}}(\theta_l) | 1 \leq l \leq L\}$ , and the effect of such basis extension is negligible. Therefore, the problem has been diminished to find the best  $N_{\text{RF}}$  array response vectors, and find their optimal baseband combinations. Lastly, we can establish the constraint of the analog precoder in the optimization problem to get the next equivalent simplified sparsity constrained matrix reconstruction problem

$$\begin{aligned} \{\mathbf{F}_{\text{BB}}^*[k]\}_{k=1}^K &= \underset{\mathbf{F}_{\text{BB}}[k]}{\text{argmin}} \|\mathbf{F}_{\text{svd}}[k] - \mathbf{A}_{\text{BS}}\mathbf{F}_{\text{BB}}[k]\|_{\text{F}}, \\ \text{s.t. } \|\text{diag}(\mathbf{F}_{\text{BB}}[k]\mathbf{F}_{\text{BB}}^*[k])\|_0 &= N_{\text{RF}}, \\ \|\mathbf{A}_{\text{BS}}\mathbf{F}_{\text{BB}}[k]\|_{\text{F}}^2 &\in \mathcal{U}_{N_{\text{BS}} \times N_{\text{S}}}, k = 1, 2, \dots, K, \end{aligned} \quad (2.19)$$

where  $\mathbf{A}_{\text{BS}} = [\mathbf{a}_{\text{BS}}(\phi_1), \mathbf{a}_{\text{BS}}(\phi_2), \dots, \mathbf{a}_{\text{BS}}(\phi_L)]$  is an  $N_{\text{BS}} \times L$  matrix of array response vectors.  $\mathbf{a}_{\text{BS}}(\phi) = \frac{1}{\sqrt{N_{\text{BS}}}}[1, e^{j(\frac{2\pi}{\lambda})d \sin(\phi)}, \dots, e^{j(N_{\text{BS}}-1)(\frac{2\pi}{\lambda})d \sin(\phi)}]$  for a ULPA, where  $\lambda$  is the signal wave-

length, and  $d$  is the distance between antenna elements.  $\mathbf{F}_{\text{BB}}[k]$  is an  $L \times N_{\text{S}}$  matrix, and  $L$  is the number of clusters in the channel.

Basically, the jointly non-trivial optimization problem given in (2.10) is simplified into a sparsity constrained matrix reconstruction problem with one variable. To solve the sparse problem in (2.19) we use the well-known OMP sparse recovery technique [25, 127]. This technique tries to find the best matching projections of multidimensional data onto the span of an over-complete dictionary. To grasp it more easily, let's assume that we have the simplest case of single stream beamforming, the problem in (2.19) simplifies to

$$\begin{aligned} \{\mathbf{f}_{\text{BB}}^*[k]\}_{k=1}^K &= \underset{\mathbf{f}_{\text{BB}}[k]}{\operatorname{argmin}} \|\mathbf{f}_{\text{svd}}[k] - \mathbf{A}_{\text{BS}}\mathbf{f}_{\text{BB}}[k]\|_{\text{F}}, \\ \text{s.t. } \|\mathbf{f}_{\text{BB}}[k]\|_0 &= N_{\text{RF}}, \\ \|\mathbf{A}_{\text{BS}}\mathbf{f}_{\text{BB}}[k]\|_{\text{F}}^2 &\in \mathcal{U}_{N_{\text{BS}} \times N_{\text{S}}}, k = 1, 2, \dots, K, \end{aligned} \quad (2.20)$$

in which the sparsity constraint is now on the vector  $\mathbf{f}_{\text{BB}}[k]$ . Such beamforming problem can now be solved through relaxing the sparsity constraint and through exploiting convex optimization to solve the  $\ell_2$ ,  $\ell_1$  relaxation. Accordingly, (2.20) can be solved using tools from [97, 154, 155], please refer to section 1.5 for more details.

The pseudo-code of the proposed FS hybrid precoding design algorithm is given in Algorithm 1, which is similar to [127] with some modifications to be well suited for FS systems. Algorithm 1 is divided into three main parts. In the initialization part, we set the residual RF precoding matrix  $\mathbf{F}_{\text{rf}}$  to an empty matrix in step 1. Then in step 2 we propose to stack the optimal SVD precoders obtained from the channels  $\{\mathbf{H}[k]\}_{k=1}^K$  in a column-wise manner in matrix  $\mathbf{F}_{\text{H}}$ . Afterwards, we initialize the residual matrix  $\mathbf{F}_{\text{res}}$  to  $\mathbf{F}_{\text{H}}$  in step 3. Subsequently, the second part of the algorithm which is the RF precoder design part starts. The essential steps of algorithm 1 are step 5 and step 6, in which for each RF chain in the system, the algorithm aims to find the best vector  $\mathbf{a}_{\text{BS}}(\phi_l)$  in  $\mathbf{A}_{\text{BS}}$  that has the maximum projection on  $\mathbf{F}_{\text{res}}$ . After that, the chosen column vector is column-wise appended to the residual matrix  $\mathbf{F}_{\text{rf}}$  in step 7. In step 9, the least squares (LS) solution is used from step 8 to delete the contribution of the selected vector from  $\mathbf{F}_{\text{res}}$ , along with a normalization

process. The RF precoder design procedure is continued by going back to step 5 until all  $N_{\text{RF}}$  beamforming vectors are selected. In step 11, the quantization of the angles of  $\mathbf{F}_{\text{rf}}$  is performed to meet the constraint on the available angles of the practical phase shifters. Finally, the digital precoder design part is made up of a for loop, for each subcarrier  $k$ , steps 13 and 14 are performed. These steps calculate the digital precoders and ensure that the transmit power constraint is exactly satisfied, respectively.

---

**Algorithm 1** Spatially Sparse Precoding for FS MmWave Channel via Orthogonal Matching Pursuit

---

**Require:**  $\{\mathbf{H}[k]\}_{k=1}^K, \mathbf{A}_{\text{BS}}$

**Initialization**

- 1:  $\mathbf{F}_{\text{rf}} = \text{Empty Matrix}$
- 2:  $\mathbf{F}_{\text{H}} = [\mathbf{F}_{\text{svd}}[1], \mathbf{F}_{\text{svd}}[2], \dots, \mathbf{F}_{\text{svd}}[K]] \in \mathbb{C}^{N_{\text{BS}} \times N_{\text{S}}K}$
- 3:  $\mathbf{F}_{\text{res}} = \mathbf{F}_{\text{H}}$

**RF Precoder Design**

- 4: **for**  $i = 1, 2, \dots, N_{\text{RF}}$  **do**
- 5:    $\Psi = \mathbf{A}_{\text{BS}}^* \mathbf{F}_{\text{res}}$
- 6:    $u^* = \text{argmax}_{u=1,2,\dots,L} \|\Psi\|_{:,u}\|_2$
- 7:    $\mathbf{F}_{\text{rf}} = [\mathbf{F}_{\text{rf}} | \mathbf{A}_{\text{BS}}^{(u^*)}]$
- 8:    $\mathbf{F}_{\text{LS}} = (\mathbf{F}_{\text{rf}}^* \mathbf{F}_{\text{rf}})^{-1} \mathbf{F}_{\text{rf}}^* \mathbf{F}_{\text{H}}$
- 9:    $\mathbf{F}_{\text{res}} = \frac{\mathbf{F}_{\text{H}} - \mathbf{F}_{\text{rf}} \mathbf{F}_{\text{LS}}}{\|\mathbf{F}_{\text{H}} - \mathbf{F}_{\text{rf}} \mathbf{F}_{\text{LS}}\|_{\text{F}}}$
- 10: **end for**
- 11:  $\mathbf{F}_{\text{RF}} \leftarrow$  Approximate the angles of  $\mathbf{F}_{\text{rf}}$  to the closest quantized angles of the available phase shifters and save them in  $\mathbf{F}_{\text{RF}}$

**Digital Precoder Design**

- 12: **for**  $k = 1, 2, \dots, K$  **do**
  - 13:    $\mathbf{F}[k] = \frac{\mathbf{F}_{\text{rf}}^* \mathbf{F}_{\text{rf}}}{\mathbf{F}_{\text{rf}}^* \mathbf{F}_{\text{svd}}[k]}$
  - 14:    $\mathbf{F}[k] = \sqrt{N_{\text{S}}K} \left( \frac{\mathbf{F}[k]}{\|\mathbf{F}_{\text{rf}} \mathbf{F}[k]\|_{\text{F}}} \right)$
  - 15: **end for**
- 

## 2.5 Spatially Sparse MMSE Combining

In order to simplify the precoding design in section 2.4, we have decoupled the transceiver design to only concentrate on the precoding part. Basically, we have assumed that the RX can perform optimal nearest neighbor decoding based on the  $N_{\text{MS}}$ -dimensional received signal with fully-digital

hardware. In practice, such an assumption imposes prohibitively high complexity for MIMO systems, thus it is unrealistic for practical mmWave systems.

A compromised solution for such problem can be offered by the well-known linear MMSE RX design. This solution relaxes the constraint for a fully-digital hardware, and utilizes both the digital and analog processing. The MMSE solution aims to design the hybrid combiners  $\mathbf{W}_{\text{RF}}, \{\mathbf{W}[k]\}_{k=1}^K$  that minimize the MSE between the transmitted and received signals. The MMSE combining design problem can be expressed as

$$\begin{aligned} (\mathbf{W}_{\text{RF}}^*, \{\mathbf{W}^*[k]\}_{k=1}^K) = & \underset{\mathbf{W}_{\text{RF}}, \{\mathbf{W}[k]\}_{k=1}^K}{\text{argmin}} \mathbb{E}[\|\mathbf{d}[k] - \mathbf{W}^*[k]\mathbf{W}_{\text{RF}}^*\tilde{\mathbf{y}}[\bar{k}]\|_2^2], \\ \text{s.t. } & \mathbf{W}_{\text{RF}} \in \mathcal{W}_{\text{RF}}, \end{aligned} \quad (2.21)$$

where  $\mathcal{W}_{\text{RF}}$  is the set of feasible RF combining matrices, that means the set of matrices having elements satisfying the phase shifters' constraints of constant modulus and only phase values.  $\tilde{\mathbf{y}}[\bar{k}]$  is the received vector of symbols after performing digital combining at frequency  $k$ ,  $\mathbf{d}[k]$  is the transmitted vector at frequency  $k$  as in (2.1), where we have dropped the time index for simplicity. Assuming no hardware limitations, the exact solution of (2.21) is given as [127]

$$\mathbf{W}_{\text{MMSE}}^*[k] = \frac{1}{\sqrt{P}} (\mathbf{F}^*[k]\mathbf{F}_{\text{RF}}^*\mathbf{H}^*[k]\mathbf{H}[k]\mathbf{F}_{\text{RF}}\mathbf{F}[k] + \frac{N_{\text{S}}}{\rho}\mathbf{I}_{N_{\text{MS}}})^{-1}\mathbf{F}^*[k]\mathbf{F}_{\text{RF}}^*\mathbf{H}^*[k] \quad (2.22)$$

However, the optimal unconstrained MMSE combiner  $\mathbf{W}_{\text{MMSE}}^*[k]$  in (2.22) is not a combination of digital and analog combiners, hence it is not suitable for our hybrid system. Nonetheless,  $\mathbf{W}_{\text{MMSE}}^*[k]$  will still be used in the combining method that we will show in the upcoming sequel.

Following the same demonstrations as in [127], the optimal feasible solution of the MMSE problem given in (2.21) is provided as

$$\begin{aligned}
\mathbf{W}^*[k] &= \underset{\mathbf{W}[k]}{\operatorname{argmin}} \|\mathbb{E}[\tilde{\mathbf{y}}[\bar{k}]\tilde{\mathbf{y}}^*[\bar{k}]]^{\frac{1}{2}} \mathbf{W}_{\text{MMSE}}[k] \\
&\quad - \mathbb{E}[\tilde{\mathbf{y}}[\bar{k}]\tilde{\mathbf{y}}^*[\bar{k}]]^{\frac{1}{2}} \mathbf{A}_{\text{MS}} \mathbf{W}[k]\|_{\text{F}}, \\
\text{s.t.} \quad &\|\operatorname{diag}(\mathbf{W}[k]\mathbf{W}^*[k])\|_0 = N_{\text{RF}},
\end{aligned} \tag{2.23}$$

where  $\mathbf{A}_{\text{MS}} = [\mathbf{a}_{\text{MS}}(\theta_1), \mathbf{a}_{\text{MS}}(\theta_2), \dots, \mathbf{a}_{\text{MS}}(\theta_L)]$  is an  $N_{\text{MS}} \times L$  matrix of array response vectors, and  $\mathbf{W}[k]$  is an  $L \times N_{\text{S}}$  matrix.

Therefore, as seen from (2.23), the MMSE combining problem is transformed to a sparse signal recovery problem again as in (2.19). The solution is once more done via OMP method. The pseudo-code of the MMSE combining design algorithm is illustrated in Algorithm 3. The procedure and steps of this algorithm are similar to Algorithm 1, please refer to section 2.4. We shall notice that we propose to stack the covariance matrices  $\mathbb{E}[\tilde{\mathbf{y}}[\bar{k}]\tilde{\mathbf{y}}^*[\bar{k}]]$  in one big matrix  $\mathbf{Y}_{\text{H}}$  in a column-wise manner as we have done for  $\mathbf{F}_{\text{H}}$  in Algorithm 1.

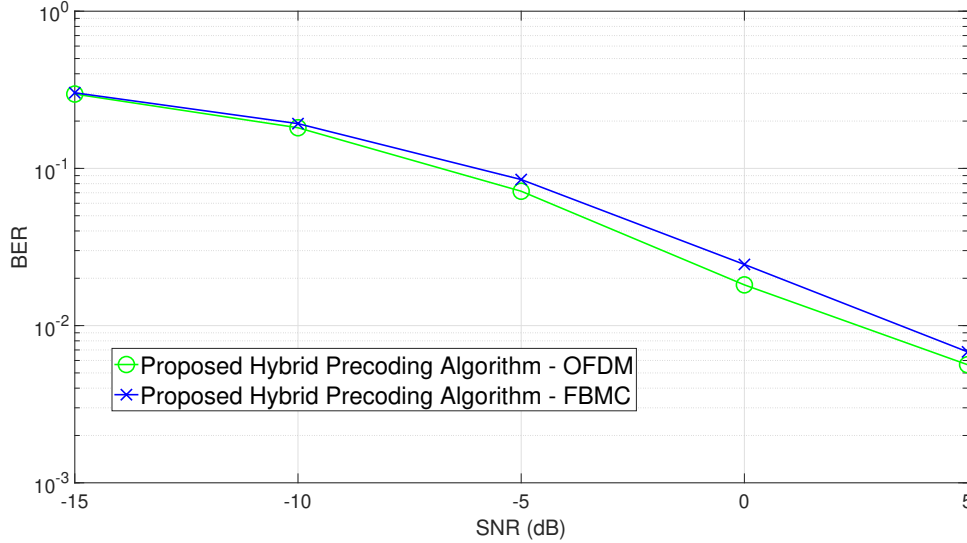


Figure 2.2: The BER versus SNR of the proposed hybrid algorithms for mmWave  $32 \times 16$  MIMO FBMC-OQAM system, compared to the OFDM counterpart,  $N_S = 2, N_{RF} = 4$ .

---

**Algorithm 2** Spatially Sparse MMSE Combining For FS MmWave Channel Via Orthogonal Matching Pursuit

---

**Require:**  $\mathbf{Y}_H, \mathbf{W}_{MMSE}, \mathbf{A}_{MS}$

---

**Initialization**

- 1:  $\mathbf{W}_{rf} = \text{Empty Matrix}$
- 2:  $\mathbf{W}_{res} = \mathbf{Y}_H$

**RF Combiner Design**

- 3: **for**  $i = 1, 2, \dots, N_{RF}$  **do**
- 4:    $\Psi = \mathbf{A}_{MS}^* \mathbf{W}_{res}$
- 5:    $u^* = \text{argmax}_{u=1,2,\dots,L} \|\Psi_{:,u}\|_2$
- 6:    $\mathbf{W}_{rf} = [\mathbf{W}_{rf} | \mathbf{A}_{MS}^{(u^*)}]$
- 7:    $\mathbf{W}_{LS} = (\mathbf{W}_{rf}^* \mathbf{W}_{rf})^{-1} \mathbf{W}_{rf}^* \mathbf{Y}_H$
- 8:    $\mathbf{W}_{res} = \frac{\mathbf{Y}_H - \mathbf{W}_{rf} \mathbf{W}_{LS}}{\|\mathbf{Y}_H - \mathbf{W}_{rf} \mathbf{W}_{LS}\|_F}$
- 9: **end for**
- 10:  $\mathbf{W}_{RF} \leftarrow$  Approximate the angles of  $\mathbf{W}_{rf}$  to the closest quantized angles of the available phase shifters and save them in  $\mathbf{W}_{RF}$

**Digital Combiner Design**

- 11: **for**  $k = 1, 2, \dots, K$  **do**
  - 12:    $\mathbf{W}[k] = \frac{\mathbf{W}_{rf}^* \mathbf{W}_{rf}}{\mathbf{W}_{rf}^* \mathbf{W}_{MMSE}[k]}$
  - 13:    $\mathbf{W}[k] = \sqrt{N_S} \left( \frac{\mathbf{W}[k]}{\|\mathbf{W}^*[k] \mathbf{W}_{rf}^*\|_F} \right)$
  - 14: **end for**
-

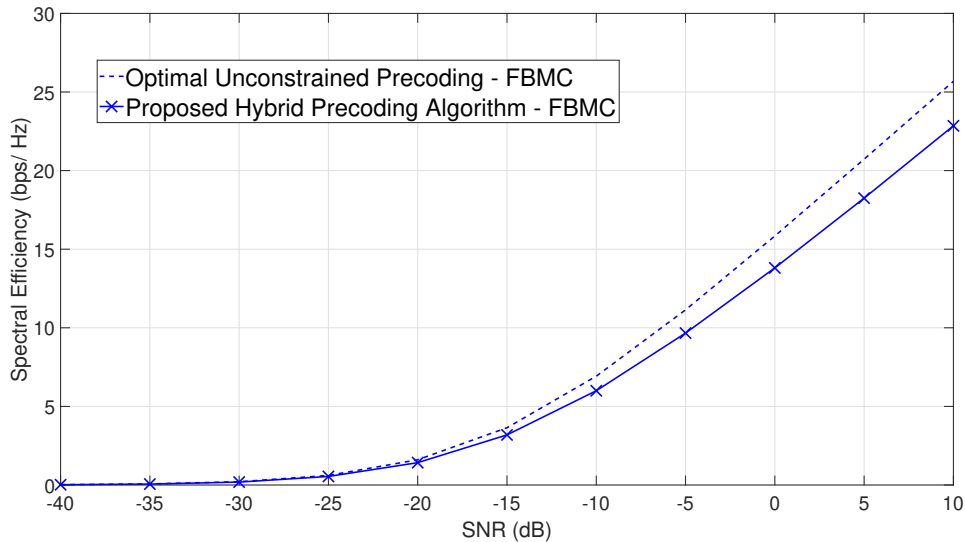


Figure 2.3: The SEs of the proposed hybrid precoding and digital SVD algorithms versus SNR for mmWave  $32 \times 16$  MIMO FBMC-OQAM system,  $N_S = N_{RF} = 3$ .

## 2.6 Results

We evaluate by simulation the performance of FBMC-OQAM with the proposed FS hybrid precoding and combining designs for mmWave MIMO systems.  $N_{BS} = 32, N_{MS} = 16$ , unless stated otherwise. We assume in these simulations that both the BS and MS have a ULPA. The data symbols are drawn from the real and imaginary parts of 4-QAM symbols. We adopt a wideband mmWave channel model with  $L = 6$  clusters. Furthermore, concerning the dynamics of the channel, we restricted our work to scenarios where the channel is invariant over several FBMC-OQAM symbols. The number of subcarriers is  $K = 512$ , with 16 MCM symbols and 6 quantization bits for the phase shifters, unless stated otherwise. We assume that the center AoAs/AoDs of the  $L$  clusters  $\theta_l, \phi_l$  are uniformly distributed over  $[0, 2\pi)$ . We adopt the so called PHYDYAS prototype filter for the pulse shaping function for the FBMC-OQAM system [83], with  $O = 4$  overlapping factor.

Fig. 2.2 represents the BER versus SNR of the proposed algorithms for mmWave hybrid MIMO FBMC-OQAM system compared with OFDM system as a benchmark. These systems have been compared with  $N_S = 2, N_{RF} = 4$ , and  $K = 64$ , where 20000 Monte Carlo repetitions have been conducted over 20000 new channel realizations. Fig. 2.2 shows that the BER achieved by the

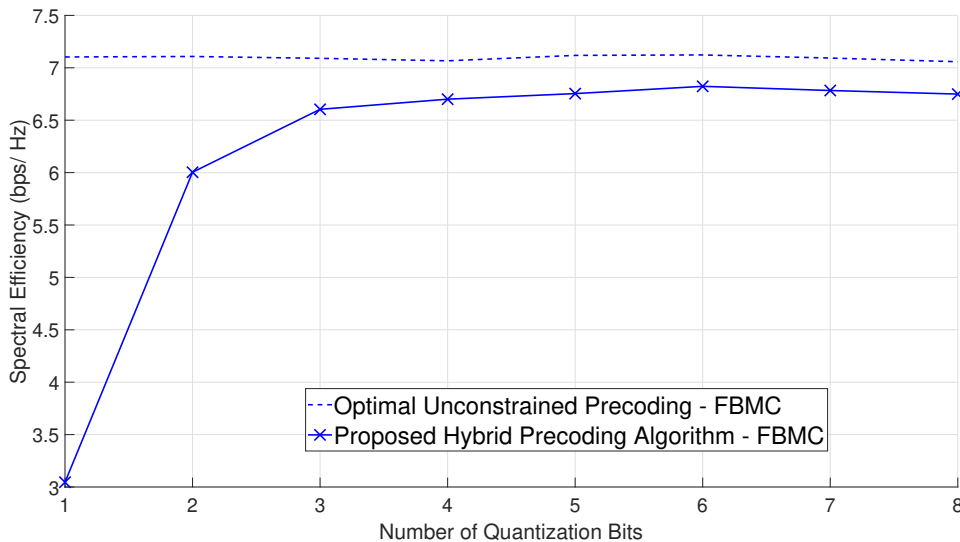


Figure 2.4: The SEs of the proposed hybrid precoding and digital SVD algorithms versus the number of quantization bits for mmWave  $32 \times 16$  MIMO FBMC-OQAM system,  $N_S = 1$ ,  $N_{RF} = 2$ , SNR = 0 dB.

OFDM system is slightly better in comparison to the FBMC-OQAM system, this was expected due to the intrinsic interference in FBMC-OQAM system [145]. This interference can be fully eliminated using interference cancellation techniques, or it can be totally ignored without loss in performance if we assume that the CFR is the same for each three consecutive subcarriers [86].

In Figures 2.3, 2.4, 2.5, the SEs achieved by the proposed hybrid algorithms are compared with the optimal unconstrained SVD technique for mmWave hybrid MIMO FBMC-OQAM system over 100 different channel realizations for 16 MCM symbols. In Fig. 2.3, the SEs are plotted versus SNR with  $N_S = N_{RF} = 3$ . As can be seen, the SE achieved by the proposed algorithms is close to the optimal SVD technique. The SE performance attained by the proposed algorithm for our FBMC system is the same for the OFDM system counterpart. This was expected, since we are using the same number of subcarriers and hence the same bandwidth. However, if the system is restricted to low OOB emission, then FBMC should be chosen over OFDM. For the sake of clarity, the SEs for OFDM system have not been presented in the figure. In Fig. 2.4, the SEs are plotted versus the number of quantization bits with  $N_S = 1$ ,  $N_{RF} = 2$  and for SNR = 0 dB. As can be concluded from the figure, 4 to 6 quantization bits would be enough to have good performance.

In Fig. 2.5, the SEs are shown for different numbers of transmitted data streams. We adopt the same setup as before but with  $N_{MS} = 8$ , and the number of RF chains equals to the number

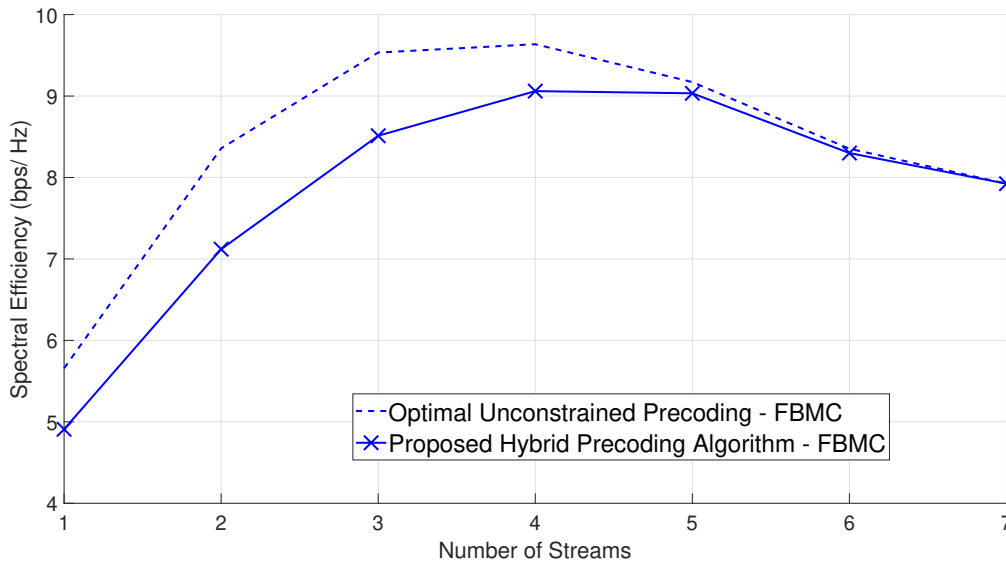


Figure 2.5: The SEs of the proposed hybrid precoding and digital SVD algorithms versus the number of streams for mmWave  $32 \times 8$  MIMO FBMC-OQAM system,  $N_S = N_{RF}$ , SNR = 0 dB.

of data streams and for SNR = 0 dB. First, Fig. 2.5 shows that the performance of both the unconstrained precoding and the hybrid precoding increases then decreases again with the number of data streams. This decrease with large numbers of transmitted data streams is a result of the sparse mmWave channels and the equal power allocation among the different streams, which causes some power to be allocated to less important multi-path components. Furthermore, observation of the figure shows that the gap between the proposed hybrid precoding algorithms and digital SVD solution is small when the number of streams is large, which also follows from the sparsity of mmWave channels.

## 2.7 Conclusions

In this chapter, we considered single-user precoding and combining and investigated the feasibility of adopting FBMC-OQAM signaling waveform for next generation mmWave communications, where the strong dependency on RF precoding makes typical MIMO solutions unfeasible. We created a low-hardware-complexity precoding approach by utilizing the structure of realistic mmWave channels. We formulated the problem of mmWave precoder design as a sparsity-constrained signal

---

recovery problem, then we offered an algorithmic solution employing OMP. The same approach may be used to solve the problem of designing realistic MMSE combiners for mmWave systems, as we demonstrated. We showed that the proposed precoders can be efficiently quantized, and the precoding technique is well-suited for restricted feedback systems. Finally, numerical results on the performance of spatially sparse mmWave processing were provided, demonstrating that it allows systems to operate more efficiently. Furthermore, simulation results showed that FBMC-OQAM waveform can be a convenient candidate for future mmWave MIMO communication systems, especially when high SE is the primary goal. Future extensions of this work may explore the high mobility scenarios, such as vehicular mmWave systems, and MU communications scenarios.





# Chapter 3

## Hybrid Precoding And Channel Estimation For Frequency-Selective MmWave MIMO OFDM Systems

### 3.1 Introduction

Several works have been proposed to estimate the mmWave channel with its new hybrid architecture. Most of these works assume an FF narrowband mmWave channel model [156, 157]. However, mmWave channels are wideband FS in reality, hence some recent papers have been published considering this aspect [158, 159].

In this chapter we propose two algorithms for FS OFDM mmWave systems under the hybrid architecture: 1) An FS codebook design algorithm based on the OMP technique. 2) An FS channel estimation algorithm that generalizes the work in [156] to FS channels. The design of the FS hybrid codebook is based on the well-known OMP technique. On the other hand, the proposed channel estimation algorithm is inspired by the novel FF channel estimation algorithm proposed in [156]. The main contributions of this chapter can be summarized as follows:

- The design of an FS hybrid codebook to train precoders. In the proposed codebook, in contrast to other works, our designed baseband training precoders are FS matrices, and not FF matrices as usual, thus can be different for each subcarrier.

- The design of an adaptive compressive sensing based algorithm that efficiently estimates the multi-path mmWave channel using the proposed FS codebook.

Before delving into the codebook design and our proposed channel estimation algorithm, we provide in the following section a detailed comprehensive review of the channel estimation techniques for mmWave systems.

## 3.2 Review of Channel Estimation Techniques for Hybrid Architecture Systems

For the sake of attaining more precoding gains as well as to be able to precode simultaneously multiple data streams, numerous studies have been proposed to split the precoding process into analog and digital domains [111, 53]. Moreover, to overcome the limitations of analog-only beamforming mmWave systems, constrained by the analog phase shifters amplitude which has to be constant, and by the potentially low-resolution signal phase control, several works have adopted the joint analog-digital hybrid architecture. Some channel estimation methods with this hybrid architecture have been proposed taking into account the aforementioned constraints. Most of these works assume a FF narrowband mmWave channel model [55, 160, 161, 111, 162, 103, 163, 164]. However, several papers have been proposed focusing on the FS channel case [118, 119, 120]. In the following paragraphs, we will first present the different approaches for mmWave channel estimation with hybrid architecture when the system is narrowband, before presenting the research works under the FS channel assumption.

### 3.2.1 Techniques for Narrowband Systems

Different approaches are employed to estimate the FF mmWave channel including divide-and-conquer, ping-pong, mode-by-mode approaches and many others. These approaches are explained below in addition to other methods, and they are listed in Table 3.1 with their respective references.

Table 3.1: Channel estimation algorithms for narrowband hybrid mmWave systems.

Reference	Year	Approach	Scenario	UL/DL	2D/3D	Complexity	Description
Alkhateeb <i>et al.</i> [111]	2014	Divide-and-conquer	Single-user	DL	2D	$\mathcal{O}(VL^2[VL/N_{\text{RF}}] \log_V(N/L))$	OMP, LSE
Lee <i>et al.</i> [103]	2014	Open-loop	Single-user	Not specified	2D	$\mathcal{O}(LV^2N^2)$	OMP, MG-OMP, LSE
He <i>et al.</i> [165]	2014	Mode-by-mode	Single-user	UL/DL	2D	Not specified	A temporally correlated NLOS channel, based on the TDD correlation statistics
Schniter <i>et al.</i> [87]	2014	Aperture shaping	Not specified	Not specified	2D	Not specified	LASSO, LMMSE
Alkhateeb <i>et al.</i> [112]	2014	Ping-ping	Single-user	UL/DL	2D	$\mathcal{O}(VL^2N_{\text{BS}} \log_V(N/L))$	OMP, no feedback is needed
Payami <i>et al.</i> [166]	2015	Ping-pong	Single-user	Not specified	2D	$\lceil N/N_{\text{RF}} \rceil$ measurements to scan all $N$ directions	The training time doesn't scale with the number of multi-path components
Kokshoorn <i>et al.</i> [167]	2015	Overlapped beam patterns	Single-user	Not specified	2D	$\frac{V^2}{\log_2^2(V+1)}$ reduction compared to [111]	MRC, used to track fast changing channels
Peng <i>et al.</i> [113]	2015	AAVE	Single-user	UL	2D	$2N_{\text{RF}}$ time slots	CS-based technique, enhances the angular estimation resolution
Montagner <i>et al.</i> [168]	2015	2D DFT	Single-user	Not specified	2D	$\lceil \frac{N_{D_T}}{N_{\text{RF,MS}}} \rceil \lceil \frac{N_{D_B}}{N_{\text{RF,BS}}} \rceil N_{\text{RF,BS}}$ time slots	DFT, iterative cancellation method
Mendez-rial <i>et al.</i> [114]	2015	Switches	Single-user	DL	2D	Not specified	OMP, M-OMP
Chiang <i>et al.</i> [115]	2016	SVD avoidance	Single-user	Not specified	Not specified	Not specified	OMP, it exploits the orthogonality between the array propagation vectors
Lu <i>et al.</i> [169]	2016	Adaptive DFT	Single-user	DL	2D	$\lceil \frac{N_{D_T}}{N_{\text{RF,MS}}} \rceil \lceil \frac{N_{D_B}}{N_{\text{RF,BS}}} \rceil N_{\text{RF,BS}}$ time slots	DFT, a feedback is adopted to improve the accuracy
Han <i>et al.</i> [116]	2016	Two-stage asymmetric	Multi-user	DL	2D	Not specified	Exhaustive search, CS
Park <i>et al.</i> [117]	2016	Spatial covariance	Single-user	UL	Not specified	Not specified	OMP, S-OMP, C-OMP, DS-OMP, DC-OMP
Zhou <i>et al.</i> [170]	2016	CANDECOMP/-PARAFAC (C/P)	Multi-user	UL	2D	$\mathcal{O}(G_1^2G_2^2 + T'TN_{\text{RF,BS}})$	C/P, referred to as tensor rank decomposition
Guo <i>et al.</i> [171]	2017	2D beamspace MUSIC	Single-user	Not specified	2D	The main complexity comes from (i) the eigenvalue decomposition: $\mathcal{O}(N_{\text{RF,BS}}^3 N_{\text{RF,MS}}^3)$ (ii) the grid search: $\mathcal{O}(G_2G_1N_{\text{RF,BS}}^2 N_{\text{RF,MS}}^2)$	MUSIC, LSE, it exploits the large-scale fading property of path directions
Guo <i>et al.</i> [172]	2019	Dimension-deficient	Single-user	UL	2D	$\mathcal{O}(N_{\text{RF}}N_{\text{BS}}(N_{\text{MS}}L)^3)$	CoSaMP, it reduces the influence of accidental errors

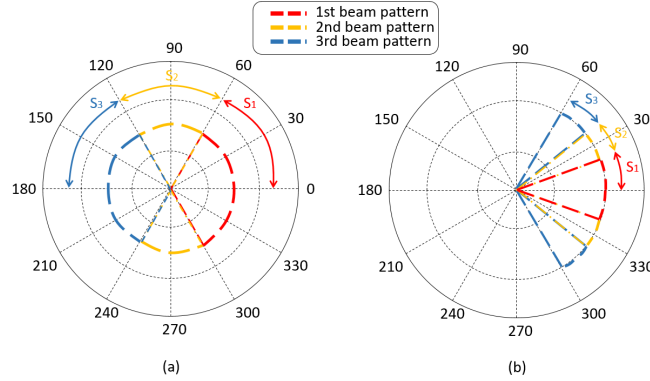


Figure 3.1: An example of the beam patterns adopted in the first (a) and second (b) stages in [111] when  $K = 3$ , where  $S_k, k \in \{1, \dots, K\}$  denotes the sub-ranges in each stage.

### Divide-and-conquer approach

In [111] a low-complexity adaptive channel estimation algorithm has been proposed for narrowband mmWave channel with large antenna arrays and a few number of RF units at both the BS and MS sides. The authors assumed that the amplitude of phase shifters is constant, and that the phases are quantized. The algorithm *divides* the estimation process into several stages as shown in figure 3.1. At each stage, the AoAs/AoDs angular ranges are divided into  $V$  non-overlapped angular sub-ranges,  $V$  beam patterns are used to send the pilot signal and  $V$  beam patterns are used to combine the signal at the RX. So each beam pattern at the TX is combined by  $V$  beam patterns at the RX, as a result, each stage needs  $V^2$  time slots to span all the combinations of transmit-receive beam patterns. The beam patterns are taken from a predefined codebook designed and proposed by the authors. The process is then continued by calculating the magnitudes of the  $V^2$  received signals to determine or *conquer* the next AoAs/AoDs angular sub-range for the next stage. At each stage, the process pursues the same way as in the previous stage, in which it divides the chosen AoDs sub-range at the TX and AoAs sub-range at the RX into  $V$  sub-ranges. It proceeds this way until it achieves the desired AoAs/AoDs resolution. This algorithm, initially proposed for single-path and multi-path cases, needs  $V^2 \lceil \log_V(\max(N_{BS}, N_{MS})) \rceil$  time slots for each channel path. Such algorithm is not fast enough to track the rapid variations of mmWave channels which could be a major drawback. Moreover, this algorithm requires an exclusive feedback channel.

### Ping-pong approaches

Based on the same codebook design of [111], the authors appended their work in [112] by proposing another estimation algorithm that doesn't need feedback. The developed algorithm uses *ping-pong* iterations and requires a complexity of  $\mathcal{O}(VL^2N_{\text{BS}}\log_V(N/L))$ , to acquire the channel parameters, where the AoAs, and AoDs are taken from a uniform grid of  $N$  points. Two ping-pong stages are done in each stage of the adaptive algorithm in [112]. In the first stage, the BS utilizes a relatively wide beamforming vector, while the MS uses a number of beamforming vectors to sense the received signal. The BS-MS roles are switched in the second ping-pong stage, allowing the BS to choose a narrower beamforming vector. In [166] a two-stage algorithm for single-user (SU) channel estimation is presented as well as a codebook design which is similar to that in [112]. The algorithm is characterized by a two-stage handshaking between the TX and the RX. During the first stage, the TX uses one transmit antenna to send an omni-directional signal and correspondingly the RX senses and scans its multiple directions to detect the AoAs, subsequently the roles are exchanged at the second stage such that the RX sends a pilot signal at the detected angles only. The two-stage estimation algorithm is illustrated in figure 3.2. It needs  $\lceil N/N_{\text{RF}} \rceil$  measurements to scan all  $N$  required directions, where  $N_{\text{RF}}$  is the number of the RF chains in the system. Moreover, its training time doesn't scale with the number of multi-path components, unlike the channel estimation method in [112].

### Overlapped beam patterns approach

[167] outlined a fast channel estimation algorithm by proposing the *overlapped beam patterns* estimation concept. This concept reduces the time slots needed to estimate the channel by  $\frac{V^2}{\log_2^2(V+1)}$  compared to [111], with a slight degradation in performance. This small sacrifice in degradation can be accepted when tracking fast changing channels is required. Indeed, the concept is to use a smaller number of overlapped beam patterns for the same number of sub-ranges to estimate the channel, instead of assigning one beam pattern for each sub-range as in [111] in which the number of beam patterns should be equal to the number of sub-ranges. The algorithm is illustrated in figure 3.3.

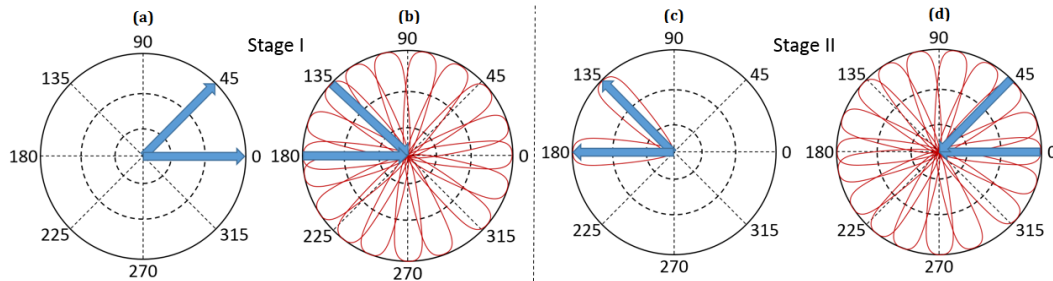


Figure 3.2: Illustration of the two-stage estimation algorithm in [166], the blue colored arrows represent the AoAs and AoDs at the BS and MS; (a) the BS sends an omni-directional signal over all directions, (b) the MS scans the directions, in this case we have two AoAs at MS at  $135^\circ$  and  $180^\circ$ , (c) the MS sends through its AoDs, (d) the BS scans the directions, in this case we have two AoAs at BS at  $0^\circ$  and  $45^\circ$ .

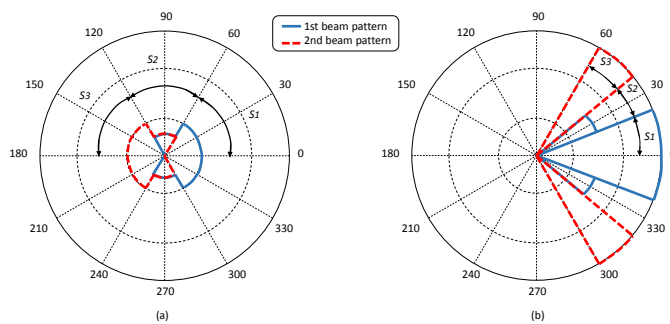


Figure 3.3: The overlapped beam patterns adopted in the first (a) and second (b) stages when  $V = 3$

### Open-loop approach

An *open-loop* channel estimation technique that doesn't need a feedback loop was proposed in [103]. The algorithm is provided for an SU mmWave system, and is based on CS techniques. As for many channel estimation algorithms, the authors used the OMP and least-squares estimation (LSE) techniques to perform the estimation of the AoAs/AoDs and gains, respectively. However, they also proposed the adaptive MG-OMP, this new version of OMP enhances the estimates of AoAs/AoDs by refining these estimates just around the regions where the AoAs/AoDs are present which reduces MG-OMP complexity over OMP. Through their computer simulations, the authors showed that CS techniques, OMP and MG-OMP, outperforms the LSE ones. In addition, the complexity reduction gained by the MG-OMP was estimated.

### Mode-by-mode approach

Another scheme was proposed in [165] to estimate a temporally correlated NLOS mmWave MIMO channel. The authors, first modified the parametric channel model to an evolution temporally correlated MIMO channel model to successfully track the channel variations. The system is based on the TDD correlation statistics and it exploits the reciprocity of the channel. The proposed algorithm updates each column of the analog precoder and combiner, this approach is called the *mode-by-mode* approach, in which each mode represents one column of the analog precoder and combiner. For each mode, a codebook is built using a group of rotation matrices that rotate the previous mode to reconstruct the new mode, then the algorithm chooses the codeword that maximizes the received power. The digital precoder and combiner are then constructed using conventional pilot-aided estimation of the effective channel.

### Aperture shaping approach

In [87], P. Schniter and A. Sayeed proposed a technique termed as *aperture shaping* to enhance the sparsity of the mmWave MIMO channel. Briefly, aperture shaping is performed by applying a fixed gain at each antenna at both the TX and RX. The shaping coefficients are optimised to maximize the signal-to-interference ratio. In addition, they implemented a mmWave system that uses modulation and demodulation techniques based on FFT to further expose the channel sparsity. They solved the sparsity problem using LASSO [101], where it was shown that their procedure approaches the perfect-CSI capacity for a mmWave system.

### AAVE approach

Based on the same assumptions as in [111], the authors in [113] proposed a new concept called antenna array with virtual elements (*AAVE*), that extends the real antenna arrays at both the TX and RX to a new one by appending some  $A_v$  virtual antennas without affecting the physical array. The idea behind AAVE is to add some virtual antennas to the real physical antennas at both the BS and MS, in order to enhance the angular estimation resolution. However, the scheme assures that no data is sent over the virtual antennas to guarantee that no physical change has been

introduced to the antenna arrays. Based on AAVE, [113] develops a CS angle estimation method with less overhead and delay than [111]. The proposed method with AAVE can obtain a resolution of  $\mathcal{O}(1/A_v)$  which is better than  $\mathcal{O}(1/N)$  in [111, 173, 167], remind that  $N$  is the number of points of the uniform grid.

## 2D DFT approach

In [168], a mmWave channel estimation method was proposed based on the *2D DFT* of the two-dimensional complex modes based on the AoDs and AoAs. The estimation of the channel parameters is done using the iterative cancellation method. In detail, the approach estimates the channel parameters for each path using the DFT samples, after cancelling the previous estimated parameters in each iteration. This technique requires a training sequence of  $N_{\text{TS}} = \lceil \frac{N_{D_T}}{N_{\text{RF,MS}}} \rceil \lceil \frac{N_{D_B}}{N_{\text{RF,BS}}} \rceil N_{\text{RF,BS}}$  time slots, where  $N_{\text{RF,BS}}, N_{\text{RF,MS}}$  are the number of RF chains at the BS and MS, respectively.  $N_{\text{D}}$  and  $M_{\text{D}}$  are two suitable integer parameters to be chosen depending on the length of the training sequence  $N_{\text{TS}}$ . The method showed low complexity and performed close to a known channel system. Another channel estimation algorithm for a DL SU mmWave system was proposed in [169] based on the *DFT* algorithm in [168]. The algorithm uses exactly the same DFT technique provided in [168], while adopting a feedback to the BS to improve the estimation accuracy. The algorithm is illustrated as follows: First, the BS sends its training sequence to the MS, the MS estimates the channel using the DFT technique, and determines if the estimation is accurate based on an adjustable threshold. Second, the MS returns *YES* or *NO* to the BS depending on the accuracy of its estimation. Third, the BS readjusts the length of the training sequence *adaptively* according to the feedback.

## Switches approach; SVD avoidance approach

In [114], the authors proposed a new hybrid architecture for a DL SU mmWave system using *switches* as an alternative for phase shifters, to reduce cost, complexity and power consumption, especially at MSs where these parameters are crucial. Figure 3.4 depicts the proposed hybrid architecture which is slightly different from the aforementioned one as it was presented in figure 1.2(b). A new CS-based channel estimation algorithm was also developed. A multiple measurement

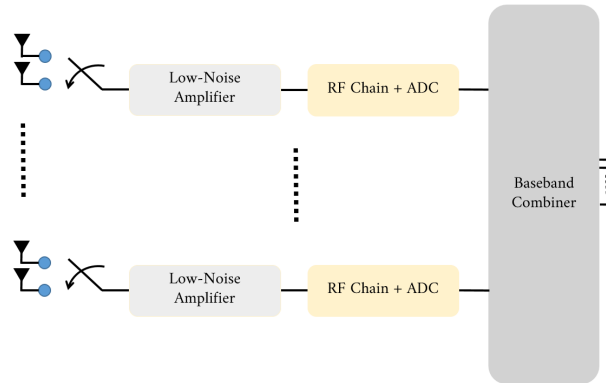


Figure 3.4: Hybrid mmWave MS architecture implementing switches instead of phase shifters

vector OMP (M-OMP) was considered in [174] instead of the single measurement vector OMP. Phase shifters architecture versus switches architecture were compared, the results showed a slight better performance of the architecture implementing switches over phase shifters one. A modified version of the aforementioned algorithm was proposed in [115] for an SU mmWave system. The authors intended to reduce the computational complexity and feedback overhead to the TX. The algorithm is also based on the OMP, but unlike to [114] it *avoids* the computation of the channel *SVD* at the RX by exploiting the orthogonality between the array propagation vectors. In contrast to [114], where the whole reconstructed precoder is sent back to the TX through the feedback link, the algorithm in [115] diminishes the feedback overhead, since it aims to reconstruct the precoder at the TX, after obtaining the codebook indices through the feedback link.

### Two-stage asymmetric approach

An asymmetric channel estimation approach was proposed in [116] for a DL MU mmWave system. The MU system is characterized by a hybrid BS and analog-only beamforming at the MSs with one RF chain for each MS. The proposed algorithm is a *two-stage asymmetric* approach, an exhaustive search stage, followed by a CS estimation stage. At the first phase, the BS sends the omni-directional training signals to the MSs, the MSs search in exhaustive manner for the best combining vectors to find the AoAs. Following the first phase, a second phase of CS estimation is performed, where the MSs fix their receiving beams to the best ones found at the first phase, while utilizing CS tools to estimate their channel parameters. The two-stage algorithm is depicted in figure 3.5.

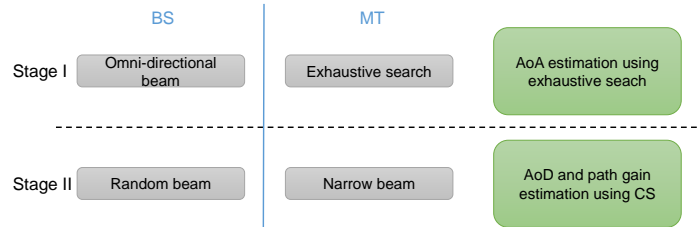


Figure 3.5: The two-stage asymmetric estimation approach in [116]

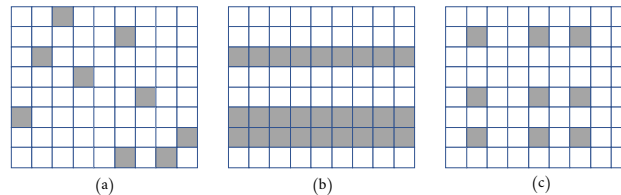


Figure 3.6: Different sparse matrix types (a) unstructured sparse matrix (b) sparse rows matrix (c) sparse Hermitian matrix.

### Spatial covariance approach

In [117], a channel estimation algorithms based on estimating the *spatial covariance* for a TDD UL SU mmWave channel were proposed. Unlike the two-step approach, where first it is needed to estimate the channel, followed by a second step of channel covariance calculation. The authors proposed to estimate the channel covariance directly, and without estimating the channel explicitly. To overcome the need for estimating the channel explicitly, the authors exploited the Hermitian property of the spatial covariance channel matrix. A sparse Hermitian matrix is shown in figure 3.6(c). Furthermore, the authors designed the covariance OMP (C-OMP) algorithm, which is based on the OMP and simultaneous OMP (S-OMP), to exploit this property and to estimate the covariance of the channel. C-OMP employs a quadratic form in its covariance calculations unlike OMP and S-OMP where a linear form is used. As known, for a perfect recovery using CS techniques, many measurements are required especially for time-varying channels. Accordingly, the authors also proposed dynamic S-OMP (DS-OMP), which was inspired by S-OMP, to mitigate the number of measurements, similarly, dynamic C-OMP (DC-OMP) was introduced. Both DS-OMP and DC-OMP can be applied to a time-varying analog combining matrix in a time-varying channel.

### Over-complete dictionary approach

Another channel estimation algorithm for a fully-connected UL SU mmWave system has been developed in [172]. The authors described the channel estimation problem by *dimension-deficient* which results from the fact that the number of RF chains is a lot smaller than the number of antennas, hence the received signal does not contain full CSI. The authors treated this issue by adopting an adaptive over-complete dictionary, then by estimating the channel parameters using CoSaMP which improves the OMP technique by reducing the influence of accidental errors. The proposed algorithm showed more robustness against noise, better performance compared with non-adaptive CS techniques, with SE close to perfect CSI.

### Other approaches

Some works tried to compete with CS algorithms in estimating the mmWave channel. Based on a technique termed *CANDECOMP/PARAFAC* (C/P) decomposition, an interesting method was carried out in [170] and was also compared to some CS techniques. In this regard, the UL MU mmWave channel can be estimated by means of the C/P decomposition method. This procedure also referred to as tensor rank decomposition, can be viewed as a generalisation of the matrix SVD to tensors. Please refer to [175] for more details. The authors stated that the C/P method can be advantageous when compared to CS techniques in terms of computational complexity due to the utilization of tensors. In addition, while it is somewhat troublesome to examine the right recovery condition for generic dictionaries, this is not the case for the C/P method, hence it is more easier to analyze and find the exact size of training overhead. Moreover, unlike CS methods, the C/P doesn't require the quantization of the continuous parameter space, consequently, no grid quantization errors. The overall computational complexity of the proposed C/P method was shown to be  $\mathcal{O}(G_1^2 G_2^2 + T' T N_{\text{RF,BS}})$ , where  $T$  and  $T'$  are respectively the number of frames and sub-frames (each frame is divided into a number of sub-frames), and  $G_2$  and  $G_1$  are respectively the search grid sizes within the considered beamforming sectors.

Another contribution to estimate an SU mmWave channel was achieved in [171] based on a 2D beamspace *multiple signal classification* (MUSIC) method. The MUSIC method is used to estimate

Table 3.2: Channel estimation algorithms for wideband hybrid mmWave systems.

Reference	Year	Scenario	UL/DL	2D/3D	Complexity	Description
Venugopal <i>et al.</i> [118]	2017	Single-user or multi-user	DL	2D	Not specified	CS, LSE, high complexity
Venugopal <i>et al.</i> [119]	2017	Single-user or multi-user	Not specified	2D or 3D	Not specified	OMP, DGMP, LSE, MMSE, SC-FDE or OFDM are considered
Rodriguez-fernandez <i>et al.</i> [120]	2017	Single-user	Not specified	2D	Not specified	OMP, MSE, LSE, exploits the common support between the subcarriers to reduce complexity
Rodriguez-fernandez <i>et al.</i> [121]	2018	Not specified	Not specified	2D	SW-OMP: $\mathcal{O}(N_{\text{RF,MS}}T(K(G_1G_2 - (j-1))))$ ; SS-SW-OMP+Th: $\mathcal{O}(N_{\text{RF,MS}}T(K_p(G_1G_2 - (j-1))))$	SW-OMP, SS-SW-OMP+Th, provides a trade-off between complexity and achievable rate
Gao <i>et al.</i> [122]	2016	Multi-user	UL	2D	Not specified	DGMP, exploits the angle-domain sparsity of FS fading channels
Zhou <i>et al.</i> [176]	2017	Multi-user	DL	2D	$\mathcal{O}(T^2TK)$	C/P, higher estimation accuracy compared to OMP
Araujo <i>et al.</i> [123]	2014	Single-user	DL	3D	$\mathcal{O}(\log(N_{\text{RF,BS}}))$	OMP, <i>search region</i> , a coarse stage followed by a refinement stage
Gonzalez-coma <i>et al.</i> [64]	2018	Multi-user	UL	2D	$\mathcal{O}(N_{\text{RF,MS}}T(K(G_1G_2 - (j-1))))$	SW-OMP

the path directions while the LSE one estimates the path gains. The suggested algorithm reduces the computational overhead by exploiting the large-scale fading property of the path directions which are believed to remain unchanged for each frame according to the measurement results obtained in [20]. Hence the costly computation of path directions is executed only once per each frame. The main computational complexity analysis of the algorithm brings out two major tasks (i) the eigenvalue decomposition whose complexity is  $\mathcal{O}(N_{\text{RF,BS}}^3 N_{\text{RF,MS}}^3)$  (ii) the grid search whose complexity is  $\mathcal{O}(G_2 G_1 N_{\text{RF,BS}}^2 N_{\text{RF,MS}}^2)$ .

### 3.2.2 Techniques for Wideband Systems

Most of the work done on mmWave channels estimation assumed the narrowband case. Such assumption was found to be not realistic for aforementioned channels, but was considered as a first step in the development of mmWave channel estimation. MmWave channels are wideband channels in reality, and to be useful, channel estimation algorithms have to take this into consideration. Recently, some works have been proposed to estimate the FS channels for mmWave hybrid systems,

we review these works in the following. Table 3.2 provides a list of these research works.

### **Time-domain approach**

In [118] a time-domain channel estimation algorithm was proposed for both single- and multi-user fully-connected hybrid single-carrier mmWave systems. The authors have taken into account the bandlimiting filter and the time required to reconfigure RF circuits. The proposed algorithm is based on CS to estimate the AoAs/AoDs, and on the LSE or the MMSE to estimate the path gains. Simulation results showed that the proposed algorithm provides low estimation error using small training overhead, but the main drawback of this algorithm lies into its complexity.

### **Frequency-domain approaches**

In [121], two frequency-domain channel estimation algorithms for a fully-connected OFDM mmWave system were proposed based on the S-OMP method [177] and tested on real FS channel models. The proposed algorithms provide a trade-off between complexity and achievable rate, and consider the effects of the bandlimiting filter and the time required to reconfigure RF circuits. The first algorithm termed as the simultaneous weighted OMP (SW-OMP) provides the best performance compared to the second one since it exploits the information on the support coming from every subcarrier of the OFDM system. While the second algorithm termed as subcarrier selection SW-OMP + thresholding (SS-SW-OMP+Th) aims to exploit information from a reduced number of subcarriers, hence it provides a lower complexity compared to SW-OMP. Both algorithms achieve the Cramer-Rao lower bound. Comparisons were done for the proposed algorithms and other FS mmWave channel estimation algorithms including structured sparsity adaptive matching pursuit (SSAMP) [178] and distributed grid matching pursuit (DGMP) [122]. The simulation results show a very good performance of the proposed algorithms.

Another frequency-domain algorithm was developed in [120], for a fully-connected OFDM mmWave system. The algorithm was compared with the time-domain algorithm proposed in [118], where it provides the same estimation error as the time-domain one, however with a lesser complexity. The authors opted to use OMP and LSE techniques to estimate the sparse channel, and exploited the common support between the subcarriers to gain more reduction in estimation com-

plexity. In addition, they proposed to refine more the estimates using an algorithm they termed as the joint channel estimation + local search (JCE+LS), which is based on MSE to know whether an improvement of the estimates is needed or not.

In [122], a frequency-domain CS-based UL MU channel estimation algorithm was proposed for OFDM mmWave system. The proposed DGMP algorithm aims to exploit the angle-domain sparsity of FS fading channels, and solves the problem of the leakage power caused by the continuous AoAs/AoDs. The simulation results showed a good performance of the proposed algorithm.

Based on the SW-OMP algorithm developed in [121], the authors in [64] proposed a joint UL MU channel estimation method for an OFDM mmWave system. Afterwards, the UL channel estimates and the reciprocity of TDD scheme were exploited to jointly design the precoders and combiners in the DL.

### Two-stage approach

A two-stage channel estimation algorithm has been proposed in [123] for an indoor SU DL mmWave system, implementing FDD and OFDM, and operating at 60 GHz. The estimation algorithm is based on two stages, a coarse stage followed by an amelioration stage. The first stage of the algorithm is performed based on the OMP CS technique, which estimates the parameters of the channel coarsely. Subsequently, the second stage is carried out to refine the estimates based on the maximization of the energy of the received signal and using the so-called *search region* algorithm as described in the paper. The proposed method can achieve a low pilot overhead of  $\mathcal{O}(\log N_{\text{BS}})$  compared to the traditional LSE that requires a length of  $\mathcal{O}(N_{\text{BS}})$ , and shows a quite well performance.

### Other approaches

The authors in [119] developed channel estimation algorithms in the frequency-domain, in the time-domain, as well as in the combined time/frequency domain. The basic concept is to use compressive sensing in the frequency domain to estimate the AoAs/AoDs, and then use those estimates to evaluate the channel gains and path delays in the time domain to acquire the full channel. Both single- and multi-user fully-connected hybrid mmWave systems implementing either

single carrier-frequency domain equalization (SC-FDE) or OFDM are considered. The estimators are based on CS, where OMP is the dominant technique used to estimate AoAs/AoDs, while LSE is used to estimate channel gains, whether for the time-domain or the frequency-domain. However, for the combined time/frequency domain, OMP or DGMP [122] are used to estimate AoAs/AoDs, and LSE or MMSE to recover the gains. The results showed a good error performance with low overhead, and a further reduction in complexity offered by the combined time/frequency algorithm.

Similarly to the CANDECOMP/PARAFAC narrowband mmWave channel estimation algorithm proposed in [170], a MU DL channel estimation technique for OFDM mmWave systems was proposed in [176]. The authors developed the Cramer-Rao bound results to describe the best asymptotically achievable performance of the algorithm, then they compared the proposed algorithm to the OMP method, where it was shown to provide a complexity similar to the OMP method, but with higher estimation accuracy.

### 3.2.3 Conclusions

The usage of analog-only beamforming for channel estimation in mmWave systems is constrained by many limitations, which can be avoided using the hybrid architecture. In this section we have seen different channel estimation techniques for both narrowband and wideband hybrid mmWave OFDM systems. Clearly the aim of most of the work that has been delivered so far for hybrid architecture was for 2D channel estimation, this work should be extended to the 3D case also. It can be also observed that there exist plenty of research works on channel estimation for the narrowband case, while only few papers have been proposed for the wideband one. It is known that mmWave channels are wideband in nature, hence some further future steps have to be taken in this regard which supported our motivation to study more in this regard.

## 3.3 System Model

Consider the OFDM system model given in Figure 3.7, where we have a BS with  $N_{\text{BS}}$  antennas and  $N_{\text{RF}}$  RF chains is communicating with a MS with  $N_{\text{MS}}$  antennas and  $N_{\text{RF}}$  RF chains. We assume that the BS is using  $N_{\text{S}} = 1$  stream of data, where the stream is length- $K$  symbol block as

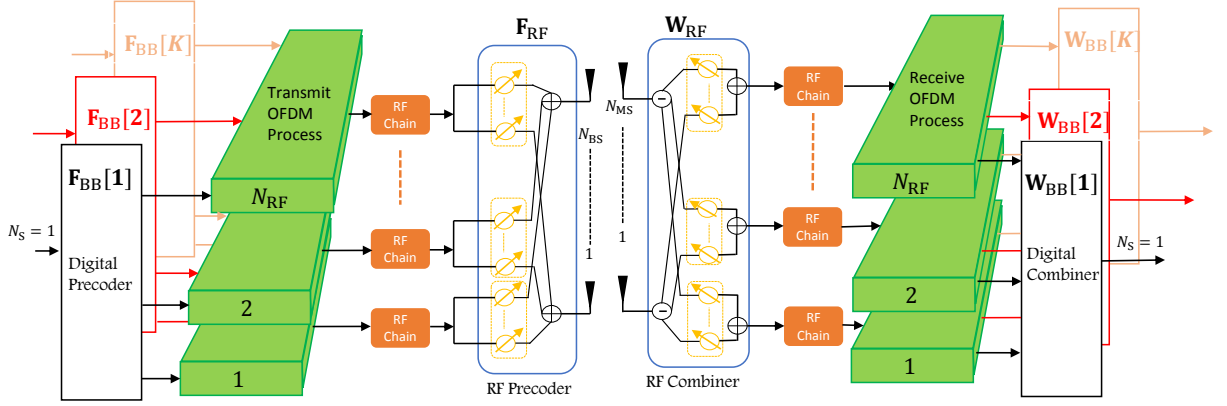


Figure 3.7: Architecture of mmWave hybrid MIMO OFDM TX and RX.

seen in Figure 3.7, such that  $N_S \leq N_{RF} \leq N_{BS}$  and  $N_S \leq N_{RF} \leq N_{MS}$ . During the training phase, we assume that the BS uses the digital precoders  $\mathbf{F}_{BB}[k] \in \mathbb{C}^{N_{RF} \times N_S}$ , and the analog precoder  $\mathbf{F}_{RF} \in \mathbb{C}^{N_{BS} \times N_{RF}}$ , with training symbols satisfying  $\mathbb{E}[\mathbf{s}[k]\mathbf{s}^*[k]] = \frac{1}{N_S} \mathbf{I}_{N_S}$ . Note that, in contrast to other works, our baseband training precoders  $\mathbf{F}_{BB}[k]$  are FS matrices, thus can be different for each subcarrier, and, as usual, the analog precoder  $\mathbf{F}_{RF}$  is an FF matrix.

At the MS, assuming perfect carrier and frequency offset synchronization, after combining with the analog and digital combiners  $\mathbf{W}_{RF} \in \mathbb{C}^{N_{MS} \times N_{RF}}$ ,  $\mathbf{W}_{BB}[k] \in \mathbb{C}^{N_{RF} \times N_S}$ , respectively, the received signal can be expressed as

$$\mathbf{y}[k] = \mathbf{W}_{BB}^*[k] \mathbf{W}_{RF}^* \mathbf{H}[k] \mathbf{F}_{RF} \mathbf{F}_{BB}[k] \mathbf{s}[k] + \mathbf{n}[k], \quad (3.1)$$

where  $\mathbf{n}[k]$  is the noise vector corrupting the received signal, such that  $\mathbb{E}[\mathbf{n}[k]\mathbf{n}[k]^*] = \sigma^2 \mathbf{W}_{BB}^*[k] \mathbf{W}_{RF}^* \mathbf{W}_{RF} \mathbf{W}_{BB}[k]$ , and  $\sigma$  is the noise variance. The main objective of the proposed channel estimation algorithm is to estimate  $\mathbf{H}[k]$  by estimating its parameters.

## 3.4 Frequency-Selective Hybrid Training Codebook Design

A lot of studies have been conducted on designing a multi-resolution codebook as in [43, 179, 45, 180, 181]. These works concentrated on analog-only beamforming and on the physical design of the beam patterns. Analog-only beamforming is not optimal and has some drawbacks, especially for mmWave systems, we list some of them:

1. Designing non-overlapping beam patterns is troublesome due to the quantized phase shifters, thus it may require to perform an exhaustive search over a large space of the large number of antennas.
2. For non-ULAs, designing the analog-only beamforming vectors is not intuitive and complicated compared to systems with ULAs.

In this section, we present the design of a multi-resolution beamforming codebook based on the approach used in [182]. While the algorithm in [182] assumes perfect channel state information (PCSI), this work handles mmWave systems without a prior knowledge of the channel. We explain the proposed algorithm for the DL model, the same algorithm, however, can be directly applied to the UL system. Here, we focus on the design of the BS training precoding codebook  $\mathcal{F}$ , a similar approach can be followed to construct the MS training codebook  $\mathcal{W}$ . Absolutely, the RF limitations including the constant amplitude phase shifters with quantized phases is considered. The codebook is general for ULAs/non-ULAs, and its complexity is low, furthermore, it performs better than the analog-only beamforming codebooks due to the additional digital processing.

### 3.4.1 Codebook Structure

The multi-resolution codebook as the name tells is made up of  $S$  levels with different resolutions,  $\mathcal{F}_s, s = 1, 2, \dots, S$ . For each level, specific designed beamforming vectors with specific beamwidths will be used in the corresponding training stage to estimate the mmWave channel. An example of the beam patterns for the apoted codebook has been shown in Fig. 3.1.

For each codebook level  $s$ , the beamforming vectors are divided into  $V^{s-1}$  subsets of  $V$  beamforming vectors. A certain range of AoDs is provided for each subset  $v$  in each level  $s$ . This AoDs range is further partitioned into  $V$  sub-ranges, such that each of the  $V$  beamforming vectors for each subset is designed to have an almost equal projection on the vectors  $\mathbf{a}_{\text{BS}}(\bar{\phi}_u)$ , with  $u$  in this sub-range, and zero projection on the other vectors. Physically, this entails the creation of a beamforming vector with a specific beamwidth given by these sub-ranges and directed in predetermined directions.

While this codebook structure is similar to that of [43, 45], which also contain many levels with beamforming vectors of varying beamwidths, this codebook's strategy defines each beamforming vector in terms of the set of quantized angles which it covers in a different way. This differs from prior work [43, 45], which defined each vector in terms of the center beamforming angle and beamwidth. This distinction leads to a new formulation of the arbitrary beamwidth beamforming design problem, as well as an entirely new method for generating these vectors using analog/digital architecture, as will be discussed shortly. As mentioned earlier, this codebook design incorporates the digital layer along with the analog one, this additional digital processing layer provides greater levels of freedom to the beamforming design problem which can be leveraged to obtain better performance in the beamforming patterns.

### 3.4.2 Design of the Codebook Beamforming Vectors

For each codebook level  $s$ , and subset  $v$ , we have  $M$  beamforming vectors  $[\mathbf{F}_{(s,v)}]_{:,m}$ ,  $m = 1, 2, \dots, M$ , which are designed such that

$$[\mathbf{F}_{(s,v)}]_{:,m} \mathbf{a}_{\text{BS}}(\bar{\phi}_u) = \begin{cases} C_s & \text{if } u \in \mathcal{I}_{(s,v,m)} \\ 0 & \text{if } u \notin \mathcal{I}_{(s,v,m)} \end{cases},$$

where

$$\mathcal{I}_{(s,v,m)} = \left\{ \frac{N}{LV^s}(V(v-1) + m - 1) + 1, \dots, \frac{N}{LV^s}(V(v-1) + m) \right\},$$

is the set that defines the sub-range of AoDs associated with the beamforming vector  $[\mathbf{F}_{(s,v)}]_{:,m}$ , and  $C_s$  is a normalization constant that satisfies  $\|\mathbf{F}_{(s,v)}\|_F = V$ .

The design objective of the beamforming vectors  $\mathbf{F}_{(s,v)}$  in (3.4.2) can be expressed in a more compact form as

$$\mathbf{A}_{\text{BS,D}}^* \mathbf{F}_{(s,v)} = C_s \mathbf{G}_{(s,v)}[k], \quad (3.2)$$

where  $\mathbf{G}_{(s,v)}[k]$  is an  $N \times V$  matrix in which for each column  $m$ , it contains 1's in the locations  $u$ ,  $u \in \mathcal{I}_{(s,v,m)}$ , and nulls in the locations  $u$ ,  $u \notin \mathcal{I}_{(s,v,m)}$ . Notice that the BS AoDs matrix  $\mathbf{A}_{\text{BS,D}}$  is an over-complete dictionary with  $N \geq N_{\text{BS}}$ , where  $N$  is the resolution of the codebook also defined in section 1.5. In other words, (3.2) represents an inconsistent system of which the approximate solution is provided by

$$\mathbf{F}_{(s,v)}[k] = C_s (\mathbf{A}_{\text{BS,D}} \mathbf{A}_{\text{BS,D}}^*)^{-1} \mathbf{A}_{\text{BS,D}}^* \mathbf{G}_{(s,v)}[k], \quad (3.3)$$

As every beamforming vector will be individually utilized in a particular time instant, we will design each of them independently in terms of the hybrid analog/digital precoders. In consequence, the design of the hybrid analog and digital training precoding matrices is accomplished by solving [127]

$$\begin{aligned} & (\mathbf{F}_{\text{RF},(s,v)}^*, [\mathbf{F}_{\text{BB},(s,v)}^*[k]]_{:,m}) = \\ & \arg \min \|\mathbf{F}_{(s,v)}[k]_{:,m} - \mathbf{F}_{\text{RF},(s,v)}[\mathbf{F}_{\text{BB},(s,v)}[k]]_{:,m}\|_F, \\ & \text{s.t. } \mathbf{F}_{\text{RF},(s,v)}[:,i] \in \{\mathbf{A}_{\text{can}}[:,q] \mid 1 \leq q \leq N_{\text{can}}\}, \\ & \quad i = 1, 2, \dots, N_{\text{RF}} \\ & \|\mathbf{F}_{\text{RF},(s,v)}[\mathbf{F}_{\text{BB},(s,v)}[k]]_{:,m}\|_F^2 = 1, \end{aligned} \quad (3.4)$$

where

$$[\mathbf{F}_{(s,v)}[k]]_{:,m} = C_s(\mathbf{A}_{\text{BS,D}}\mathbf{A}_{\text{BS,D}}^*)^{-1}\mathbf{A}_{\text{BS,D}}^*[\mathbf{G}_{(s,v)}[k]]_{:,m}, \quad (3.5)$$

and the beamforming candidate matrix  $\mathbf{A}_{\text{can}}$  is an  $N_{\text{BS}} \times N_{\text{can}}$  matrix carrying the finite set of possible analog beamforming vectors. In fact, the columns of the candidate matrix  $\mathbf{A}_{\text{can}}$  can be generated to satisfy arbitrary analog beamforming constraints. We consider on our simulation a candidate matrix  $\mathbf{A}_{\text{can}}$  that has elements satisfying the  $N_{\text{Q}}$ -bit quantized phase shifts as  $e^{jk_{\text{Q}}2\pi/2^{N_{\text{Q}}}}$ ,  $k_{\text{Q}} = 1, 2, \dots, 2^{N_{\text{Q}}} - 1$ , and  $N_{\text{can}}$  is the number of possible analog beamforming vectors.

We solve this problem using the same methodology given in chapter 2 in section 2.4. Therefore the solution is provided in Algorithm 1 illustrated in chapter 2.

## 3.5 Channel Model

In this section we propose an algorithm that uses the proposed codebook developed in section 2.4 to estimate the multi-path mmWave channel. We will explain the proposed algorithm for the DL model. The same algorithm, however, can be directly applied to the UL system.

### 3.5.1 Channel in the Time-Domain

We assume that the MIMO channel between the BS and MS is FS mmWave channel, with a delay tap length  $N_c$  in the time domain. The  $d$ -th delay tap of the channel is represented by an  $N_{\text{RF}} \times N_{\text{BS}}$  matrix denoted as  $\mathbf{H}_d$ ,  $d = 1, \dots, N_c - 1$ , which can be represented according to the geometric model [129]

$$\mathbf{H}_d = \sqrt{\frac{N_{\text{BS}}N_{\text{MS}}}{L\varrho}} \sum_{l=1}^L \alpha_l p_{\text{rc}}(dT_s - \tau_l) \mathbf{a}_{\text{BS}}(\phi_l) \mathbf{a}_{\text{MS}}^*(\theta_l), \quad (3.6)$$

where  $\varrho$  denotes the path-loss between the BS and MS,  $L$  denotes the number of paths,  $p_{\text{rc}}(\tau)$  is a filter that includes the effects of pulse-shaping and other lowpass filtering evaluated at  $\tau$ ,  $T_s$  and  $\tau_l$  are the sampling period and the delay, respectively.  $\alpha_l \in \mathbb{C}$  is the complex gain of the  $l$ th path,  $\theta_l \in [0, 2\pi)$  and  $\phi_l \in [0, 2\pi)$  are the AoAs/AoDs, of the  $l$ th path, and  $\mathbf{a}_{\text{MS}}(\theta_l) \in \mathbb{C}^{N_{\text{MS}} \times 1}$  and  $\mathbf{a}_{\text{BS}}(\phi_l) \in \mathbb{C}^{N_{\text{BS}} \times 1}$  are the array steering vectors for the receive and transmit antennas, respectively.

We can further exhibit each of the channel matrices in eq (3.6) in a more compact form as

$$\mathbf{H}_d = \mathbf{A}_{\text{MS}} \mathbf{\Delta}_d \mathbf{A}_{\text{BS}}^*, \quad (3.7)$$

where  $\mathbf{\Delta}_d \in \mathbb{C}^{L \times L}$  is diagonal with non-zero complex entries, and  $\mathbf{A}_{\text{MS}} \in \mathbb{C}^{N_{\text{MS}} \times L}$  and  $\mathbf{A}_{\text{BS}} \in \mathbb{C}^{N_{\text{BS}} \times L}$  contain the receive and transmit array steering vectors  $\mathbf{a}_{\text{MS}}(\theta_l)$  and  $\mathbf{a}_{\text{BS}}(\phi_l)$ , respectively.

### 3.5.2 Channel in the Frequency-Domain

On the other hand, the channel in the frequency-domain for each subcarrier  $k$  can be expressed in terms of the different delay taps as

$$\mathbf{H}[k] = \sum_{d=0}^{N_c-1} \mathbf{H}_d e^{-j \frac{2\pi k}{K} d} = \mathbf{A}_{\text{MS}} \mathbf{\Delta}[k] \mathbf{A}_{\text{BS}}^*, \quad (3.8)$$

where  $\mathbf{\Delta}[k]$  contains the path gains, pulse shaping filter, and delays of the channel in the frequency-domain.

### 3.5.3 Grid Quantization

We assume in our system that the AoAs/AoDs are taken from a uniform grid of points. Mathematically, we can describe this as follows:  $\phi_l \in \{0, 2\pi/G_{\text{BS}}, \dots, 2\pi(G_{\text{BS}} - 1)/G_{\text{BS}}\}$ ,  $\theta_l \in \{0, 2\pi/G_{\text{MS}}, \dots, 2\pi(G_{\text{MS}} - 1)/G_{\text{MS}}\}$ ,  $l = 1, 2, \dots, L$ , where  $G_{\text{BS}}, G_{\text{MS}}$  are the number of points in the uniform grid at BS and MS, respectively.

#### Channel in the Time-Domain with Grid Quantization

Now by neglecting the grid quantization error, and using the quantization development which has been just described, we can approximate the channel in (3.7) using the extended virtual channel model defined in [65]

$$\mathbf{H}_d \approx \tilde{\mathbf{A}}_{\text{MS}} \mathbf{\Delta}_d^v \tilde{\mathbf{A}}_{\text{BS}}^*, \quad (3.9)$$

where  $\mathbf{\Delta}_d^v \in \mathbb{C}^{G_{\text{MS}} \times G_{\text{BS}}}$  is a sparse matrix which contains the path gains of the quantized spatial

frequencies in the non-zero elements. The dictionary matrices  $\tilde{\mathbf{A}}_{\text{BS}}$  and  $\tilde{\mathbf{A}}_{\text{MS}}$  contain the TX and RX array response vectors evaluated on a grid of size  $G_{\text{MS}}$  for the AoAs and a grid of size  $G_{\text{BS}}$  for the AoDs.

### Channel in the Frequency-Domain with Grid Quantization

The matrix in (3.8) can be expressed in terms of the sparse matrices  $\Delta_d^v$  and the dictionaries

$$\mathbf{H}[k] \approx \tilde{\mathbf{A}}_{\text{MS}} \left( \sum_{d=0}^{N_c-1} \Delta_d^v e^{-j\frac{2\pi k}{K}d} \right) \tilde{\mathbf{A}}_{\text{BS}}^* \approx \tilde{\mathbf{A}}_{\text{MS}} \Delta^v[k] \tilde{\mathbf{A}}_{\text{BS}}^*, \quad (3.10)$$

to aid exhibit the sparse structure later.

## 3.6 A Sparse Formulation of the mmWave Channel Estimation Problem

Consider the system described in section 3.3. It is important to rewrite again equation (3.1)

$$\mathbf{y}[k] = \mathbf{W}_{\text{BB}}^*[k] \mathbf{W}_{\text{RF}}^* \mathbf{H}[k] \mathbf{F}_{\text{RF}} \mathbf{F}_{\text{BB}}[k] \mathbf{s}[k] + \mathbf{n}[k], \quad (3.11)$$

Using the result  $\text{vec}\{\mathbf{A}\mathbf{X}\mathbf{C}\} = (\mathbf{C}^T \otimes \mathbf{A}) \text{vec}\{\mathbf{X}\}$ , the received signal in (3.11) can be written as

$$\mathbf{y}_{\text{vec}}[k] = \text{vec}\{\mathbf{W}_{\text{BB}}^*[k] \mathbf{W}_{\text{RF}}^* \mathbf{H}[k] \mathbf{F}_{\text{RF}} \mathbf{F}_{\text{BB}}[k] \mathbf{s}[k]\} + \text{vec}\{\mathbf{n}[k]\} \quad (3.12)$$

$$= (\mathbf{s}[k]^T \mathbf{F}_{\text{BB}}[k]^T \mathbf{F}_{\text{RF}}^T \otimes \mathbf{W}_{\text{BB}}^*[k] \mathbf{W}_{\text{RF}}^*) \text{vec}\{\mathbf{H}[k]\} + \text{vec}\{\mathbf{n}[k]\}, \quad (3.13)$$

now, again using the result  $\text{vec}\{\mathbf{A}\mathbf{X}\mathbf{C}\} = (\mathbf{C}^T \otimes \mathbf{A}) \text{vec}\{\mathbf{X}\}$ , with the frequency-domain channel in (3.8), equation (3.13) can be rewritten as

$$\mathbf{y}_{\text{vec}}[k] = (\mathbf{s}[k]^T \mathbf{F}_{\text{BB}}[k]^T \mathbf{F}_{\text{RF}}^T \otimes \mathbf{W}_{\text{BB}}^*[k] \mathbf{W}_{\text{RF}}^*) (\mathbf{A}_{\text{BS}}^T \circ \mathbf{A}_{\text{MS}}) \text{vec}\{\Delta[k]\} + \text{vec}\{\mathbf{n}[k]\}, \quad (3.14)$$

the matrix  $(\mathbf{A}_{\text{BS}}^T \circ \mathbf{A}_{\text{MS}})$  is an  $N_{\text{BS}}N_{\text{MS}} \times L$  matrix in which each column has the form  $(\mathbf{a}_{\text{BS}}^*(\phi_l) \otimes \mathbf{a}_{\text{MS}}(\theta_l)), l = 1, 2, \dots, L$ , i.e., each column  $l$  represents the Kronecker product of the BS and MS array response vectors associated with the AoAs/AoDs of the  $l$ th path of the channel, and  $\circ$  represents the matrix entrywise product.

To complete the problem formulation, we utilize the quantization process defined in subsection 3.5.3 for a uniform grid of  $G_{\text{BS}} = G_{\text{MS}} = N$  points, with  $N \gg L$ . Neglecting the grid quantization error, we can approximate  $\text{vec}\{\mathbf{y}[k]\}$  in (3.14) as

$$\mathbf{y}_{\text{vec}}[k] = (\mathbf{s}[k]^T \mathbf{F}_{\text{BB}}[k]^T \mathbf{F}_{\text{RF}}^T \otimes \mathbf{W}_{\text{BB}}^*[k] \mathbf{W}_{\text{RF}}^*) (\tilde{\mathbf{A}}_{\text{BS}}^T \circ \tilde{\mathbf{A}}_{\text{MS}}) \text{vec}\{\Delta^v[k]\} + \text{vec}\{\mathbf{n}[k]\} \quad (3.15)$$

$$= (\mathbf{s}[k]^T \mathbf{F}_{\text{BB}}[k]^T \mathbf{F}_{\text{RF}}^T \otimes \mathbf{W}_{\text{BB}}^*[k] \mathbf{W}_{\text{RF}}^*) \mathbf{A}_{\text{D}} \mathbf{z}[k] + \text{vec}\{\mathbf{n}[k]\}, \quad (3.16)$$

where  $\mathbf{A}_{\text{D}} = (\tilde{\mathbf{A}}_{\text{BS}}^T \circ \tilde{\mathbf{A}}_{\text{MS}})$  is an  $N_{\text{BS}}N_{\text{MS}} \times N^2$  dictionary matrix that consists of the column vectors of the form  $(\mathbf{a}_{\text{BS}}^*(\bar{\phi}_u) \otimes \mathbf{a}_{\text{MS}}(\bar{\theta}_v))$ , in which  $\bar{\phi}_u$ , and  $\bar{\theta}_v$  the  $u$ th, and  $v$ th points, respectively, of the angles uniform grid, in other words,  $\bar{\phi}_u = 2\pi u/N, u = 1, 2, \dots, N-1$ , and  $\bar{\theta}_v = 2\pi v/N, v = 1, 2, \dots, N-1$ .  $\mathbf{z}[k] = \text{vec}\{\Delta^v[k]\}$  is an  $N^2 \times 1$  vector that contains the path gains of the corresponding quantized directions. Note that in order to detect the AoAs and AoDs of the dominant paths of the channel, we need to detect the columns of  $\mathbf{A}_{\text{D}}$  that correspond to non-zero elements of  $\mathbf{z}[k]$ . Afterwards, the values of the path gains can be obtained through computing the values of the corresponding elements in  $\mathbf{z}[k]$ .

The formulation of the vectorized received signal, which is given in (3.16), is a sparse formulation of the channel estimation problem, since  $\mathbf{z}[k]$  has  $L$  non-zero elements out of  $N$  elements, where  $L \ll N$ . Basically, the number of measurements needed to detect  $\mathbf{z}[k]$  is very small compared to  $N^2$ . Given the obtained formulation in (3.16), CS tools as described in chapter 1 section 1.5 can be exploited to design estimation algorithms to obtain the quantized AoAs/AoDs.

In order to make things less complex, we prefer to utilize the Kronecker product properties and rewrite ((3.16)) as [181]

$$\mathbf{y}_{\text{vec}}[k] = (\mathbf{s}[k]^T \mathbf{F}_{\text{BB}}[k]^T \mathbf{F}_{\text{RF}}^T \mathbf{A}_{\text{BS,D}}^T \otimes \mathbf{W}_{\text{BB}}^*[k] \mathbf{W}_{\text{RF}}^* \mathbf{A}_{\text{MS,D}}) \mathbf{A}_{\text{D}} \mathbf{z}[k] + \text{vec} \{ \mathbf{n}[k] \} \quad (3.17)$$

$$= \mathbf{s}[k]^T \mathbf{F}_{\text{BB}}[k]^T \mathbf{F}_{\text{RF}}^T \mathbf{A}_{\text{BS,D}}^T \mathbf{z}_{\text{BS}}[k] \otimes \mathbf{W}_{\text{BB}}^*[k] \mathbf{W}_{\text{RF}}^* \mathbf{A}_{\text{MS,D}} \mathbf{z}_{\text{MS}}[k] + \text{vec} \{ \mathbf{n}[k] \}, \quad (3.18)$$

where  $\mathbf{z}_{\text{BS}}[k]$ , and  $\mathbf{z}_{\text{MS}}[k]$  are two  $N \times 1$  sparse vectors that have non-zero elements in the locations that correspond to the AoDs, and AoAs, respectively.  $\mathbf{A}_{\text{BS,D}}$ , and  $\mathbf{A}_{\text{MS,D}}$  are  $N_{\text{BS}} \times N$ , and  $N_{\text{MS}} \times N$  dictionary matrices that consist of column vectors of the form  $\mathbf{a}_{\text{BS}}^*(\bar{\phi}_u)$ , and  $\mathbf{a}_{\text{MS}}(\bar{\theta}_v)$ , the quantized AoDs, and AoAs, respectively.

The standard CS theory tells us that the number of measurements needed to assure the detection of the  $L$ -sparse vector with high probability is of order  $\mathcal{O}(L \log(N/L))$  [183]. In fact, as these results are theoretically proved, unfortunately, they lack extensive implementations for practical applications. Hence, we focus on adaptive CS tools which provides some ideas on the design of the training vectors.

### 3.7 Channel Estimation for Frequency-Selective MmWave Channels

In this section, we examine the sparse channel estimation problem formulated in (3.6), and we propose an algorithm that adaptively uses the proposed hierarchical codebook developed in section 2.4 to estimate the multi-path mmWave channel. We explain the proposed algorithm for the DL model. The same algorithm, however, can be directly applied to the UL system.

As mention earlier, we focus on adaptive CS [161, 184, 185], in which the training process is partitioned into a number of stages. For each stage, the precoding and combining matrices are calculated using the output of the earlier stages, hence they are so called 'adaptive' CS. Basically, if we divide the training process into  $S$  stages, then the vectorized received signals of these stages are

$$\begin{aligned}
 \mathbf{y}_{(1)}[k] &= (\mathbf{s}[k]_{(1)}^T \mathbf{F}_{\text{BB},(1)}[k]^T \mathbf{F}_{\text{RF},(1)}^T \mathbf{A}_{\text{BS},\text{D}}^T \otimes \mathbf{W}_{\text{BB},(1)}^*[k] \mathbf{W}_{\text{RF},(1)}^* \mathbf{A}_{\text{MS},\text{D}}) \mathbf{A}_{\text{D}} \mathbf{z}[k] + \mathbf{n}_1[k] \\
 \mathbf{y}_{(2)}[k] &= (\mathbf{s}[k]_{(2)}^T \mathbf{F}_{\text{BB},(2)}[k]^T \mathbf{F}_{\text{RF},(2)}^T \mathbf{A}_{\text{BS},\text{D}}^T \otimes \mathbf{W}_{\text{BB},(2)}^*[k] \mathbf{W}_{\text{RF},(2)}^* \mathbf{A}_{\text{MS},\text{D}}) \mathbf{A}_{\text{D}} \mathbf{z}[k] + \mathbf{n}_2[k] \\
 &\vdots \\
 \mathbf{y}_{(s)}[k] &= (\mathbf{s}[k]_{(s)}^T \mathbf{F}_{\text{BB},(s)}[k]^T \mathbf{F}_{\text{RF},(s)}^T \mathbf{A}_{\text{BS},\text{D}}^T \otimes \mathbf{W}_{\text{BB},(s)}^*[k] \mathbf{W}_{\text{RF},(s)}^* \mathbf{A}_{\text{MS},\text{D}}) \mathbf{A}_{\text{D}} \mathbf{z}[k] + \mathbf{n}_s[k] \quad (3.19)
 \end{aligned}$$

As mentioned earlier, the design of the training precoding and measurements matrices for each stage  $s$ , depend on the previous vectorized received vectors  $\mathbf{y}_{(1)}[k], \mathbf{y}_{(2)}[k], \dots, \mathbf{y}_{(s)}[k]$ . Adaptive CS algorithms performs better compared to standard CS tools for low SNR [161, 184, 185], which is the typical case for mmWave systems. In addition, these adaptive CS tools, especially those rely in successive bisections, provide some insights that can be used to design the training precoding and combining matrices.

In the proposed channel estimation algorithm presented in subsection 3.7, the training precoding and combining matrices are adaptively designed based on the codebook defined in section 3.4. Basically, the algorithm begins initially by splitting the received vector in (3.19) into a number of partitions, which in turns divides the AoAs/AoDs range into a number of intervals, then design the training precoding and combining matrices of the first stage to sense those partitions. Afterwards, the algorithm tries to find the partition(s) which contain the non-zero element(s), which in turns will be further divided into smaller partitions in the later stages until all the non-zero elements, with the AoAs/AoDs with the required resolution are found.

## Adaptive Estimation Algorithm for MmWave Channels

The pseudo-code of the proposed channel estimation algorithm is given in Algorithm 3. As opposed to the algorithm in [156], which was mainly proposed for narrowband mmWave channels with FF codebook, our proposed algorithm handles FS mmWave systems and uses our proposed FS codebook.

Algorithm 3 has two main parts. In the initialization part, the history matrices  $\mathbf{T}^{\text{BS}}$  and  $\mathbf{T}^{\text{MS}}$

are initialized. These matrices are used to save the trajectories of the obtained paths at the BS and MS, respectively, in order to remove the contributions of these obtained paths in the next iterations. Moreover, the algorithm divides the estimation process into  $S$  stages, which is calculated at step 2 of the initialization part.

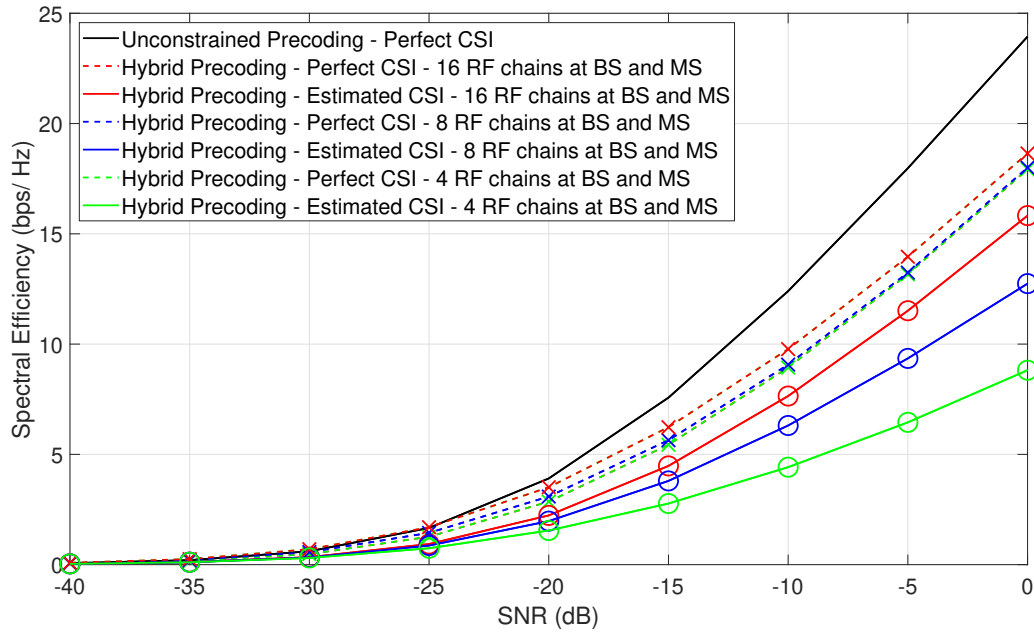


Figure 3.8: SEs of a  $64 \times 32$  MIMO OFDM mmWave system, based on the proposed hybrid precoding and channel estimation algorithms, as a function of SNR.

---

**Algorithm 3** Proposed Channel Estimation For Frequency-Selective MmWave Channels
 

---

**Require:** BS and MS know  $N, V, L$ , and have  $\mathcal{F}, \mathcal{W}$ 
**Initialization**

- 1:  $\mathbf{T}_{1,1}^{\text{BS}}[k] = \{1, \dots, 1\}$ ,  $\mathbf{T}_{1,1}^{\text{MS}}[k] = \{1, \dots, 1\}$
- 2:  $S = \log_V(N/L)$

**Channel Estimation Procedure**

- 3: **for**  $l \leq L$  **do**
  - 4:     **for**  $s \leq S$  **do**
  - 5:         **for**  $k \leq K$  **do**
  - 6:             **for**  $m_{\text{BS}} \leq VL$  **do**
  - 7:                 BS uses  $[\mathbf{F}_{\text{BB},(s,\mathbf{T}_{l,s}^{\text{BS}}[k])}[k]]_{:,m_{\text{BS}}}$
  - 8:                 BS uses  $\mathbf{F}_{\text{RF},(s,\mathbf{T}_{l,s}^{\text{BS}}[k])}$
  - 9:                 **for**  $m_{\text{MS}} \leq VL$  **do**
  - 10:                     MS uses  $\mathbf{W}_{\text{RF},(s,\mathbf{T}_{l,s}^{\text{MS}}[k])}$
  - 11:                     MS uses  $[\mathbf{W}_{\text{BB},(s,\mathbf{T}_{l,s}^{\text{MS}}[k])}[k]]_{:,m_{\text{MS}}}$
  - 12:                 **end for**
  - 13:                 After MS measurements:
  - 14:                  $\mathbf{y}_{m_{\text{BS}}}[k] = \mathbf{W}_{\text{BB},(s,\mathbf{T}_{l,s}^{\text{MS}}[k])}^* [k] \dots$   
 $\mathbf{W}_{\text{RF},(s,\mathbf{T}_{l,s}^{\text{MS}}[k])}^* \mathbf{H}[k] \mathbf{F}_{\text{RF},(s,\mathbf{T}_{l,s}^{\text{BS}}[k])} [\mathbf{F}_{\text{BB},(s,\mathbf{T}_{l,s}^{\text{BS}}[k])}[k]]_{:,m_{\text{BS}}} + \mathbf{n}[k]$
  - 15:                 **end for**
  - 16:                 After BS measurements:
  - 17:                  $\mathbf{y}_{(s)}[k] = [\mathbf{y}_1^{\text{T}}[k], \mathbf{y}_2^{\text{T}}[k], \dots, \mathbf{y}_V^{\text{T}}[k]]^{\text{T}}$
  - 18:                 **for**  $p = 1 \leq l - 1$  **do**
  - 19:                     Remove previous path contributions from the history matrix  $\mathbf{T}$
  - 20:                      $\mathbf{g} = \mathbf{s}[k]^{\text{T}} \mathbf{F}_{\text{BB},(s,\mathbf{T}_{p,s}^{\text{BS}}[k])}^{\text{T}} [k] \mathbf{F}_{\text{RF},(s,\mathbf{T}_{p,s}^{\text{BS}}[k])}^{\text{T}} \dots$   
 $[\mathbf{A}_{\text{BS},\text{D}}^{\text{T}}]_{:, \mathbf{T}_{p,s}^{\text{BS}}[k](1)} \otimes \mathbf{W}_{\text{BB},(s,\mathbf{T}_{p,s}^{\text{MS}}[k])}^* [k] \mathbf{W}_{\text{RF},(s,\mathbf{T}_{p,s}^{\text{MS}}[k])}^* [\mathbf{A}_{\text{MS},\text{D}}]_{:, \mathbf{T}_{p,s}^{\text{MS}}[k](1)}$
  - 21:                      $\mathbf{y}_{(s)}[k] = \mathbf{y}_{(s)}[k] - \mathbf{y}_{(s)}^*[k] \mathbf{g} (\mathbf{g}^* \mathbf{g}) \mathbf{g}$
  - 22:                 **end for**
  - 23:                  $\mathbf{Y}[k] = \text{matrix}(\mathbf{y}_{(s)}[k])$ , return  $\mathbf{y}_{(s)}[k]$  to the matrix form
  - 24:                  $(m_{\text{BS}}^*, m_{\text{MS}}^*) = \underset{\forall m_{\text{BS}}, m_{\text{MS}}=1,2,\dots,V}{\text{argmax}} [\mathbf{Y}[k] \odot \mathbf{Y}^*[k]]_{m_{\text{BS}}, m_{\text{MS}}}$
  - 25:                  $\mathbf{T}_{l,s+1}^{\text{BS}}[k](1) = V(m_{\text{BS}}^* - 1) + 1$
  - 26:                  $\mathbf{T}_{l,s+1}^{\text{MS}}[k](1) = V(m_{\text{MS}}^* - 1) + 1$
  - 27:                 **for**  $p = 1 \leq l - 1$  **do**
  - 28:                      $\mathbf{T}_{l,s+1}^{\text{BS}}[k](p) = \mathbf{T}_{p,s+1}^{\text{BS}}[k](1)$
  - 29:                      $\mathbf{T}_{l,s+1}^{\text{MS}}[k](p) = \mathbf{T}_{p,s+1}^{\text{MS}}[k](1)$
  - 30:                 **end for**
  - 31:             **end for**
  - 32:     **end for**
  - 33: **end for**
-

---



---

```

34: for  $k \leq K$  do
35:   for  $l \leq L$  do
36:     AoDs and AoAs estimation:
37:      $\hat{\phi}_l[k] = \hat{\phi}_{\mathbf{T}_{l,S+1}^{\text{BS}}[k](1)}, \hat{\theta}_l[k] = \hat{\theta}_{\mathbf{T}_{l,S+1}^{\text{MS}}[k](1)}$ 
38:      $\Delta[k]$  estimation:
39:      $\mathbf{g} = \mathbf{s}[k]^T \mathbf{F}_{\text{BB},(S,\mathbf{T}_{l,S}^{\text{BS}}[k])}^T [k] \mathbf{F}_{\text{RF},(S,\mathbf{T}_{l,S}^{\text{BS}}[k])}^T [\mathbf{A}_{\text{BS,D}}^T]_{:, \mathbf{T}_{l,S}^{\text{BS}}[k](1)} \otimes$ 
        $\mathbf{W}_{\text{BB},(S,\mathbf{T}_{l,S}^{\text{MS}}[k])}^* [k] \mathbf{W}_{\text{RF},(S,\mathbf{T}_{l,S}^{\text{MS}}[k])}^* [\mathbf{A}_{\text{MS,D}}]_{:, \mathbf{T}_{l,S}^{\text{MS}}[k](1)}$ 
40:      $\Delta_l[k] = \mathbf{y}_{(S)}^* [k] \mathbf{g} / \mathbf{g}^* \mathbf{g}$ 
41:   end for
42: end for

```

---

Subsequently, the second part of the algorithm starts, in which the estimation process is done. The process makes  $L$  outer iterations to detect each path. During each outer iteration,  $S$  inner iterations or stages are carried out. At each stage, the AoAs/AoDs angular ranges are divided into  $V$  non-overlapped angular sub-ranges,  $V$  beam patterns are used to send the pilot signal and  $V$  beam patterns are used to combine the signal at the RX. Hence, each stage needs  $V^2$  time slots to span all the combinations of transmit-receive beam patterns. The beam patterns are taken from the predefined codebook designed in section 2.4. Afterwards, the contributions of the detected paths that are stored in  $\mathbf{T}^{\text{BS}}$  and  $\mathbf{T}^{\text{MS}}$  are projected out at step 20. The process is then continued by calculating the magnitudes of the  $V^2$  received signals at step 24 to determine the next AoAs/AoDs angular sub-range for the next stage. At each stage, the process pursues the same way as in the previous stage, in which it divides the chosen AoDs sub-range at the TX and AoAs sub-range at the RX into  $V$  sub-ranges. It proceeds this way until it achieves the desired AoAs/AoDs resolution  $N$ .

## 3.8 Results

We evaluate by simulation the performance of the proposed FS hybrid precoding and combining designs, along with the proposed channel estimation algorithm for mmWave MIMO OFDM systems with  $N_{\text{BS}} = 64, N_{\text{MS}} = 32$ . We assume in these simulations that both the BS and MS have a ULA. We adopt a wideband mmWave channel model with  $L = 3$  paths. Furthermore, concerning the dynamics of the channel, we restricted our work to scenarios where the channel is invariant over

several OFDM symbols. We assume that the center AoAs/AoDs of the  $L$  paths are uniformly distributed in  $[0, 2\pi)$ . The number of subcarriers is  $K = 64$ , with 7 quantization bits, unless stated otherwise. The results are conducted over 100 different channel realizations for 16 symbols.

In Figure 3.8, the SEs achieved employing the proposed channel estimation algorithm are plotted versus SNR for different number of RF chains. The SEs achieved by the hybrid precoding and channel estimation algorithms are compared with both 1) the hybrid precoding with PCSI mmWave hybrid MIMO OFDM system, and 2) the optimal unconstrained SVD (fully-digital SVD precoder) with PCSI mmWave hybrid MIMO OFDM system. As expected, as the number of RF chains at the BS and MS increases, the SEs increase, and the performance becomes very close to the hybrid precoding with PCSI system for the case of 16 RF chains at the BS and MS, this illustrates the validity of the proposed channel estimation algorithm for practical mmWave systems. The SEs for the SVD optimal solution with PCSI are also presented as a benchmark.

In Figure 3.9, the improvement of the precoding gains achieved by the proposed algorithm versus the number of grid points is simulated for  $\text{SNR} = -10$  dB. These results indicate that a wise choice of the desired resolution parameter is needed in order to have a good performance. For example, the figure shows that doubling the number of grid points, i.e., from 96 to 192, achieves an improvement of only 1 bps/Hz in the SE.

In Figure 3.10, the SEs are plotted versus the number of quantization bits for  $\text{SNR} = -13$  dB. As expected and as can be seen from the figure that the performance increases as the number of quantization bits increases, and that 7 to 8 quantization bits would be enough to have good performance. The SE in the case of unconstrained precoding with PCSI has been presented for comparison.

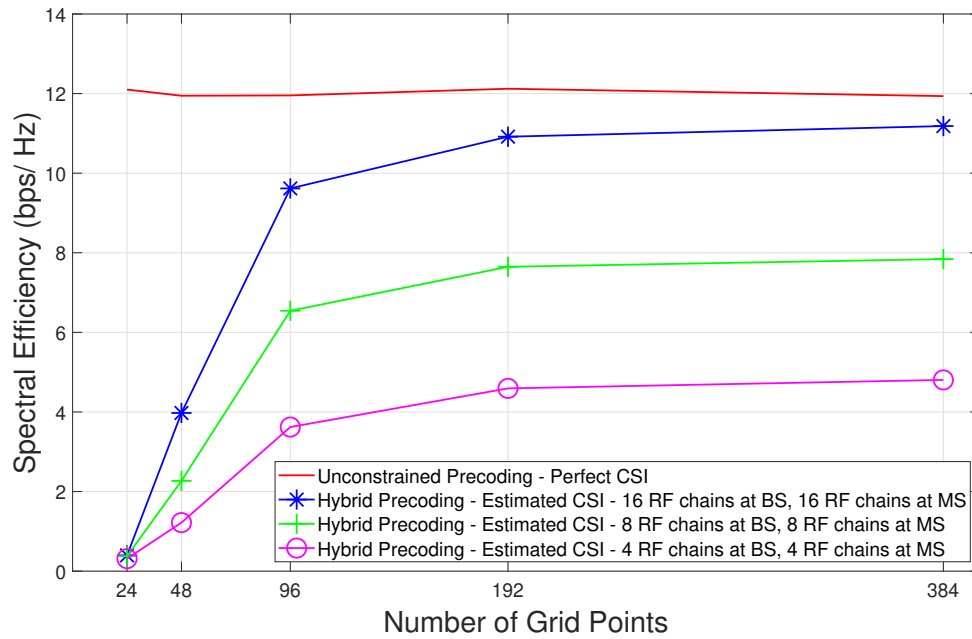


Figure 3.9: SEs of a  $64 \times 32$  MIMO OFDM mmWave system employing the proposed hybrid precoding and channel estimation algorithms versus the number of resolution  $N$  when  $\text{SNR} = 10$  dB.

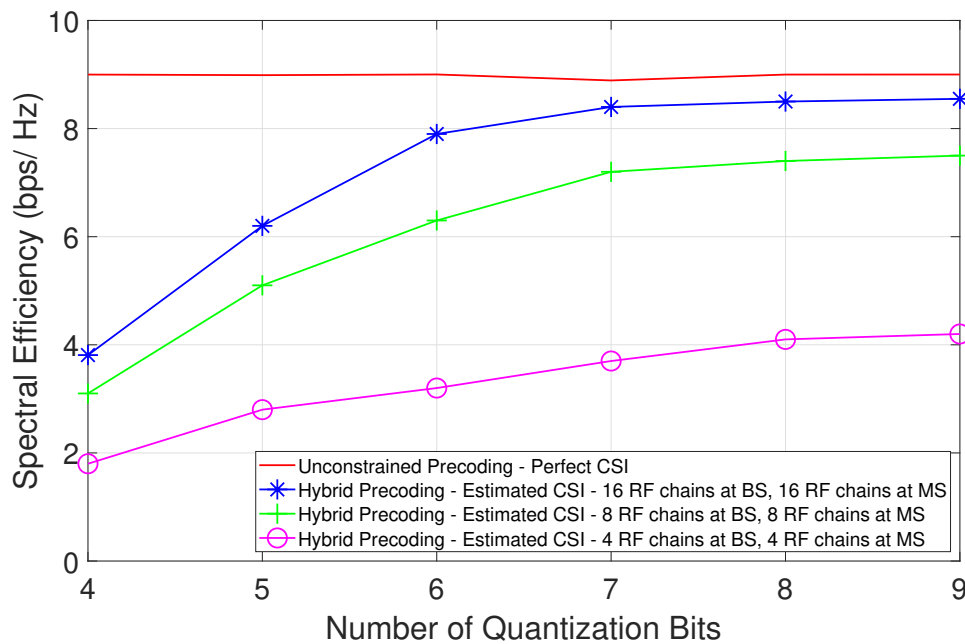


Figure 3.10: SEs of a  $64 \times 32$  MIMO OFDM mmWave system employing the proposed hybrid precoding and channel estimation algorithms versus the number of quantization bits when  $\text{SNR} = 13$  dB.

### 3.9 Conclusions

This chapter has presented two algorithms, the first being a proposed approach for designing an FS hybrid multi-resolution codebook, the second being a proposed FS channel estimation algorithm for next generation mmWave communications. An FS OMP-based codebook has been proposed to design the hybrid precoders. Afterwards, a channel estimation algorithm has been proposed for mmWave MIMO FS channels. Simulation results showed that the proposed algorithms can perform well compared to mmWave systems with PCSI when employing an appropriate number of RF chains with a wise choice of the desired resolution parameter. Basically, we have seen that the performance of the proposed algorithms approaches that of the hybrid precoding with PCSI system, demonstrating the applicability of the proposed channel estimation algorithm for actual mmWave systems. Furthermore, the proposed algorithm can be convenient for future mmWave MIMO communication systems which will use the mmWave bands.



# General Conclusions and Perspectives

Through the deployment of a high number of antennas at the transmitters and receivers, MIMO communication is expected to play a key role in future wireless systems. Massive MIMO improves the spectral efficiency of low-frequency systems by providing huge multiplexing improvements. Massive antenna arrays must be deployed at both the base station and mobile users in mmWave systems to ensure sufficient received signal power. However, putting these approaches into practice entails overcoming many major challenges, such as hardware limitations, channel acquisition overhead, and precoding design complexity. The goal of this dissertation was to propose precoding and channel estimating methods to address these key challenges in mmWave systems. First, we proposed frequency-selective hybrid analog/digital precoding algorithms adopting FBMC-OQAM signaling for MIMO mmWave systems. Second, we introduced efficient mmWave channel estimation technique that exploits the channels' sparse characteristics.

The following sections detail the major topics explored in this Ph.D. thesis, as well as our major contributions and conclusions. Following that, we present the many options and perspectives that could be explored.

## Summary and Conclusions

In chapter 1, the features of mmWave channels, such as the differences between propagation behavior in mmWave bands and sub-6 GHz bands, are first illustrated in section 1.2. This is important to aid in comprehending the technical promise of mmWave communications, the problems that must be overcome in order to realize this potential, and the enabler technologies that will address these challenges. Then, in section 1.3, we went over the various existing system architectures for massive MIMO mmWave systems that have been proposed. Before presenting the massive MIMO system model, the spatial MIMO channel models are presented, which demonstrate the unique character of highly-directive mmWave communications. We introduce multi-carrier

modulation techniques in section 1.4, and we have showed the modulation waveforms that have been used in this Ph.D. thesis, such as the FBMC-OQAM waveform in chapter 2 and the OFDM waveform in chapter 3. After that, section 1.5 introduced compressive sensing as a mathematical method for channel estimation, in which the suggested channel estimation algorithm in chapter 3 is based.

In chapter 2, we looked at single-user precoding and combining, as well as the viability of using the FBMC-OQAM signaling waveform for next-generation mmWave communications, where standard MIMO solutions aren't possible due to the high reliance on RF precoding. Using the structure of realistic mmWave channels, we developed a low-hardware-complexity precoding technique. We rephrased the mmWave precoder design problem as a sparsity-constrained signal recovery problem, and then proposed an algorithmic solution based on OMP. As we demonstrated, the problem of constructing realistic MMSE combiners for mmWave systems may be solved using the same approach using OMP method. We demonstrated that the suggested precoders can be quantized efficiently, and that the precoding technique is well-suited for restricted feedback systems. Finally, numerical results on the performance of spatially sparse mmWave processing were presented, revealing that adopting FBMC-OQAM with our proposed algorithms improves the efficiency of mmWave systems, hence, FBMC-OQAM waveform could be a good fit for future mmWave MIMO communication systems, particularly when high SE is a priority.

In chapter 3, both algorithms have been provided, the first is a proposed approach for developing an FS hybrid multi-resolution codebook, and the second is a proposed FS channel estimation algorithm for next-generation mmWave communications. To design the hybrid precoders, an FS OMP-based codebook has been proposed. Following that, a channel estimation algorithm for mmWave MIMO FS channels was suggested. The suggested algorithms outperform mmWave systems with PCSI, with performance approaching that of the hybrid precoding with PCSI system, highlighting the importance of the proposed channel estimation technique for actual mmWave systems. Hence, the suggested technique may be useful for future mmWave MIMO communication systems that employ the mmWave bands.

## Perspectives

In this section, we provide our visions and perspectives for future problems and research that need to be addressed and investigated. We have classified the perspectives into short-term perspectives and long-term perspectives.

### Short-term Perspectives

- High mobility : Accurate alignment of narrow beams of mmWave transmission is essential to avoid a significant loss in received power in the high mobility scenarios, such as vehicular mmWave systems, since the high mobility will increase the beam training and alignment overhead. In order to establish a stable link between the BS and the MS, the channel estimation, and hence the beam alignment, must be completed or joined with a beam tracking scheme in order to track the variations in AoDs/AoAs at the receiver. We didn't study the effect of mobility on our FS systems, which is not practical, since mmWave channels are time-variant channels having high mobility for some scenarios. Hence, some extensive research is needed to adapt our channel estimation technique to practical and fast estimation/tracking mmWave channels.
- Quantization errors: The beam steering directions are assumed to be quantized, i.e. the AoAs/AoDs are considered discrete against continuous ones in practice, which leads to quantization errors in channel estimation algorithms. The impact of this quantization errors on the performance of the proposed algorithms must be evaluated and new improved ones must be proposed if necessary. In other words, the values of the AoAs/AoDs are continuous in practice, hence, some other more realistic off-grid based algorithms can be used to reduce the quantization error, like continuous BP [186], Newton refinement ideas [187], sparse regularized total least squared [188]. In our work, we only exploited the case of quantized AoAs/AoDs, letting possible improvements for future work.
- Multi-user scenario: The application of mmWave communications to cellular systems implies to consider multi-user communications. This also requires to employ some multiple access

scheme such as orthogonal frequency-division multiplexing access, semi-orthogonal multiple access scheme [189], or non-orthogonal multiple access [190]. Our work has been done for single-user scenario, which is not realistic. The employed multiple access scheme must be taken into consideration in the design of channel estimation techniques. Furthermore, an additional effort must be dedicated to the pilot contamination problem which could limit the number of scheduled users and degrades the channel estimation accuracy.

## Long-term Perspectives

- Other mmWave architectures and waveforms: The wide bandwidth available in the mmWave bands leads inevitably to frequency-selective channels since the different frequency components will experience independent fadings. This problem is traditionally solved by employing appropriate waveforms such as OFDM, FBMC or UFMC, among others. Our channel estimation technique for wideband systems has been mainly proposed for hybrid architecture with OFDM. This area must be further explored to cover all the architectures and all the waveforms in order to propose tailored channel estimation solutions and to try to keep up with the latest advances in this domain.
- Graphical models: The channel estimation problem can be reformulated such as it can be represented in factor graph models which allows to employ the message passing algorithms as a powerful solution. This approach was exploited in the literature especially for the systems with few-bit ADCs. It is promising to extend this effort to hybrid architecture systems and incorporate it in our system, and to use also other variations of message passing algorithms such as expectation-propagation algorithms and belief-propagation algorithms and their different approximations.
- Machine learning: It is not complicated to collect a large amount of wireless communications data which makes worth investigating if machine learning tools are capable to inspect the structure of the received signal and hence to estimate the mmWave channel. This idea becomes more legitimate with the recent advances in machine learning fields especially the deep learning which proposes several efficient tools such as deep convolutional neural networks,

recurrent neural Networks, and Bayesian neural networks, and their different variations. We didn't exploit these promising techniques in our channel estimation technique, that is why it is deemed as promising and attractive to propose new channel estimation techniques based on these deep learning tools.

- 3D : A 3D channel estimation means that neither the elevation scattering nor the horizontal scattering is neglected. Indeed, it is more practical to know the AoAs and the AoDs in both the horizontal and the vertical plans. In our work we only explored the 2D channel estimation case. This work can be developed by introducing new 3D estimation solutions for hybrid architectures which will make these estimation techniques more robust and realistic.
- Antenna array design: Beamforming gains are enabled by antenna arrays which are composed of several antenna elements that can be distributed via different geometrical configuration (linear, planar, circular) [191] and array layouts (uniform and non-uniform) [192]. We adopted ULAs for our system. It will be useful to adopt different antenna configurations and study their impacts.
- Cognitive radio: One solution to increase the spectral efficiency and to reply to the increasing traffic demand is to combine cognitive radio and mmWave communications, this perspective had been studied in several recent research works [193, 194, 195]. In this context, the problem of joint channel estimation and spectrum sensing for the secondary and the primary users must be further investigated.



# Bibliography

- [1] Ericsson. *Ericsson Mobility Report*. Tech. rep. Stockholm, Sweden, June 2019. URL: <https://www.ericsson.com/en/mobility-report/reports/june-2019>.
- [2] M. Agiwal, A. Roy, and N. Saxena. “Next Generation 5G Wireless Networks: A Comprehensive Survey”. In: *IEEE Communications Surveys Tutorials* 18.3 (2016), pp. 1617–1655.
- [3] Yong Niu et al. “A survey of millimeter wave communications (mmWave) for 5G: opportunities and challenges”. en. In: *Wireless Networks* 21.8 (Nov. 2015), pp. 2657–2676. ISSN: 1572-8196. DOI: 10.1007/s11276-015-0942-z. (Visited on 10/03/2019).
- [4] J. G. Andrews et al. “Modeling and Analyzing Millimeter Wave Cellular Systems”. In: *IEEE Transactions on Communications* 65.1 (2017), pp. 403–430.
- [5] M. Xiao et al. “Millimeter Wave Communications for Future Mobile Networks”. In: *IEEE Journal on Selected Areas in Communications* 35.9 (2017), pp. 1909–1935.
- [6] I. A. Hemadeh et al. “Millimeter-Wave Communications: Physical Channel Models, Design Considerations, Antenna Constructions, and Link-Budget”. In: *IEEE Communications Surveys Tutorials* 20.2 (2018), pp. 870–913.
- [7] T. S. Rappaport et al. “Millimeter Wave Mobile Communications for 5G Cellular: It Will Work!” In: *IEEE Access* 1 (2013), pp. 335–349.
- [8] W. Roh et al. “Millimeter-wave beamforming as an enabling technology for 5G cellular communications: theoretical feasibility and prototype results”. In: *IEEE Communications Magazine* 52.2 (2014), pp. 106–113.
- [9] A. Alkhateeb et al. “MIMO Precoding and Combining Solutions for Millimeter-Wave Systems”. In: *IEEE Communications Magazine* 52.12 (2014), pp. 122–131.
- [10] Theodore S Rappaport et al. *Millimeter Wave Wireless Communications*. Prentice Hall, 2015.
- [11] *IEEE Standard for Information technology–Telecommunications and information exchange between systems–Local and metropolitan area networks–Specific requirements–Part 11: Wireless LAN Medium Access Control (MAC) and Physical Layer (PHY) Specifications Amendment 3: Enhancements for Very High Throughput in the 60 GHz Band*. Tech. rep. IEEE. DOI: 10.1109/IEEESTD.2012.6392842. (Visited on 10/08/2019).

- 
- [12] *IEEE Standard for Information technology– Local and metropolitan area networks– Specific requirements– Part 15.3: Amendment 2: Millimeter-wave-based Alternative Physical Layer Extension*. Tech. rep. IEEE. DOI: 10.1109/IEEESTD.2009.5284444. (Visited on 10/08/2019).
- [13] WiGig. *Defining the Future of Multi-Gigabit Wireless Communications*. White Paper. July 2010.
- [14] T. S. Rappaport et al. “Wireless Communications and Applications Above 100 GHz: Opportunities and Challenges for 6G and Beyond”. In: *IEEE Access* 7 (2019), pp. 78729–78757.
- [15] Samsung. *Feasibility of Mobility for 28 GHz millimeter-wave Systems*. Tech. rep. Sept. 2018.
- [16] Huawei. *Deutsche Telekom and Huawei Complete World’s First 5G High mmWave Technology over-the-air Field Tests*. Feb. 2018. URL: <https://www.huawei.com/en/press-events/news/2018/2/DectschTelckom-5G-High-mmWave-Technology>.
- [17] M. Marcus and B. Pattan. “Millimeter wave propagation: spectrum management implications”. In: *IEEE Microwave Magazine* 6.2 (2005), pp. 54–62.
- [18] X. Zhang and J. G. Andrews. “Downlink Cellular Network Analysis With Multi-Slope Path Loss Models”. In: *IEEE Transactions on Communications* 63.5 (2015), pp. 1881–1894.
- [19] S. Sun, G. R. MacCartney, and T. S. Rappaport. “Millimeter-wave distance-dependent large-scale propagation measurements and path loss models for outdoor and indoor 5G systems”. In: *2016 10th European Conference on Antennas and Propagation (EuCAP)*. 2016, pp. 1–5.
- [20] M. R. Akdeniz et al. “Millimeter Wave Channel Modeling and Cellular Capacity Evaluation”. In: *IEEE Journal on Selected Areas in Communications* 32.6 (2014), pp. 1164–1179.
- [21] T. S. Rappaport et al. “Wideband Millimeter-Wave Propagation Measurements and Channel Models for Future Wireless Communication System Design”. In: *IEEE Transactions on Communications* 63.9 (2015), pp. 3029–3056.
- [22] Yusra Banday, Ghulam Mohammad Rather, and Gh. Rasool Begh. “Effect of atmospheric absorption on millimetre wave frequencies for 5G cellular networks”. en. In: *IET Communications* 13.3 (Feb. 2019), pp. 265–270. ISSN: 1751-8628, 1751-8636. DOI: 10.1049/iet-com.2018.5044. (Visited on 11/13/2019).

- [23] Dalia Nandi and Animesh Maitra. “Study of rain attenuation effects for 5G Mm-wave cellular communication in tropical location”. en. In: *IET Microwaves, Antennas & Propagation* 12.9 (July 2018), pp. 1504–1507. ISSN: 1751-8725, 1751-8733. DOI: 10.1049/iet-map.2017.1029. (Visited on 11/13/2019).
- [24] H. Zhao et al. “28 GHz millimeter wave cellular communication measurements for reflection and penetration loss in and around buildings in New York city”. In: *2013 IEEE International Conference on Communications (ICC)*. 2013, pp. 5163–5167.
- [25] Kais Hassan et al. “Channel Estimation Techniques for Millimeter-Wave Communication Systems: Achievements and Challenges”. In: *IEEE Open Journal of the Communications Society* 1 (2020), pp. 1336–1363. DOI: 10.1109/OJCOMS.2020.3015394.
- [26] Z. Pi and F. Khan. “An introduction to millimeter-wave mobile broadband systems”. In: *IEEE Communications Magazine* 49.6 (2011), pp. 101–107.
- [27] Huawei Technologies. *5G spectrum public policy position*. Tech. rep. 2017.
- [28] L. Zhang et al. “A Survey on 5G Millimeter Wave Communications for UAV-Assisted Wireless Networks”. In: *IEEE Access* 7 (2019), pp. 117460–117504.
- [29] FCC. *Use of Spectrum Bands Above 24 GHz for Mobile Radio Services*. Tech. rep. 84 FR 20810. 2019.
- [30] Q. Xue et al. “Performance Analysis of Interference and Eavesdropping Immunity in Narrow Beam mmWave Networks”. In: *IEEE Access* 6 (2018), pp. 67611–67624.
- [31] E. Bjornson et al. “Massive MIMO in Sub-6 GHz and mmWave: Physical, Practical, and Use-Case Differences”. In: *IEEE Wireless Communications* 26.2 (2019), pp. 100–108.
- [32] S. Rangan, T. S. Rappaport, and E. Erkip. “Millimeter-Wave Cellular Wireless Networks: Potentials and Challenges”. In: *Proceedings of the IEEE* 102.3 (2014), pp. 366–385.
- [33] T. S. Rappaport, J. N. Murdock, and F. Gutierrez. “State of the Art in 60-GHz Integrated Circuits and Systems for Wireless Communications”. In: *Proceedings of the IEEE* 99.8 (2011), pp. 1390–1436.
- [34] C. H. Doan et al. “Design considerations for 60 GHz CMOS radios”. In: *IEEE Communications Magazine* 42.12 (2004), pp. 132–140.
- [35] Lou Zhao. “Millimeter Wave Systems for Wireless Cellular Communications”. In: *arXiv:1811.12606 [cs, math]* (Nov. 2018). arXiv: 1811.12606. (Visited on 05/28/2019).

- 
- [36] Shuguang Cui, A. J. Goldsmith, and A. Bahai. “Energy-efficiency of MIMO and cooperative MIMO techniques in sensor networks”. In: *IEEE Journal on Selected Areas in Communications* 22.6 (2004), pp. 1089–1098.
- [37] Y. Teng et al. “Resource Allocation for Ultra-Dense Networks: A Survey, Some Research Issues and Challenges”. In: *IEEE Communications Surveys Tutorials* 21.3 (2019), pp. 2134–2168.
- [38] M. Kamel, W. Hamouda, and A. Youssef. “Ultra-Dense Networks: A Survey”. In: *IEEE Communications Surveys Tutorials* 18.4 (2016), pp. 2522–2545.
- [39] S. Han et al. “Large-scale antenna systems with hybrid analog and digital beamforming for millimeter wave 5G”. In: *IEEE Communications Magazine* 53.1 (2015), pp. 186–194.
- [40] M. Boers et al. “A 16TX/16RX 60 GHz 802.11ad Chipset With Single Coaxial Interface and Polarization Diversity”. In: *IEEE Journal of Solid-State Circuits* 49.12 (2014), pp. 3031–3045.
- [41] B. Biglarbegan et al. “Optimized Microstrip Antenna Arrays for Emerging Millimeter-Wave Wireless Applications”. In: *IEEE Transactions on Antennas and Propagation* 59.5 (2011), pp. 1742–1747.
- [42] S. Kutty and D. Sen. “Beamforming for Millimeter Wave Communications: An Inclusive Survey”. In: *IEEE Communications Surveys Tutorials* 18.2 (2016), pp. 949–973.
- [43] Junyi Wang et al. “Beam codebook based beamforming protocol for multi-Gbps millimeter-wave WPAN systems”. In: *IEEE Journal on Selected Areas in Communications* 27.8 (2009), pp. 1390–1399.
- [44] S. Hur et al. “Multilevel millimeter wave beamforming for wireless backhaul”. In: *2011 IEEE GLOBECOM Workshops (GC Wkshps)*. 2011, pp. 253–257.
- [45] S. Hur et al. “Millimeter Wave Beamforming for Wireless Backhaul and Access in Small Cell Networks”. In: *IEEE Transactions on Communications* 61.10 (2013), pp. 4391–4403.
- [46] P. Xia et al. “A practical SDMA protocol for 60 GHz millimeter wave communications”. In: *2008 42nd Asilomar Conference on Signals, Systems and Computers*. 2008, pp. 2019–2023.
- [47] P. Xia et al. “Practical Antenna Training for Millimeter Wave MIMO Communication”. In: *2008 IEEE 68th Vehicular Technology Conference*. 2008, pp. 1–5.

- 
- [48] P. Xia et al. “Multi-Stage Iterative Antenna Training for Millimeter Wave Communications”. In: *IEEE GLOBECOM 2008 - 2008 IEEE Global Telecommunications Conference*. 2008, pp. 1–6.
- [49] Z. Xiao, L. Bai, and J. Choi. “Iterative Joint Beamforming Training with Constant-Amplitude Phased Arrays in Millimeter-Wave Communications”. In: *IEEE Communications Letters* 18.5 (2014), pp. 829–832.
- [50] Xinying Zhang, A. F. Molisch, and Sun-Yuan Kung. “Variable-phase-shift-based RF-baseband codesign for MIMO antenna selection”. In: *IEEE Transactions on Signal Processing* 53.11 (2005), pp. 4091–4103.
- [51] T. S. Rappaport et al. “Broadband Millimeter-Wave Propagation Measurements and Models Using Adaptive-Beam Antennas for Outdoor Urban Cellular Communications”. In: *IEEE Transactions on Antennas and Propagation* 61.4 (2013), pp. 1850–1859.
- [52] 3GPP. *Final report of {3GPP TSG RAN WG1} (85)*. Tech. rep. 3GPP, 2016.
- [53] O. E. Ayach et al. “Spatially Sparse Precoding in Millimeter Wave MIMO Systems”. In: *IEEE Transactions on Wireless Communications* 13.3 (2014), pp. 1499–1513.
- [54] X. Gao et al. “Energy-Efficient Hybrid Analog and Digital Precoding for MmWave MIMO Systems With Large Antenna Arrays”. In: *IEEE Journal on Selected Areas in Communications* 34.4 (2016), pp. 998–1009.
- [55] R. Méndez-Rial et al. “Hybrid MIMO Architectures for Millimeter Wave Communications: Phase Shifters or Switches?” In: *IEEE Access* 4 (2016), pp. 247–267.
- [56] A. Alkhateeb et al. “Massive MIMO Combining with Switches”. In: *IEEE Wireless Communications Letters* 5.3 (2016), pp. 232–235.
- [57] S. Payami et al. “Phase Shifters Versus Switches: An Energy Efficiency Perspective on Hybrid Beamforming”. In: *IEEE Wireless Communications Letters* 8.1 (2019), pp. 13–16.
- [58] J. Brady, N. Behdad, and A. M. Sayeed. “Beamspace MIMO for Millimeter-Wave Communications: System Architecture, Modeling, Analysis, and Measurements”. In: *IEEE Transactions on Antennas and Propagation* 61.7 (2013), pp. 3814–3827.
- [59] Y. Zeng and R. Zhang. “Millimeter Wave MIMO With Lens Antenna Array: A New Path Division Multiplexing Paradigm”. In: *IEEE Transactions on Communications* 64.4 (2016), pp. 1557–1571.

- [60] J. Mo and R. W. Heath. “Capacity Analysis of One-Bit Quantized MIMO Systems With Transmitter Channel State Information”. In: *IEEE Transactions on Signal Processing* 63.20 (2015), pp. 5498–5512.
- [61] T. Zhang et al. “Mixed-ADC Massive MIMO Detectors: Performance Analysis and Design Optimization”. In: *IEEE Transactions on Wireless Communications* 15.11 (2016), pp. 7738–7752.
- [62] J. Mo, P. Schniter, and R. W. Heath. “Channel Estimation in Broadband Millimeter Wave MIMO Systems With Few-Bit ADCs”. In: *IEEE Transactions on Signal Processing* 66.5 (2018), pp. 1141–1154.
- [63] H. He, C. Wen, and S. Jin. “Bayesian Optimal Data Detector for Hybrid mmWave MIMO-OFDM Systems With Low-Resolution ADCs”. In: *IEEE Journal of Selected Topics in Signal Processing* 12.3 (2018), pp. 469–483.
- [64] J. P. González-Coma et al. “Channel Estimation and Hybrid Precoding for Frequency Selective Multiuser mmWave MIMO Systems”. In: *IEEE Journal of Selected Topics in Signal Processing* 12.2 (2018), pp. 353–367.
- [65] R. W. Heath et al. “An Overview of Signal Processing Techniques for Millimeter Wave MIMO Systems”. In: *IEEE Journal of Selected Topics in Signal Processing* 10.3 (2016), pp. 436–453.
- [66] A. Kammoun et al. “Preliminary Results on 3D Channel Modeling: From Theory to Standardization”. In: *IEEE Journal on Selected Areas in Communications* 32.6 (2014), pp. 1219–1229.
- [67] M. Dong et al. “Simulation study on millimeter wave 3D beamforming systems in urban outdoor multi-cell scenarios using 3D ray tracing”. In: *2015 IEEE 26th Annual International Symposium on Personal, Indoor, and Mobile Radio Communications (PIMRC)*. 2015, pp. 2265–2270.
- [68] Dian-Wu Yue, Shuai Xu, and Ha H. Nguyen. “Diversity gain of millimeter-wave massive MIMO systems with distributed antenna arrays”. en. In: *EURASIP Journal on Wireless Communications and Networking* 2019.1 (Mar. 2019), p. 54. ISSN: 1687-1499. DOI: 10.1186/s13638-019-1366-8. (Visited on 03/20/2019).
- [69] R. Shafin et al. “DoA Estimation and Capacity Analysis for 3-D Millimeter Wave Massive-MIMO/FD-MIMO OFDM Systems”. In: *IEEE Transactions on Wireless Communications* 15.10 (2016), pp. 6963–6978.
- [70] W. Ma and C. Qi. “Channel Estimation for 3-D Lens Millimeter Wave Massive MIMO System”. In: *IEEE Communications Letters* 21.9 (2017), pp. 2045–2048.

- [71] T. Cheng et al. “Low-Complexity Channel Estimation in 3D Lens Millimeter-Wave Massive MIMO Systems”. In: *2018 24th Asia-Pacific Conference on Communications (APCC)*. 2018, pp. 347–352.
- [72] Andreas F. Molisch. *Wireless Communications*. Second. Wiley-IEEE Press, 2011.
- [73] Shahid Mumtaz, Jonathan Rodriguez, and Linglong Dai. *mmWave Massive MIMO - 1st Edition*. Elsevier, 2017. (Visited on 03/20/2019).
- [74] L. Yang, Y. Zeng, and R. Zhang. “Channel Estimation for Millimeter-Wave MIMO Communications With Lens Antenna Arrays”. In: *IEEE Transactions on Vehicular Technology* 67.4 (2018), pp. 3239–3251.
- [75] M. L. Doelz, E. T. Heald, and D. L. Martin. “Binary Data Transmission Techniques for Linear Systems”. In: *Proceedings of the IRE* 45.5 (1957), pp. 656–661. DOI: 10.1109/JRPROC.1957.278415.
- [76] “Orthogonal Frequency Division Multiplexing”. In: *U.S. Patent No. 3,488,4555, filed November 14, 1966, issued January 6, 1970*. ().
- [77] J.A.C. Bingham. “Multicarrier modulation for data transmission: an idea whose time has come”. In: *IEEE Communications Magazine* 28.5 (1990), pp. 5–14. DOI: 10.1109/35.54342.
- [78] Zhendao Wang and G.B. Giannakis. “Wireless multicarrier communications”. In: *IEEE Signal Processing Magazine* 17.3 (2000), pp. 29–48. DOI: 10.1109/79.841722.
- [79] Richard DJ Van Nee and Ramjee Prasad. “OFDM for wireless multimedia communications”. In: (2000).
- [80] Paolo Banelli et al. “Modulation Formats and Waveforms for 5G Networks: Who Will Be the Heir of OFDM?: An overview of alternative modulation schemes for improved spectral efficiency”. In: *IEEE Signal Processing Magazine* 31.6 (2014), pp. 80–93. DOI: 10.1109/MSP.2014.2337391.
- [81] Alphan Sahin et al. “An Improved Unique Word DFT-Spread OFDM Scheme for 5G Systems”. In: *2015 IEEE Globecom Workshops (GC Wkshps)*. 2015, pp. 1–6. DOI: 10.1109/GLOCOMW.2015.7414173.
- [82] R. Zayani et al. “WOLA-OFDM: A Potential Candidate for Asynchronous 5G”. In: *2016 IEEE Globecom Workshops (GC Wkshps)*. 2016, pp. 1–5. DOI: 10.1109/GLOCOMW.2016.7849087.

- 
- [83] Ronald Nissel, Stefan Schwarz, and Markus Rupp. “Filter Bank Multicarrier Modulation Schemes for Future Mobile Communications”. In: *IEEE Journal on Selected Areas in Communications* 35.8 (2017), pp. 1768–1782. DOI: 10.1109/JSAC.2017.2710022.
- [84] Vida Vakilian et al. “Universal-filtered multi-carrier technique for wireless systems beyond LTE”. In: *2013 IEEE Globecom Workshops (GC Wkshps)*. 2013, pp. 223–228. DOI: 10.1109/GLOCOMW.2013.6824990.
- [85] Xi Zhang et al. “Filtered-OFDM - Enabler for Flexible Waveform in the 5th Generation Cellular Networks”. In: *2015 IEEE Global Communications Conference (GLOBECOM)*. 2015, pp. 1–6. DOI: 10.1109/GLOCOM.2015.7417854.
- [86] Ana I. Pérez-Neira et al. “MIMO Signal Processing in Offset-QAM Based Filter Bank Multicarrier Systems”. In: *IEEE Transactions on Signal Processing* 64.21 (2016), pp. 5733–5762. DOI: 10.1109/TSP.2016.2580535.
- [87] P. Schniter and A. Sayeed. “Channel estimation and precoder design for millimeter-wave communications: The sparse way”. In: *2014 48th Asilomar Conference on Signals, Systems and Computers*. 2014, pp. 273–277.
- [88] A. Ghosh et al. “Millimeter-Wave Enhanced Local Area Systems: A High-Data-Rate Approach for Future Wireless Networks”. In: *IEEE Journal on Selected Areas in Communications* 32.6 (2014), pp. 1152–1163.
- [89] S. Sun and T. S. Rappaport. “Millimeter Wave MIMO channel estimation based on adaptive compressed sensing”. In: *2017 IEEE International Conference on Communications Workshops (ICC Workshops)*. 2017, pp. 47–53.
- [90] Emmanuel J. Candès and Michael B. Wakin. “An Introduction To Compressive Sampling [A sensing/sampling paradigm that goes against the common knowledge in data acquisition]”. In: *IEEE Signal Processing Magazine* 25 (Mar. 2008), pp. 21–30. ISSN: 1053-5888. (Visited on 09/13/2019).
- [91] R. G. Baraniuk. “Compressive Sensing [Lecture Notes]”. In: *IEEE Signal Processing Magazine* 24.4 (2007), pp. 118–121.
- [92] David L. Donoho, Arian Maleki, and Andrea Montanari. “Message-passing algorithms for compressed sensing”. en. In: *Proceedings of the National Academy of Sciences* 106.45 (Nov. 2009), pp. 18914–18919. ISSN: 0027-8424, 1091-6490. DOI: 10.1073/pnas.0909892106. (Visited on 09/13/2019).
- [93] J. W. Choi et al. “Compressed Sensing for Wireless Communications: Useful Tips and Tricks”. In: *IEEE Communications Surveys Tutorials* 19.3 (2017), pp. 1527–1550.

- [94] E. J. Candes, J. Romberg, and T. Tao. “Robust uncertainty principles: exact signal reconstruction from highly incomplete frequency information”. In: *IEEE Transactions on Information Theory* 52.2 (2006), pp. 489–509.
- [95] David L. Donoho and Michael Elad. “Optimally sparse representation in general (nonorthogonal) dictionaries via  $l_1$  minimization”. en. In: *Proceedings of the National Academy of Sciences* 100.5 (Mar. 2003), pp. 2197–2202. ISSN: 0027-8424, 1091-6490. DOI: 10.1073/pnas.0437847100. (Visited on 11/06/2019).
- [96] E. J. Candes and T. Tao. “Decoding by linear programming”. In: *IEEE Transactions on Information Theory* 51.12 (2005), pp. 4203–4215.
- [97] J. A. Tropp and A. C. Gilbert. “Signal Recovery From Random Measurements Via Orthogonal Matching Pursuit”. In: *IEEE Transactions on Information Theory* 53.12 (2007), pp. 4655–4666.
- [98] M. Rani, S. B. Dhok, and R. B. Deshmukh. “A Systematic Review of Compressive Sensing: Concepts, Implementations and Applications”. In: *IEEE Access* 6 (2018), pp. 4875–4894.
- [99] S. Chen, D. Donoho, and M. Saunders. “Atomic Decomposition by Basis Pursuit”. In: *SIAM Review* 43.1 (Jan. 2001), pp. 129–159. ISSN: 0036-1445. DOI: 10.1137/S003614450037906X. (Visited on 06/27/2019).
- [100] Emmanuel Candes and Terence Tao. “The Dantzig selector: Statistical estimation when  $p$  is much larger than  $n$ ”. EN. In: *The Annals of Statistics* 35.6 (Dec. 2007), pp. 2313–2351. ISSN: 0090-5364, 2168-8966. DOI: 10.1214/009053606000001523. (Visited on 09/16/2019).
- [101] *Regression Shrinkage and Selection Via the Lasso - Tibshirani - 1996 - Journal of the Royal Statistical Society: Series B (Methodological) - Wiley Online Library*. URL: <https://rss.onlinelibrary.wiley.com/doi/abs/10.1111/j.2517-6161.1996.tb02080.x> (visited on 09/17/2019).
- [102] S. G. Mallat and Zhifeng Zhang. “Matching pursuits with time-frequency dictionaries”. In: *IEEE Transactions on Signal Processing* 41.12 (1993), pp. 3397–3415.
- [103] J. Lee, G. Gil, and Y. H. Lee. “Exploiting spatial sparsity for estimating channels of hybrid MIMO systems in millimeter wave communications”. In: *2014 IEEE Global Communications Conference*. 2014, pp. 3326–3331.
- [104] D. Needell and J.A. Tropp. “CoSaMP: Iterative signal recovery from incomplete and inaccurate samples”. en. In: *Applied and Computational Harmonic Analysis* 26.3 (May 2009), pp. 301–321. ISSN: 10635203. DOI: 10.1016/j.acha.2008.07.002. (Visited on 12/01/2019).

- [105] Thomas Blumensath and Mike E. Davies. “Iterative hard thresholding for compressed sensing”. In: *Applied and Computational Harmonic Analysis* 27.3 (Nov. 2009), pp. 265–274. ISSN: 1063-5203. DOI: 10.1016/j.acha.2009.04.002. (Visited on 10/10/2019).
- [106] S. Ji, Y. Xue, and L. Carin. “Bayesian Compressive Sensing”. In: *IEEE Transactions on Signal Processing* 56.6 (2008), pp. 2346–2356.
- [107] J. Haupt and R. Nowak. “Signal Reconstruction From Noisy Random Projections”. In: *IEEE Transactions on Information Theory* 52.9 (2006), pp. 4036–4048.
- [108] S. Kwon, J. Wang, and B. Shim. “Multipath Matching Pursuit”. In: *IEEE Transactions on Information Theory* 60.5 (2014), pp. 2986–3001.
- [109] J. Wang, S. Kwon, and B. Shim. “Generalized Orthogonal Matching Pursuit”. In: *IEEE Transactions on Signal Processing* 60.12 (2012), pp. 6202–6216.
- [110] A. N. Uwaechia and N. M. Mahyuddin. “Stage-Determined Matching Pursuit for Sparse Channel Estimation in OFDM Systems”. In: *IEEE Systems Journal* 13.3 (2019), pp. 2240–2251.
- [111] A. Alkhateeb et al. “Channel Estimation and Hybrid Precoding for Millimeter Wave Cellular Systems”. In: *IEEE Journal of Selected Topics in Signal Processing* 8.5 (2014), pp. 831–846.
- [112] A. Alkhateeb et al. “Single-sided adaptive estimation of multi-path millimeter wave channels”. In: *2014 IEEE 15th International Workshop on Signal Processing Advances in Wireless Communications (SPAWC)*. 2014, pp. 125–129.
- [113] Y. Peng, Y. Li, and P. Wang. “An Enhanced Channel Estimation Method for Millimeter Wave Systems With Massive Antenna Arrays”. In: *IEEE Communications Letters* 19.9 (2015), pp. 1592–1595.
- [114] R. Méndez-Rial et al. “Channel estimation and hybrid combining for mmWave: Phase shifters or switches?” In: *2015 Information Theory and Applications Workshop (ITA)*. 2015, pp. 90–97.
- [115] H. Chiang et al. “Low-complexity spatial channel estimation and hybrid beamforming for millimeter wave links”. In: *2016 IEEE 27th Annual International Symposium on Personal, Indoor, and Mobile Radio Communications (PIMRC)*. 2016, pp. 1–7.
- [116] Y. Han and J. Lee. “Asymmetric channel estimation for multi-user millimeter wave communications”. In: *2016 International Conference on Information and Communication Technology Convergence (ICTC)*. 2016, pp. 4–6.

- [117] S. Park and R. W. Heath. “Spatial channel covariance estimation for mmWave hybrid MIMO architecture”. In: *2016 50th Asilomar Conference on Signals, Systems and Computers*. 2016, pp. 1424–1428.
- [118] K. Venugopal et al. “Time-domain channel estimation for wideband millimeter wave systems with hybrid architecture”. In: *2017 IEEE International Conference on Acoustics, Speech and Signal Processing (ICASSP)*. 2017, pp. 6493–6497.
- [119] K. Venugopal et al. “Channel Estimation for Hybrid Architecture-Based Wideband Millimeter Wave Systems”. In: *IEEE Journal on Selected Areas in Communications* 35.9 (2017), pp. 1996–2009.
- [120] J. Rodríguez-Fernández et al. “A frequency-domain approach to wideband channel estimation in millimeter wave systems”. In: *2017 IEEE International Conference on Communications (ICC)*. 2017, pp. 1–7.
- [121] J. Rodríguez-Fernández et al. “Frequency-Domain Compressive Channel Estimation for Frequency-Selective Hybrid Millimeter Wave MIMO Systems”. In: *IEEE Transactions on Wireless Communications* 17.5 (2018), pp. 2946–2960.
- [122] Z. Gao et al. “Channel Estimation for Millimeter-Wave Massive MIMO With Hybrid Precoding Over Frequency-Selective Fading Channels”. In: *IEEE Communications Letters* 20.6 (2016), pp. 1259–1262.
- [123] D. C. Araújo et al. “Channel estimation for millimeter-wave Very-Large MIMO systems”. In: *2014 22nd European Signal Processing Conference (EUSIPCO)*. 2014, pp. 81–85.
- [124] A. Kaushik et al. “Efficient Channel Estimation in Millimeter Wave Hybrid MIMO Systems with Low Resolution ADCs”. In: *2018 26th European Signal Processing Conference (EUSIPCO)*. 2018, pp. 1825–1829.
- [125] J. Sung, J. Choi, and B. L. Evans. “Narrowband Channel Estimation for Hybrid Beamforming Millimeter Wave Communication Systems with One-Bit Quantization”. In: *2018 IEEE International Conference on Acoustics, Speech and Signal Processing (ICASSP)*. 2018, pp. 3914–3918.
- [126] J. Mo et al. “Channel estimation in millimeter wave MIMO systems with one-bit quantization”. In: *2014 48th Asilomar Conference on Signals, Systems and Computers*. 2014, pp. 957–961.
- [127] Omar El Ayach et al. “Spatially Sparse Precoding in Millimeter Wave MIMO Systems”. In: *IEEE Transactions on Wireless Communications* 13.3 (2014), pp. 1499–1513. DOI: 10.1109/TWC.2014.011714.130846.

- [128] Ahmed Alkhateeb et al. “MIMO Precoding and Combining Solutions for Millimeter-Wave Systems”. In: *IEEE Communications Magazine* 52.12 (2014), pp. 122–131. DOI: 10.1109/MCOM.2014.6979963.
- [129] Philip Schniter and Akbar Sayeed. “Channel estimation and precoder design for millimeter-wave communications: The sparse way”. In: *2014 48th Asilomar Conference on Signals, Systems and Computers*. 2014, pp. 273–277. DOI: 10.1109/ACSSC.2014.7094443.
- [130] Ahmed Alkhateeb and Robert W. Heath. “Frequency Selective Hybrid Precoding for Limited Feedback Millimeter Wave Systems”. In: *IEEE Transactions on Communications* 64.5 (2016), pp. 1801–1818. DOI: 10.1109/TCOMM.2016.2549517.
- [131] Amir Aminjavaheri et al. “Impact of timing and frequency offsets on multicarrier waveform candidates for 5G”. In: *2015 IEEE Signal Processing and Signal Processing Education Workshop (SP/SPE)*. 2015, pp. 178–183. DOI: 10.1109/DSP-SPE.2015.7369549.
- [132] Jiening Mao et al. “Over-Sampling Codebook-Based Hybrid Minimum Sum-Mean-Square-Error Precoding for Millimeter-Wave 3D-MIMO”. In: *IEEE Wireless Communications Letters* 7.6 (2018), pp. 938–941. DOI: 10.1109/LWC.2018.2839723.
- [133] Michel Saideh et al. “Performance Evaluation of Multi-Carrier Modulation Techniques in High Speed Railway Environment with Impulsive Noise”. In: *2019 IEEE 2nd 5G World Forum (5GWF)*. 2019, pp. 243–248. DOI: 10.1109/5GWF.2019.8911645.
- [134] Michel Saideh, Iyad Dayoub, and Marion Berbineau. “Efficient Equalization for FBMC-OQAM Under Doubly Selective Channel Estimation Errors”. In: *IEEE Communications Letters* 23.5 (2019), pp. 863–866. DOI: 10.1109/LCOMM.2019.2907938.
- [135] Jun Li et al. “Receiver Design for Alamouti Coded FBMC System in Highly Frequency Selective Channels”. In: *IEEE Transactions on Broadcasting* 65.3 (2019), pp. 601–608. DOI: 10.1109/TBC.2018.2874547.
- [136] Prem Singh et al. “Semi-Blind, Training, and Data-Aided Channel Estimation Schemes for MIMO-FBMC-OQAM Systems”. In: *IEEE Transactions on Signal Processing* 67.18 (2019), pp. 4668–4682. DOI: 10.1109/TSP.2019.2925607.
- [137] Arman Farhang et al. “Filter Bank Multicarrier for Massive MIMO”. In: *2014 IEEE 80th Vehicular Technology Conference (VTC2014-Fall)*. 2014, pp. 1–7. DOI: 10.1109/VTCFall.2014.6965986.
- [138] Prem Singh et al. “Uplink Sum-Rate and Power Scaling Laws for Multi-User Massive MIMO-FBMC Systems”. In: *IEEE Transactions on Communications* 68.1 (2020), pp. 161–176. DOI: 10.1109/TCOMM.2019.2950216.

- [139] Prem Singh, Rohit Budhiraja, and Kasturi Vasudevan. “Probability of Error in MMSE Detection For MIMO-FBMC-OQAM Systems”. In: *IEEE Transactions on Vehicular Technology* 68.8 (2019), pp. 8196–8200. DOI: 10.1109/TVT.2019.2920475.
- [140] Prem Singh, Rohit Budhiraja, and K. Vasudevan. “SER Analysis of MMSE Combining For MIMO FBMC-OQAM Systems With Imperfect CSI”. In: *IEEE Communications Letters* 23.2 (2019), pp. 226–229. DOI: 10.1109/LCOMM.2018.2884932.
- [141] Prem Singh et al. “CFO and Channel Estimation for Frequency Selective MIMO-FBMC/OQAM Systems”. In: *IEEE Wireless Communications Letters* 7.5 (2018), pp. 844–847. DOI: 10.1109/LWC.2018.2830777.
- [142] Han Wang. “Sparse Channel Estimation for MIMO-FBMC/OQAM Wireless Communications in Smart City Applications”. In: *IEEE Access* 6 (2018), pp. 60666–60672. DOI: 10.1109/ACCESS.2018.2875245.
- [143] Amir Aminjavaheri et al. “Frequency spreading equalization in multicarrier massive MIMO”. In: *2015 IEEE International Conference on Communication Workshop (ICCW)*. 2015, pp. 1292–1297. DOI: 10.1109/ICCW.2015.7247356.
- [144] Suraj Srivastava et al. “Bayesian Learning-Based Doubly-Selective Sparse Channel Estimation for Millimeter Wave Hybrid MIMO-FBMC-OQAM Systems”. In: *IEEE Transactions on Communications* 69.1 (2021), pp. 529–543. DOI: 10.1109/TCOMM.2020.3029568.
- [145] Ronald Nissel et al. “Low-latency MISO FBMC-OQAM: It works for millimeter waves!” In: *2017 IEEE MTT-S International Microwave Symposium (IMS)*. 2017, pp. 673–676. DOI: 10.1109/MWSYM.2017.8058660.
- [146] Kiran Venugopal, Nuria González-Prelcic, and Robert W. Heath. “Optimality of Frequency Flat Precoding in Frequency Selective Millimeter Wave Channels”. In: *IEEE Wireless Communications Letters* 6.3 (2017), pp. 330–333. DOI: 10.1109/LWC.2017.2686854.
- [147] A. Goldsmith et al. “Capacity limits of MIMO channels”. In: *IEEE Journal on Selected Areas in Communications* 21.5 (2003), pp. 684–702. DOI: 10.1109/JSAC.2003.810294.
- [148] John M Lee. “Smooth manifolds”. In: *Introduction to Smooth Manifolds*. Springer, 2013, pp. 1–31.
- [149] Stephen Boyd, Stephen P Boyd, and Lieven Vandenberghe. *Convex optimization*. Cambridge university press, 2004.

- [150] J Lindenstrauss. “The dimension of almost spherical sections of convex bodies”. In: *Séminaire d’Analyse fonctionnelle (dit” Maurey-Schwartz”)* (1977), pp. 1–13.
- [151] Nojun Kwak. “Principal Component Analysis Based on L1-Norm Maximization”. In: *IEEE Transactions on Pattern Analysis and Machine Intelligence* 30.9 (2008), pp. 1672–1680. DOI: 10.1109/TPAMI.2008.114.
- [152] J.A. Tropp et al. “Designing structured tight frames via an alternating projection method”. In: *IEEE Transactions on Information Theory* 51.1 (2005), pp. 188–209. DOI: 10.1109/TIT.2004.839492.
- [153] Omar El Ayach et al. “The capacity optimality of beam steering in large millimeter wave MIMO systems”. In: *2012 IEEE 13th International Workshop on Signal Processing Advances in Wireless Communications (SPAWC)*. 2012, pp. 100–104. DOI: 10.1109/SPAWC.2012.6292865.
- [154] J.A. Tropp. “Greed is good: algorithmic results for sparse approximation”. In: *IEEE Transactions on Information Theory* 50.10 (2004), pp. 2231–2242. DOI: 10.1109/TIT.2004.834793.
- [155] Stephen J. Wright, Robert D. Nowak, and Mário A. T. Figueiredo. “Sparse Reconstruction by Separable Approximation”. In: *IEEE Transactions on Signal Processing* 57.7 (2009), pp. 2479–2493. DOI: 10.1109/TSP.2009.2016892.
- [156] Ahmed Alkhateeb et al. “Channel Estimation and Hybrid Precoding for Millimeter Wave Cellular Systems”. In: *IEEE Journal of Selected Topics in Signal Processing* 8.5 (2014), pp. 831–846. DOI: 10.1109/JSTSP.2014.2334278.
- [157] Zhenyu Xiao, Pengfei Xia, and Xiang-Gen Xia. “Channel Estimation and Hybrid Precoding for Millimeter-Wave MIMO Systems: A Low-Complexity Overall Solution”. In: *IEEE Access* 5 (2017), pp. 16100–16110. DOI: 10.1109/ACCESS.2017.2724037.
- [158] Kiran Venugopal et al. “Channel Estimation for Hybrid Architecture-Based Wideband Millimeter Wave Systems”. In: *IEEE Journal on Selected Areas in Communications* 35.9 (2017), pp. 1996–2009. DOI: 10.1109/JSAC.2017.2720856.
- [159] Javier Rodríguez-Fernández et al. “A frequency-domain approach to wideband channel estimation in millimeter wave systems”. In: *2017 IEEE International Conference on Communications (ICC)*. 2017, pp. 1–7. DOI: 10.1109/ICC.2017.7997047.
- [160] M. L. Malloy and R. D. Nowak. “Near-Optimal Adaptive Compressed Sensing”. In: *IEEE Transactions on Information Theory* 60.7 (2014), pp. 4001–4012.

- [161] Matthew L. Malloy and Robert D. Nowak. “Near-Optimal Compressive Binary Search”. In: *arXiv:1203.1804 [cs, math]* (Mar. 2012). arXiv: 1203.1804. (Visited on 06/28/2019).
- [162] D. E. Berraki, S. M. D. Armour, and A. R. Nix. “Application of compressive sensing in sparse spatial channel recovery for beamforming in mmWave outdoor systems”. In: *2014 IEEE Wireless Communications and Networking Conference (WCNC)*. 2014, pp. 887–892.
- [163] Z. Marzi, D. Ramasamy, and U. Madhow. “Compressive Channel Estimation and Tracking for Large Arrays in mm-Wave Picocells”. In: *IEEE Journal of Selected Topics in Signal Processing* 10.3 (2016), pp. 514–527.
- [164] Z. Xiao, P. Xia, and X. Xia. “Channel Estimation and Hybrid Precoding for Millimeter-Wave MIMO Systems: A Low-Complexity Overall Solution”. In: *IEEE Access* 5 (2017), pp. 16100–16110.
- [165] J. He et al. “Millimeter wave MIMO channel tracking systems”. In: *2014 IEEE Globecom Workshops (GC Wkshps)*. 2014, pp. 416–421.
- [166] S. Payami et al. “Effective RF codebook design and channel estimation for millimeter wave communication systems”. In: *2015 IEEE International Conference on Communication Workshop (ICCW)*. 2015, pp. 1226–1231.
- [167] M. Kokshoorn et al. “Fast channel estimation for millimetre wave wireless systems using overlapped beam patterns”. In: *2015 IEEE International Conference on Communications (ICC)*. 2015, pp. 1304–1309.
- [168] S. Montagner, N. Benvenuto, and P. Baracca. “Channel Estimation Using a 2D DFT for Millimeter-Wave Systems”. In: *2015 IEEE 81st Vehicular Technology Conference (VTC Spring)*. 2015, pp. 1–5.
- [169] L. Wenlü, Z. Weixia, and L. Xuefeng. “An Adaptive Channel Estimation Algorithm for Millimeter Wave Cellular Systems”. In: *Journal of Communications and Information Networks* 1.2 (2016), pp. 37–44.
- [170] Z. Zhou et al. “Channel Estimation for Millimeter-Wave Multiuser MIMO Systems via PARAFAC Decomposition”. In: *IEEE Transactions on Wireless Communications* 15.11 (2016), pp. 7501–7516.
- [171] Z. Guo, X. Wang, and W. Heng. “Millimeter-Wave Channel Estimation Based on 2-D Beamspace MUSIC Method”. In: *IEEE Transactions on Wireless Communications* 16.8 (2017), pp. 5384–5394.

- [172] Y. Xiao, Y. Wang, and W. Xiang. “Dimension-Deficient Channel Estimation of Hybrid Beamforming Based on Compressive Sensing”. In: *IEEE Access* 7 (2019), pp. 13791–13798.
- [173] W. U. Bajwa, A. Sayeed, and R. Nowak. “Compressed sensing of wireless channels in time, frequency, and space”. In: *2008 42nd Asilomar Conference on Signals, Systems and Computers*. 2008, pp. 2048–2052.
- [174] S. F. Cotter et al. “Sparse solutions to linear inverse problems with multiple measurement vectors”. In: *IEEE Transactions on Signal Processing* 53.7 (2005), pp. 2477–2488.
- [175] A. Cichocki et al. “Tensor Decompositions for Signal Processing Applications: From two-way to multiway component analysis”. In: *IEEE Signal Processing Magazine* 32.2 (2015), pp. 145–163.
- [176] Z. Zhou et al. “Low-Rank Tensor Decomposition-Aided Channel Estimation for Millimeter Wave MIMO-OFDM Systems”. In: *IEEE Journal on Selected Areas in Communications* 35.7 (2017), pp. 1524–1538.
- [177] J. A. Tropp, A. C. Gilbert, and M. J. Strauss. “Simultaneous sparse approximation via greedy pursuit”. In: *Proceedings. (ICASSP '05). IEEE International Conference on Acoustics, Speech, and Signal Processing, 2005*. Vol. 5. 2005, v/721–v/724 Vol. 5.
- [178] Z. Gao, L. Dai, and Z. Wang. “Channel estimation for mmWave massive MIMO based access and backhaul in ultra-dense network”. In: *2016 IEEE International Conference on Communications (ICC)*. 2016, pp. 1–6.
- [179] Li Chen et al. “Multi-stage beamforming codebook for 60GHz WPAN”. In: *2011 6th International ICST Conference on Communications and Networking in China (CHINACOM)*. 2011, pp. 361–365. DOI: 10.1109/ChinaCom.2011.6158179.
- [180] Y. Ming Tsang and Ada S. Y. Poon. “Successive AoA estimation: Revealing the second path for 60 GHz communication system”. In: *2011 49th Annual Allerton Conference on Communication, Control, and Computing (Allerton)*. 2011, pp. 508–515. DOI: 10.1109/Allerton.2011.6120209.
- [181] HLV Trees. *Optimum array processing (detection, estimation, and modulation theory, part iv)* wiley. 2002.
- [182] Mohammad Masarra et al. “FBMC-OQAM for frequency-selective mmWave hybrid MIMO systems”. In: *2022 IEEE Wireless Communications and Networking Conference (WCNC)*. 2022, pp. 1593–1598. DOI: 10.1109/WCNC51071.2022.9771667.

- 
- [183] D.L. Donoho. “Compressed sensing”. In: *IEEE Transactions on Information Theory* 52.4 (2006), pp. 1289–1306. DOI: 10.1109/TIT.2006.871582.
- [184] Matthew L. Malloy and Robert D. Nowak. “Near-Optimal Adaptive Compressed Sensing”. In: *IEEE Transactions on Information Theory* 60.7 (2014), pp. 4001–4012. DOI: 10.1109/TIT.2014.2321552.
- [185] Mark A. Iwen and Ahmed H. Tewfik. “Adaptive Strategies for Target Detection and Localization in Noisy Environments”. In: *IEEE Transactions on Signal Processing* 60.5 (2012), pp. 2344–2353. DOI: 10.1109/TSP.2012.2187201.
- [186] Chaitanya Ekanadham, Daniel Tranchina, and Eero P. Simoncelli. “Recovery of Sparse Translation-Invariant Signals With Continuous Basis Pursuit”. In: *IEEE Transactions on Signal Processing* 59.10 (2011), pp. 4735–4744. DOI: 10.1109/TSP.2011.2160058.
- [187] Dinesh Ramasamy, Sriram Venkateswaran, and Upamanyu Madhow. “Compressive Parameter Estimation in AWGN”. In: *IEEE Transactions on Signal Processing* 62.8 (2014), pp. 2012–2027. DOI: 10.1109/TSP.2014.2306180.
- [188] Hao Zhu, Geert Leus, and Georgios B. Giannakis. “Sparse regularized total least squares for sensing applications”. In: *2010 IEEE 11th International Workshop on Signal Processing Advances in Wireless Communications (SPAWC)*. 2010, pp. 1–5. DOI: 10.1109/SPAWC.2010.5671061.
- [189] A. Kabiri, M. J. Emadi, and M. N. Khormuji. “Optimal Design of Semi-Orthogonal Multiple-Access Massive MIMO Systems”. In: *IEEE Communications Letters* 21.10 (2017), pp. 2230–2233.
- [190] L. Dai et al. “A Survey of Non-Orthogonal Multiple Access for 5G”. In: *IEEE Communications Surveys Tutorials* 20.3 (2018), pp. 2294–2323.
- [191] P. Ioannides and C. A. Balanis. “Uniform circular and rectangular arrays for adaptive beamforming applications”. In: *IEEE Antennas and Wireless Propagation Letters* 4 (2005), pp. 351–354.
- [192] S. Ghosh and D. Sen. “An Inclusive Survey on Array Antenna Design for Millimeter-Wave Communications”. In: *IEEE Access* 7 (2019), pp. 83137–83161.
- [193] Y. Song et al. “Physical Layer Security in Cognitive Millimeter Wave Networks”. In: *IEEE Access* 7 (2019), pp. 109162–109180.
- [194] C. G. Tsinos, S. Chatzinotas, and B. Ottersten. “Hybrid Analog-Digital Transceiver Designs for Multi-User MIMO mmWave Cognitive Radio Systems”. In: *IEEE Transactions on Cognitive Communications and Networking* 6.1 (2020), pp. 310–324.

- 
- [195] Y. Song et al. “An Analysis on Secure Millimeter Wave NOMA Communications in Cognitive Radio Networks”. In: *IEEE Access* 8 (2020), pp. 78965–78978.